Norwegian University
of Life Sciences

Master's Thesis 2024 60 ECTS
Faculty of Environmental Sciences and Natural Resource Management

Evaluating the Use of ^{129}I and ^{236}U as Oceanographic Tracers in Combination with Marine Transport Modeling

Jonas Kildahl Lauritsen
Master's Degree in Chemistry

Acknowledgements

This master's thesis concludes my five-year education at the Norwegian University of Life Sciences (NMBU). The journey was an enlightening one, full of interesting education and good companionship. I have discovered new interests through various courses, resulting in this personalized thesis.

First and foremost, I would like to express my gratitude to my main supervisor Ole Christian Lind (NMBU) for making this project possible. Your guidance and enthusiasm throughout the project have been highly appreciated and motivating. I would also like to show my gratitude to my co-supervisors, Simon Jerome (NMBU), for your guidance in radiochemistry and sample preparations, and Magne Simonsen (MET), for setting up the ocean model and your continuous work with the model scripts. Thanks for all the discussions, feedback, advice and weekly meetings.

I also want to show my appreciation to Jan John (CTU), Mojmír Němec (CTU), Tomáš Prášek (CTU), Miriam Mindová (CTU), Martin Dano (CTU) and Petros Leivadaros (CTU). Thank you for helping me with sample preparations and introducing me to the accelerator mass spectrometer, as well as enjoyable lunches, coffees and chocolates. I would also like to thank Rafael García-Tenorio (CNA), Jose Maria López-Gutiérrez (CNA) and Elena Chamizo (CNA) for being able to measure my samples at such short notice.

Furthermore, I want to show my gratitude towards the Institute of Marine Research (IMR), and especially Hilde Elise Heldal (IMR) and Patrick Andre Korneliussen (frm. IMR) for providing the samples. In addition, I would also like to thank Hans-Christian Teien (NMBU) for providing ^{129}I data from Komsomolets and Øyvind Sætra (MET) for your valuable modeling advice shared during discussions.

Finally, I want to show my appreciation to friends and family for your continuous encouragement and support throughout the project. A special thanks to Petronelle for your valuable insights, discussions and support.

Norwegian University of Life Sciences (NMBU)

Ås, 15th of May 2024

Jonas Kildahl Lauritsen

Abstract

Anthropogenic radionuclides are introduced to the global marine environment from a range of different sources, such as global fallout from atmospheric weapon tests and nuclear accidents as well as operational or accidental discharges from nuclear installations. Transportation of radionuclides in the marine environment depends on the physico-chemical properties and different oceanic processes. Long-lived radionuclides like ^{129}I and ^{236}U are commonly utilized as tracers of ocean currents due to conservative behavior and the relatively well-documented discharges from nuclear installations. Discharges of ^{129}I and ^{236}U from Sellafield and La Hague reprocessing plants can be used as model input in ocean models to predict ocean transport.

These oceanographic models are used to study ocean processes, including climate changes such as ocean acidification and ice melting, and predict potential consequences of various contaminant releases to the marine environment. Regarding nuclear events, these models can be valuable pre-accident to simulate different scenarios to predict the transport and fate of radionuclides, while also contributing to emergency decision-making. Models can also be utilized post-accident to assess consequences and future measures. However, an oceanographic model needs calibration and validation before being used as an emergency preparedness tool.

In the present work, a hydrodynamic ocean model in combination with an ocean transport model was utilized to simulate the ocean transport of Lagrangian particles representing ^{129}I and ^{236}U discharges released from Sellafield and La Hague. The ocean transport model is an open-source trajectory model called OpenDrift, developed by the Norwegian Meteorological Institute (MET). The model simulations aimed to improve the source term by investigating the source contribution of ^{129}I and ^{236}U originating from Sellafield and La Hague and to validate the transport model by comparing model estimations to observations.

To validate OpenDrift, an extensive literature search of existing ^{129}I and ^{236}U observations within the model domain was carried out. The search resulted in observations in the North Sea, Irish Sea and Barents Sea which could be compared to model estimations. The literature search revealed a lack of ^{129}I and ^{236}U observations in the Norwegian Sea. Some of the identified data gaps were filled by providing seawater samples from various sampling stations in the Norwegian Sea through collaboration with the Institute of Marine Research (IMR). These samples were then analyzed using accelerator mass spectrometry (AMS) through collaboration with the Czech Technical University (CTU) and the University of Seville (USEV).

The preparation of the seawater samples was conducted at the Norwegian University of Life Sciences (NMBU) in Ås and at the Czech Technical University (CTU) in Prague. The preparations consisted of radiochemical separations and aimed to reduce the sample volume and obtain a high purity and yield of the analyte for measurements with mass spectrometric techniques. The samples were prepared into

a fine homogenous powder and shipped to Centro Nacional de Aceleradores (CNA) in Seville for accelerator mass spectrometer (AMS) measurements. Since the AMS measurements yielded $^{129}I/^{236}U$ ratios, ^{127}I was analyzed using inductively coupled plasma spectrometry (ICP-MS) at NMBU, enabling the conversion of the AMS results to ^{129}I concentrations (atoms/l). The measured concentrations of ^{129}I and existing literature data of ^{129}I and ^{236}U from different locations and sampling dates were compared to model outputs to validate OpenDrift.

Model simulations and observations provided ^{129}I and ^{236}U concentrations as well as $^{129}I/^{236}U$ atom ratios at nine different locations, including the Irish Sea, English Channel, North Sea (south, east and north), Norwegian Sea, Barents Sea, Fram Strait and Komsomolets. The ^{129}I concentrations (atoms/l) measured with AMS from samples in the Norwegian Sea ranged from 0.63 to 35.0 x 10^9 atoms/l. The $^{129}I/^{236}U$ ratios tended to be more comparable to the model outputs further away from the discharge sources when water masses are better mixed and local currents play a lesser role in the transport. The model estimations aimed to improve the source terms of ^{129}I and ^{236}U by comparing literature and unpublished data with observations, and separate source contributions from Sellafield and La Hague.

General trend observations indicated a higher ^{129}I contribution from La Hague and a higher ^{236}U contribution from Sellafield in most model locations, reflecting the reprocessing discharges. Based on comparisons of model outputs with field observation data, an alleged substantial retention of ^{236}U in the Irish Sea could not be confirmed. This interpretation is based on 1) the model underestimated ^{236}U concentrations and 2) the estimated $^{129}I/^{236}U$ ratios were relatively comparable to corresponding observations, varying within a factor ranging between 1 and 38. Whereas the opposite outcomes would be expected in case of substantial retention.

Analysis of Lagrangian model particle ages revealed transportation time differences between particles released from Sellafield and La Hague. Between 2003 and 2023, the average particle ages from Sellafield (6.98 and 7.53 years) were older than for La Hague (3.54 and 4.12 years) in the Norwegian and Barents Seas. In the Irish Sea, however, the model particles released from La Hague were over three times older, implying longer transportation time. In most parts of the North Sea, particles from Sellafield were older, meaning La Hague particles are transported faster due to the strong coastal currents along the northwestern European coast into the Barents Sea and the Arctic Ocean.

The ocean model simulations provided valuable information regarding source contributions, transportation pathways and model particle ages. The validation of the ocean model provided relatively comparable ratios, the most favorable validations of $^{129}I/^{236}U$ ratios being further away from the discharge sources. More refinements should be considered in the simulations to achieve more accurate predictions from the ocean model. The speciation of radionuclides, the background signal from global fallout and nuclear reprocessing discharges pre-1990 should be implemented in the model for future research.

Sammendrag

Antropogene radionuklider introduseres til det globale marine miljøet fra mange forskjellige kilder, inkludert global nedfall fra atmosfæriske våpentester og atomulykker, samt operasjonelle- eller utilsiktede utslipp fra atominstallasjoner. Transport av radionuklider i det marine miljøet er avhengig av deres fysisk-kjemiske egenskaper og ulike oseaniske prosesser. Langlivede radionuklider som ^{129}I og ^{236}U blir ofte brukt som tracere av havstrømmer på grunn av deres konservative egenskaper og relativt godt dokumenterte utslipp fra atominstallasjoner. Utslipp av ^{129}I og ^{236}U fra Sellafield og La Hague reprosesseringsanlegg kan brukes som modellinput i havmodeller for å forutsi havtransport.

Disse oseanografiske modellene kan brukes til å studere havprosesser, inkludert klimaendringer som havforsuring og havissmelting, samt å forutsi potensielle konsekvenser av ulike kontaminantutslipp til det marine miljøet. Når det gjelder nukleære hendelser, kan disse modellene være verdifulle før ulykker for å simulere ulike scenarier for å forutsi transporten og skjebnen til radionuklider, samt bidra til å ta beslutninger i krisesituasjoner. Modellene kan også benyttes etter ulykker for å vurdere konsekvenser og fremtidige tiltak. Oseanografiske modeller behøver kalibrering og validering før de kan benyttes som beredskapsverktøy under nødssituasjoner.

I denne forskningen benyttes en hydrodynamisk havmodell i kombinasjon med en havtransportmodell for å simulere havtransport av modellpartikler som representerer ^{129}I og ^{236}U utslipp fra Sellafield og La Hague. Havtransportmodellen som benyttes er en åpen kildekode banemodell kalt OpenDrift, utviklet av Metrologisk Institutt (MET). Målet med modellsimuleringene var å forbedre kildetermen ved å undersøke kildebidragene av ^{129}I og ^{236}U fra Sellafield og La Hague, og å validere transportmodellen ved å sammenlikne modellestimeringer med observasjoner.

For å validere OpenDrift, ble det utført omfattende litteratursøk av eksisterende ^{129}I og ^{236}U observasjoner innenfor modelldomenet. Søket resulterte i flere observasjoner i Nordsjøen, Irskesjøen og Barentshavet som kunne sammenliknes med modellestimater. Litteratursøket avdekket mangler på ^{129}I og ^{236}U observasjoner i Norskehavet. Noen av de identifiserte datahullene ble fylt ved å ta sjøvannsprøver fra ulike prøvetakingsstasjoner i Norskehavet gjennom et samarbeid med Havforskningsinstituttet (HI). Disse prøvene ble deretter analysert ved hjelp av akseleratormassespektrometri (AMS) gjennom samarbeid med Czech Technical University (CTU) og University of Seville (USEV).

Prøveprepareringen av sjøvannsprøvene ble utført ved Norges miljø- og biovitenskapelige universitet (NMBU) i Ås og ved Czech Technical University (CTU) i Praha. Prepareringene besto av radiokjemiske separasjoner, og hadde som hensikt å redusere prøvevolumet og å oppnå høyt utbytte av analytten for målinger med massespektrometriske teknikker. Prøvene ble preparert til et homogent pulver og sendt til Centro Nacional de Aceleradores (CNA) i Sevilla for målinger med akselerator massespektrometer (AMS). AMS-målingene resulterte i ^{129}I/^{236}U ratioer, så ^{127}I-målinger ble utført

med et induktivt koblet plasmaspektrometer (ICP-MS) ved NMBU for å konvertere AMS-resultatene til ^{129}I-konsentrasjoner (atomer/l). De målte ^{129}I-konsentrasjonene ble brukt sammen med eksisterende ^{129}I og ^{236}U litteraturdata fra ulike lokasjoner og prøvetakingsdatoer for å sammenlikne modellestimatene med observasjonene, og validere OpenDrift.

Modellsimuleringer og observasjoner ga ^{129}I og ^{236}U konsentrasjoner, samt ^{129}I/^{236}U atomratioer ved ni ulike lokasjoner, inkludert Irskesjøen, den engelske kanal, Nordsjøen (sør, øst og nord), Norskehavet, Barentshavet, Framstredet og Komsomolets. De målte ^{129}I konsentrasjonene (atomer/l) i prøvene fra Norskehavet varierte fra 0.63 til 35.0 x 10^9 atomer/l. De målte ^{129}I/^{236}U ratioene hadde en tendens til å være mer sammenliknbare lenger unna utslippskilden, der vannmassene er bedre blandet og lokale strømmer spiller en mindre rolle for transporteringen. Modellestimeringene hadde som mål å forbedre kildetermen til ^{129}I og ^{236}U ved å sammenlikne litteratur- og upubliserte data med estimeringene, og ved å separere de individuelle kildebidragene fra Sellafield og La Hague.

Generelle trendobserveringer indikerte et høyere ^{129}I-bidrag fra La Hague og et høyere ^{236}U-bidrag fra Sellafield for de fleste modellområder, noe som gjenspeilet seg i reprosesseringsutslippene. Basert på sammenlikningene av modelloutput med feltobservasjonsdata, kunne ikke en påstått betydelig retensjon av ^{236}U i Irskesjøen bekreftes. Denne tolkningen er basert på 1) at modellen underestimerte ^{236}U konsentrasjoner og 2) De estimerte ^{129}I/^{236}U ratioene var relativt sammenliknbare med korresponderende observasjoner, som varierte innenfor en faktor mellom 1 og 38. Mens de motsatte utfallene ville forventes dersom det var betydelig retensjon.

Analyse av modellpartikkelalder informerte om transporttidsforskjeller mellom partikler fra Sellafield og La Hague. Mellom 2003 og 2023 var gjennomsnittlig partikkelalder fra Sellafield (6.98 og 7.53) eldre enn for La Hague (3.54 og 4.12) i Norskehavet og Barentshavet. I Irskesjøen var modellpartiklene fra La Hague over tre ganger eldre, noe som indikerer lenger transporttid. I de fleste deler av Nordsjøen, var partikler fra Sellafield eldre, noe som betyr at La Hague-partikler transporteres raskere på grunn av sterke kyststrømmene langs den nordvest-europeiske kysten og inn i Barentshavet og Polhavet.

Havmodellsimuleringene ga verdifull informasjon om kildebidrag, transportveier og modellpartikkelalder. Valideringen av havmodellen ga relativt sammenliknbare ratioer, og de mer gunstige valideringene av ^{129}I/^{236}U-ratioer var lenger unna utslippskildene. Flere forbedringer bør vurderes i simuleringene for å oppnå mer nøyaktige predikteringer fra havmodellen. Spesiering av radionuklider, bakgrunnssignaler fra globalt nedfall og utslipp fra kjernefysisk reprosessering før 1990 bør implementeres i modellen i fremtidig forskning.

Table of Contents

List of Figures

List of Tables

List of Abbreviations

^{129}I – iodine-129
^{236}U – uranium-236
AMS – accelerator mass spectrometry
CNA – Centro Nacional de Aceleradores
cps – counts per second
CTU – Czech Technical University
Cs – cesium
DTU – Technical University of Denmark
DSA – Norwegian Radiation and Nuclear Safety Authority
EM – electron multiplier
ESA - electrostatic analyzer
GGR – gas-cooled reactor
GF – global fallout
GIC – gas ionization chamber
HMM – high molecular mas
HVEE – high Voltage Engineering Europe
ICP-MS – inductively coupled plasma – mass spectrometry
IMR – Institute of Marine Research
LEM – low energy magnet
LMM – low molecular mas
LOD – limit of detection
LOQ – limit of quantification
LWR – light-water reactor
Magnox – magnesium non-oxidizing
m/z – mass-to-charge
MET – Norwegian Meteorological Institute
Nb – niobium
RSD – relative standard deviation
SD – standard deviation
THORP – thermal oxide reprocessing plant
USEV – University of Seville
UTVEA – uranium and tetravalents actinides

1 Introduction

The global ocean covers approximately 70% of the Earth, and acts as a major sink for natural- and anthropogenic radionuclides from various sources. Major anthropogenic sources of contamination include global fallout from atmospheric weapon testing of the 1950s and 1960s, nuclear accidents like The Chernobyl Accident and water-borne discharges from European nuclear reprocessing plants (IAEA, 2012).

Radionuclides are introduced to the marine environment through various pathways, both by direct and indirect transport. Direct contamination includes fallout and accidental and authorized discharges from nuclear installations into the ocean. Contamination could also occur indirectly when radionuclides deposited in the terrestrial environment are transported into catchments and run off to the marine environment. Therefore, the marine environment will be at constant risk of radioactive contamination from a range of sources including nuclear reprocessing facilities. Ocean models are valuable for analyzing and predicting the behavior of ocean currents, and thereby contributing to assessing climate change impacts. However, to ensure accurate ocean transport model predictions, there is a need for model validation.

Radionuclide discharges of ^{129}I and ^{236}U have been proven useful as oceanographic tracers because of long half-lives and conservative behavior in the ocean (Casacuberta et al., 2018; Wefing et al., 2021). Both radionuclides are primarily anthropogenic and released from two main sources, liquid discharge from nuclear reprocessing plants and global fallout from atmospheric weapon testing and major nuclear accidents. The natural background signals from ^{129}I and ^{236}U in the Arctic Ocean, however, are several orders of magnitude lower compared to the anthropogenic sources (Casacuberta et al., 2016). Historical discharges of ^{129}I and ^{236}U from nuclear installations can provide information regarding ocean currents and predict the dispersion of contaminants in the marine environment. Combining radionuclide oceanographic tracers and ocean models is an essential tool during preparedness for assessing consequences and measures of marine contamination events. Oceanographic radionuclide tracers in ocean models can also be utilized to gather data on changing ocean currents, which serve as an indicator of climate change.

Hydrodynamic ocean models are often used to describe physical variables like temperature, salinity and ocean current strength and direction according to variability in space and time (Albretsen, 2019). These hydrodynamic ocean models are typically based on basic physical laws called primitive equations, which are simplified understandings of the physical laws that apply to flow fields in the atmosphere and oceans (Albretsen, 2019). These equations are typically computationally demanding and could require access to high-performance computers (Albretsen, 2019). Lagrangian ocean transport models utilize flow fields from hydrodynamic simulations to estimate the transportation of

trajectories in the marine environment. The two models can be combined to provide estimations of dispersion of particles, such as radionuclides, in the marine environment.

The utility of ^{129}I and ^{236}U as oceanographic tracers has been proven in research conducted by several authors, including (Wefing et al., 2021), (Casacuberta et al., 2018) and (Christl et al., 2015a). However, previous studies tend not to consider source separation, and instead assume that the North Sea functions as a single mixed source of ^{129}I and ^{236}U from nuclear reprocessing plants (Christl et al., 2015a). Thus, there seems to be an opportunity to improve and employ more detailed source terms. Ocean models could provide the source separation to improve the source term, and retrieve information about transportation pathways and source origin of ^{129}I and ^{236}U discharges that would have been impossible to obtain by only concentration measurements. Therefore, these models would need to be validated to ensure the predictions are within acceptable ranges of uncertainty. In addition, a recent study suggests that a significant amount of the broadly assumed conservative ^{236}U is initially retained in the bottom sediment after discharge releases (Periáñez et al., 2023). Therefore, this modeling project also aims to evaluate potential ^{236}U retention in the Irish Sea.

Objectives and hypothesis

The main aim of this project was to investigate if ^{236}U behaves as a conservative tracer which can be assumed to have similar mobility as ^{129}I in the marine environment. To achieve the main objective, the source terms of ^{129}I and ^{236}U from Sellafield and La Hague were separated and reconstructed. This included setting up a model, running simulations and validating the model with observational data based on own analysis and literature research. Then, the behavior of ^{129}I and ^{236}U could be evaluated to determine if these radionuclides behave similarly, based on comparisons between model outputs and observations. More specifically, the objectives of the thesis were:

- O_1: To update source terms of ^{129}I and ^{236}U from Sellafield and La Hague.
- O_2: Literature research to provide observational data for validation of the marine transport model.
- O_3: Radiochemical separations and AMS-analysis to obtain observational data in marine areas where there is a lack of data.
- O_4: Validate a marine transport model by comparing model outputs and observational data with respect to concentrations and isotope ratios of ^{129}I.
- O_5: Evaluate if a conservative behavior can also be assumed for ^{236}U.

Hypothesis

This project aims to evaluate the use of ^{129}I and ^{236}U as oceanographic tracers in combination with marine transport modeling. More specifically, we use a Lagrangian model to estimate ^{129}I and ^{236}U concentrations and $^{129}I/^{236}U$ ratios as well as particle age, and compare the model outputs with observations at various locations. We also evaluate the impact of the retention of ^{236}U in the Irish Sea. The following three hypotheses were set up to investigate this:

- H_1: The Lagrangian particles from Sellafield releases are older than those released from La Hague within the modeling area.
- H_2: The model concentrations of ^{129}I and ^{236}U, as well as $^{129}I/^{236}U$ isotope ratios are more in agreement with the observations closer to the discharge sources than further away.
- H_3: A significant amount of ^{236}U discharged to the environment from the Sellafield reprocessing plant is retained in Irish Sea sediments affecting the transport.

To investigate and test hypothesis 1 (H_1), a Lagrangian transport model was utilized. The model input was the documented discharges from Sellafield and La Hague, as well as ocean currents from a hydrodynamic model. Time series of the modeled ages at different locations were extracted from the transport estimates of ^{129}I and ^{236}U released from the two sources Sellafield and La Hague.

To test hypothesis 2 (H_2), the model will estimate ^{129}I and ^{236}U concentrations as well as $^{129}I/^{236}U$ ratios through simulations. The resulting model concentrations are then compared to observed concentrations from several locations with various distances away from the discharge sources. The comparison will be visualized as time series plots, to compare concentrations at several locations at different dates.

To test hypothesis 3 (H_3), the estimated model concentrations of ^{236}U will be compared to ^{236}U observations, within all model locations, including the Irish Sea and the Norwegian Sea. In addition, the estimated $^{129}I/^{236}U$ ratio used for model validation will also be compared to corresponding observations. Since the ocean model assumed a conservative behavior of ^{236}U, potential discrepancies between model estimations and observations could provide an evaluation of ^{236}U retention.

2 Background

2.1 Sources of ^{129}I and ^{236}U in the Marine Environment

Radionuclides in the marine environment can be of both natural- or anthropogenic origin. Natural sources of radionuclides include cosmic radiation from the sun and outer space and terrestrial radiation from the crust of the Earth (U.S.NRC, 2020). Sources of anthropogenic radionuclides in the marine environment include global fallout from atmospheric weapon testing and nuclear accidents like the Chernobyl Accident, as well as waterborne discharges from nuclear reprocessing plants (IAEA, 2012). The nuclear fuel cycle processes are also sources of anthropogenic radionuclides to the marine environment. These processes include ore extraction and enrichment, fuel fabrication, electricity generation in a nuclear reactor, storage and reprocessing of spent nuclear fuel before nuclear waste disposal (Costa Peluzo & Kraka, 2022).

Trace ^{129}I levels exist in the natural environment due to spontaneous fission from cosmic ray reactions. However, ^{129}I is primarily formed during the fission of uranium- and plutonium isotopes in nuclear reactors. The main sources of ^{129}I are nuclear reprocessing plants, nuclear weapon testing and major nuclear accidents (Raisbeck & Yiou, 1999). The half-life of ^{129}I is 16.1 million years (Be et al., 2004), making it persistent in the marine environment. The release of ^{129}I from nuclear-related activities has increased the ocean inventory of ^{129}I by more than one order of magnitude (Raisbeck & Yiou, 1999). The long half-life and the conservative behavior of the released ^{129}I cause bioaccumulation in marine food chains and thereby long-term ecological effects (Snyder et al., 2010). The non-fissile nature combined with the long half-life, make ^{129}I a waste product that must be thoroughly considered during waste management of spent nuclear fuel from nuclear reprocessing plants.

Natural uranium consists primarily of ^{238}U (99.3%), ^{235}U (0.72%) and ^{234}U (0.005%) (Steier et al., 2008). The abundance of ^{235}U in natural uranium has resulted in natural production of ^{236}U through neutron capture reactions (Steier et al., 2008). However, ^{236}U is primarily an intermediate product during fission reactions of ^{235}U in nuclear reactors. With a half-life of 23.43 million years (Be et al., 2008), ^{236}U is considered a long-lived anthropogenic waste product of nuclear fission. The discharge of ^{236}U to the marine environment primarily originates from waste management and storage of nuclear waste products, especially related to nuclear reprocessing of spent fuel.

Nuclear reprocessing is a process that involves recovery of reusable fissile material from spent nuclear fuel. Spent nuclear fuel from nuclear reactors is transported to nuclear reprocessing plants where fissile materials, such as plutonium- and uranium isotopes, are extracted and separated from the waste product. Nuclear reprocessing was historically developed to recover plutonium for nuclear weapons and for reuse of uranium. However, the primary motivation of nuclear reprocessing became to contribute to economic growth and as a resource for waste management in relation to energy production (WNA, 2020). Sellafield and La Hague are two nuclear reprocessing plants which have

contributed significantly to radionuclide discharges to the marine environment. The dominating radionuclides discharged from these reprocessing plants include ^{3}H, ^{137}Cs, ^{99}Tc, ^{106}Rb, ^{125}Sb, $^{239,240}Pu$, ^{129}I, ^{236}U and ^{14}C (Simonsen, 2019).

The Sellafield site, formerly known as Windscale, began nuclear operations in the 1950s (Forwood, 2008). Nuclear reprocessing has been the dominant form of handling spent nuclear fuel from nuclear reactors and has been carried out on a commercial scale at the Sellafield site since 1952 (IAEA, 2005). Sellafield was initially utilized to separate plutonium as part of the military program, but as civil nuclear power usage expanded, the reprocessing plant was more focused on nuclear fuel recycling and resource utilization (IAEA, 2005). The Sellafield site has had several nuclear reprocessing plants for managing spent nuclear fuel types since initial operations. The first nuclear reprocessing plant operating between 1952 and 1964 was the B204, which reprocessed uranium metal fuel from atomic piles (IAEA, 2005). Since several nuclear power stations in the UK began utilizing Magnox fuel (primarily natural uranium), the B205 nuclear reprocessing plant was developed and constructed to reprocess this fuel type (IAEA, 2005). Following the need to reprocess oxide fuels, permission to construct a Thermal Oxide Reprocessing Plant (THORP) was granted in the 1970s and Thorp became operational in 1994 (IAEA, 2005). The nuclear reprocessing at Sellafield recently came to an end in 2022, but Sellafield is still operational for cleanup and decommissioning (GOV.UK, 2022).

Nuclear reprocessing in Marcoule initially operated to provide plutonium for nuclear weapon and military purposes from 1958 (Schneider & Marignac, 2008). After providing plutonium for military purposes, a new vision regarding plutonium separation for civilian purposes emerged, resulting in the opening of the La Hague plant in 1966 (Schneider & Marignac, 2008). The La Hague site consisted of two main nuclear reprocessing plants, the UP2 and the UP3. The UP2 was developed in 1966, and reprocessed fuel from gas-cooled graphite reactors (GGR) and was later developed to reprocess light water reactor (LWR) fuel as well (Schneider & Marignac, 2008). The UP3 was developed in 1989, and largely financialized by Japan and Italy to reprocess their spent nuclear fuel due to nuclear waste management limitations in these countries (Schneider & Marignac, 2008).

2.2 Radionuclide Contaminants as Ocean Tracers

Radionuclides in the marine environment can be utilized to investigate marine processes, such as ocean circulation patterns and contamination dispersion by being used as ocean tracers. Since marine processes are generally relatively slow, radionuclides with long half-lives could be beneficial as tracers. The long half-life indicates that the radionuclide will remain present and radioactive in the marine environment for long periods. Mass spectrometric measurement techniques will be able to measure trace concentrations of the radionuclide tracers in low-volume seawater samples. Radionuclides from anthropogenic sources are also somewhat documented and widely distributed across the oceans. Discharges of radionuclides from nuclear reprocessing plants are often considered

valuable ocean tracers because measurements of these radionuclides can typically be traced back to the originating source. This is possible due to known isotope ratios of releases and well-established ocean circulation patterns.

General circulation patterns affect the transportation pathways of radionuclide tracers from Sellafield and La Hague. The main, known ocean currents and flow directions in the model area are schematically presented in *Figure 1*. The dominating pathway for Sellafield trajectories is northwards through the North Channel and into the North Sea (Orre et al., 2007). The contaminants from Sellafield are mixed with La Hague contaminants, that pass through the English Channel, in the southeastern North Sea and Skagerrak (Orre et al., 2007). The Norwegian Coastal Current (NCC) is important for the transport of water masses, including radionuclide tracers, from the North Sea and Skagerrak into the Barents Sea (BS) and the Arctic Ocean, west of Svalbard (Orre et al., 2007). The water masses from the Atlantic currents dilute the water masses and the radionuclide concentrations from the North Sea along the Norwegian coast.

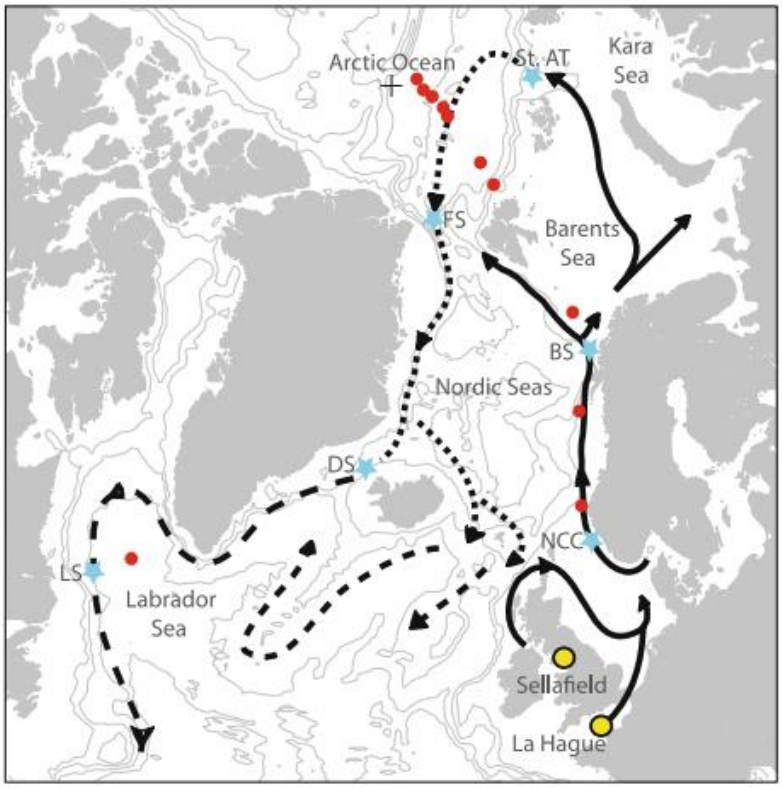

Figure 1: Schematic illustration of the main ocean circulation pathways affecting the transport of radionuclide discharges from Sellafield and La Hague. The solid line indicates transport mainly at surface levels, while the dashed line indicates surface- and deeper layer transport. Red dots mark the locations of ^{129}I observations and blue stars mark different sampling stations. Figure derived from (Orre et al., 2010). Simulating transport of ^{129}I and idealized tracers in the northern North Atlantic Ocean.

Radionuclides in the marine environment can be present in different physico-chemical forms called species, which affect properties and how effectively the radionuclide functions as oceanographic

tracers. Radionuclide species are "varying in size (nominal molecular mass), charge properties and valance, oxidation state, structure and morphology, density, degree of complexation, etc" (Salbu, 2009). The speciation of a radionuclide is considered dynamic, meaning it can be affected by the external environment and transform over time (Salbu, 2009). Radionuclide species of high molecular mass (HMM) tend to settle to bottom sediments due to gravitational forces, while low molecular mass (LMM) species are significantly more mobile and bioavailable in the marine environment. Colloidal species are defined as entities with diameters ranging from 1 nm to 0.45 µm, and do not settle as easily in the ocean due to mutual repulsion and Brownian movements (Salbu, 2009). However, some colloidal species aggregate in mixing zones between fresh- and seawater, while the remaining colloids can be transported as effectively as LMM species in the open ocean (Simonsen et al., 2019). The speciation affects the conservative behavior of the radionuclide tracer. A suitable tracer should be conservative, and thereby remain suspended in the water phase in the marine environment. A non-conservative tracer would more likely undergo adsorption onto particles or bind to the bottom sediments, making it difficult to measure the analyte concentration in a seawater sample.

The two primarily anthropogenic radionuclides, ^{129}I and ^{236}U, are broadly considered well-suited ocean tracers. Concentrations of ^{129}I and ^{236}U in the marine environment are primarily a result of anthropogenic activities, indicating that measured concentrations have a high probability of originating from Sellafield or La Hague. These radionuclides have long half-lives, significant and documented discharges and are assumed to behave conservatively in the water phase. However, a recent study (Periáñez et al., 2023) utilizing a numerical model to simulate the dispersion of ^{236}U suggests that only 52% of the total releases from Sellafield and La Hague enter the Arctic Ocean (Periáñez et al., 2018). Previous studies (Casacuberta et al., 2018; Castrillejo et al., 2018; Christl et al., 2017) have all assumed conservative behavior of ^{236}U in the marine environment, while this new statement contradicts this assumption, suggesting that ^{236}U undergoes significant adsorption onto sediments.

The ^{129}I concentrations have historically been difficult to measure due to low abundance and the presence of the highly stable ^{127}I isotope in seawater. The low radioactivity levels of ^{129}I have made it difficult to detect and quantify with radiometric measurement techniques as well. The development of the AMS has made the measurements of ^{129}I with high sensitivity and low detection limits possible. This scientific advancement has made ^{129}I, in addition to ^{236}U, an important and widely used tracer of ocean transport.

2.3 Radiochemical Separations

The purpose of radiochemical separations is to separate the radionuclides of interest from other stable or unstable elements to obtain maximum yield and purity (Trautmann et al., 2022). Radiochemical separation is especially important as pretreatment before measuring with the highly sensitive accelerator mass spectrometer as the working concentrations are trace. Even the smallest of

contaminations or interferences at these trace levels could greatly affect the measurements of the analytes.

2.3.1 Separation of ^{236}U

Since ^{236}U is not naturally abundant in seawater, and is only released from anthropogenic nuclear sources, the concentrations are very low. The trace concentrations of ^{236}U make it difficult to detect with mass spectrometric methods. To be able to measure ultra-low ^{236}U concentrations with the AMS, there is a need for sample preparation and radiochemical separation. The purpose of the separation is to remove possible isotopic interferences that might be present in the samples. A major challenge with AMS measurements of ^{236}U is to remove interferences of scattered ^{235}U and ^{238}U, as well as $^{235}UH^{3+}$ molecules (Christl et al., 2023).

A uranium separating process is illustrated in *Figure 2* and a more detailed procedure, developed at Institut de Radiophysique (IRA) can be seen in *Appendix A (Froidevaux, 2023a, 2023b)*. An iron carrier and ammonia are often added to the sample to produce a precipitate of iron- and uranium hydroxides. These precipitates are then centrifuged and washed to increase the purity of the uranium complexes, before being dissolved and treated with a UTEVA-resin. This resin is used to separate uranium from other matrix elements, such as thorium- and plutonium isotopes, based on the high affinity of uranium on this resin (Wang et al., 2021). After radiochemical separation, a high-purity sample powder is generally produced through precipitation and dissolution reactions, before drying and baking at high temperatures.

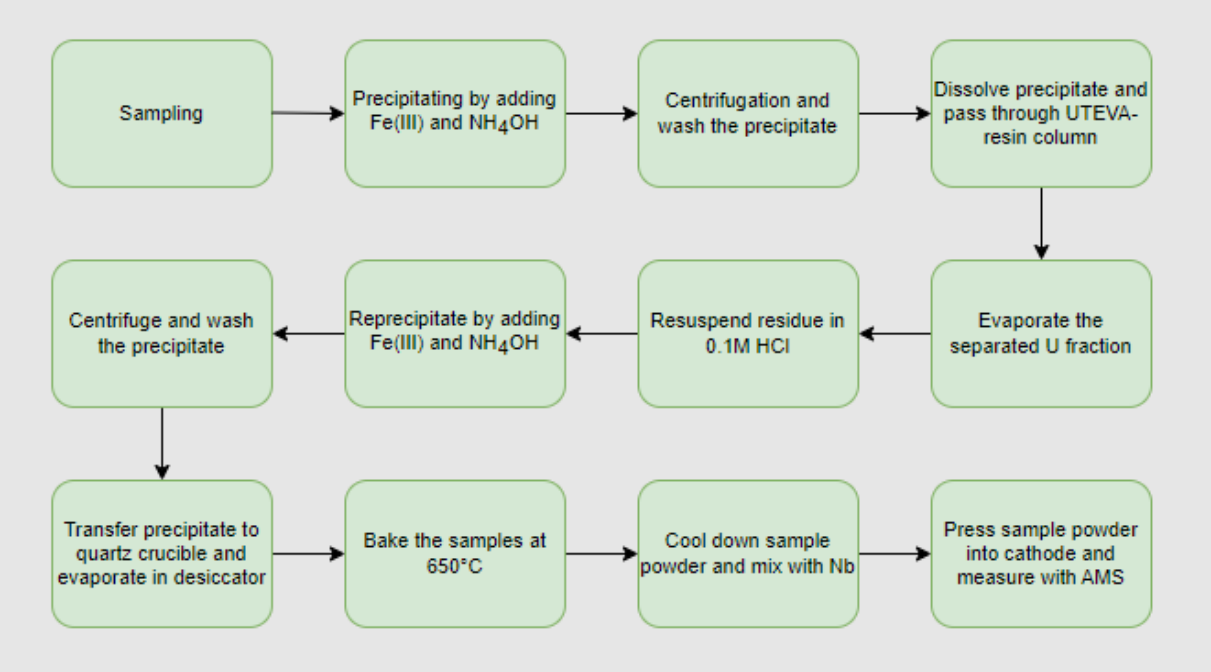

Figure 2: Flowchart illustrating a sample preparation process for uranium. From sampling to measurements with the accelerator mass spectrometer (AMS). Follow the marked arrows between the boxes for the correct step order.

2.3.2 Separation of ^{129}I

The overall purpose of ^{129}I separations is to maximize the chemical yield of the analyte through several extractions and back extractions, converting the chemical form of iodine between stable iodine (I_2) and iodide (I^-). To determine the final yield of the separation, a stable iodine carrier of known concentrations is typically added to the samples. The separation of ^{129}I in seawater samples is subjected to solvent extractions due to the highly soluble nature of molecular iodine (I_2) in nonpolar organic solvents (Thompson et al., 2023). Iodide (I^-) can be re-oxidized to I_2 by adding an oxidizing agent, like sodium nitrite ($NaNO_2$) to an acidic solution.

A summary of the iodine preparation and separation utilized in this study is illustrated in *Figure 3*, and a more detailed procedure, developed by Hou (DTU) and Mindová (CTU) can be seen in *Appendix B (Hou & Mindová, 2023)*. A stable iodine carrier is added to the sample, which is then subjected to a reducing agent to convert I_2 to I^-. The aqueous sample phase containing I^- is mixed with an organic solvent (chloroform) and an oxidizing agent to extract the I_2 to the organic phase. Then back extractions of the I_2 to I^- in the aqueous phase are conducted by adding a reducing agent.

Iodide is highly reactive, resulting in AgI (s) precipitates when adding silver nitrate ($AgNO_3$) to the I^- containing aqueous phase as illustrated by the following equation:

- $AgNO_3\,(aq) + I^-\,(aq) \rightleftharpoons AgI\,(s) + NO_3^-\,(aq)$

The resulting precipitate is washed and dried, and homogenously crushed into fine powder and pressed into an AMS cathode, ready for measurements.

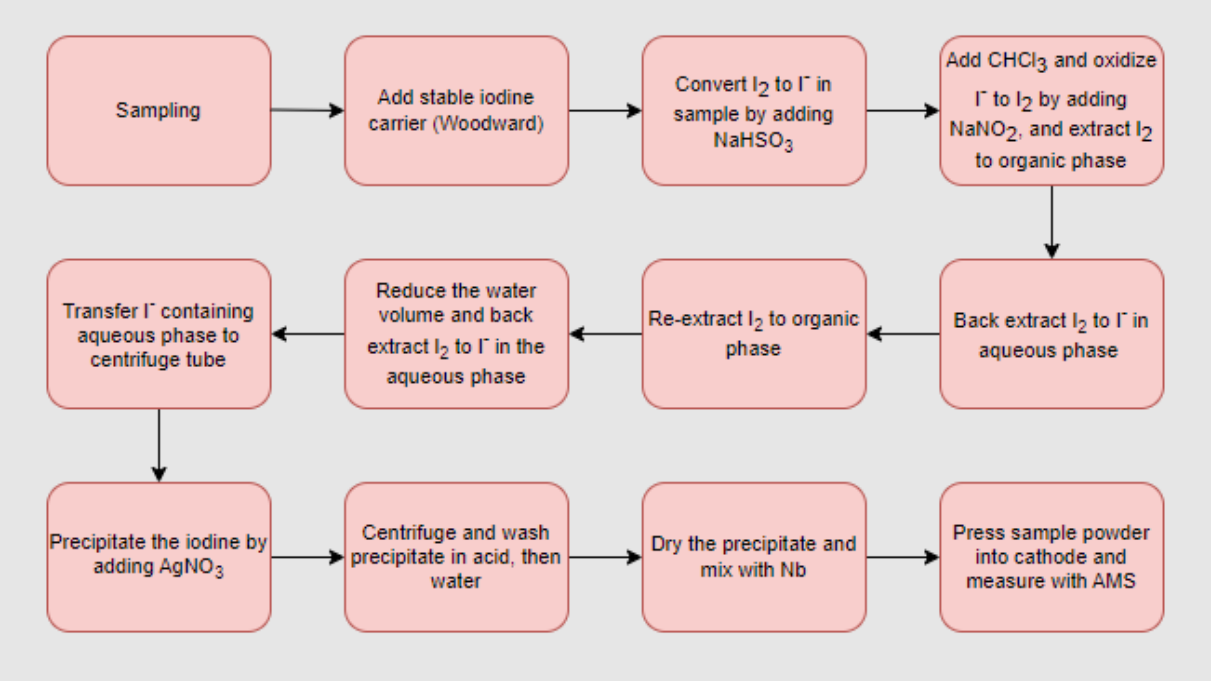

Figure 3: Flowchart illustrating a sample preparation process for iodine. From sampling to measurements with the accelerator mass spectrometer (AMS). Follow the marked arrows between the boxes for the correct step order.

2.4 Mass Spectrometric Methods

The two mass spectrometric measurement techniques utilized during this project were accelerator mass spectrometry (AMS) and inductively coupled plasma mass spectrometry (ICP-MS). The AMS typically has lower detection limits and higher sensitivity for long-lived isotopes, while the ICP-MS has high throughput and can simultaneously measure several elements.

2.4.1 Accelerator Mass Spectrometry

Accelerator Mass Spectrometry (AMS) is a mass spectrometric measurement technique that can measure, and separate different isotopes based on m/z-ratio. The AMS measurements can detect and quantify trace levels of analyte in low-volume samples, due to low detection limits and high sensitivities. The specific AMS system utilized during this study was the 1 MV AMS system at CNA in Seville, and a schematic illustration of the major components is presented in *Figure 4*.

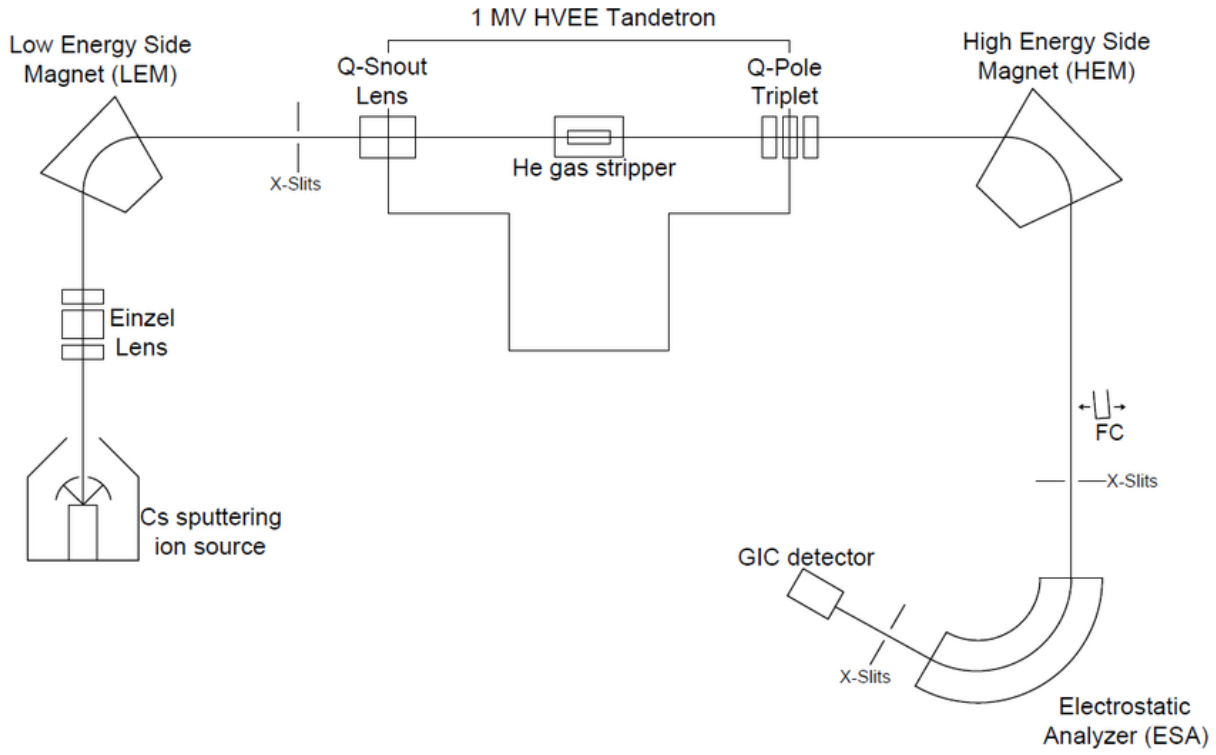

Figure 4: Schematic illustration of an accelerator mass spectrometer system and the major components. This specific AMS system was the 1 MV AMS system at CNA in Seville utilized for measurements in this project. Figure derived from Vivo-Vilches, C. (2018). ^{41}Ca measurements with Low Energy Accelerator Mass Spectrometry (LEAMS) at the Centro Nacional de Aceleradores.

The AMS system utilizes a Cs-sputtering ion source to ionize the samples. The ion source provides Cs^+ ions in the form of a vapor, so collisions between the solid sample powder and Cs^+-source causes the sample to ionize. The interaction causes the sample to "sputter" atoms from the sample surface, and a negatively charged beam, containing the atoms, continues through the AMS-system. After Cs-sputtering, the ion beam is refocused by the Einzel lens before it hits a low-energy magnet (LEM) (Vivo-Vilches, 2018). The purpose of the LEM is to bend the pathways of the negative ion beam, separating isotopes based on m/z-ratio. The bent ion beam will pass through an electrode (Q-Snout) to increase the energies of the incoming ions (Vivo-Vilches, 2018), before the ion beam enters the 1 MV HVEE Tandetron.

The ion beam accelerates to higher energies through a vacuum insulated high voltage Tandetron accelerator, and into the high-energy end of the AMS system. Helium gas is fed to the ion beam in the accelerator, where electrons are stripped off. This converts the negative ions in the beam to positively charged ions, for example $^{129}I^-$ to $^{129}I^{5+}$ and disintegrates molecular isobars (Lehto & Hou, 2010). The accelerated ion beam hits the quadrupole triplet for further mass separation and optimal focusing of the ion of interest. The accelerated ion beam strikes the high energy magnet (HEM) to bend and separate the ions in the beam based on differences in m/z ratio. The ion beam then strikes the surfaces of the Faraday cups with a specific electrical charge for different isotopes. The charge is measured as an

electrical current, and the magnitude of this current is proportional to the number of specific ions that struck the detector within a set timeframe. The ion beam passes the high-energy electrostatic analyzer (ESA), which consists of electrodes at different voltages (Vivo-Vilches, 2018). This creates an electric field and causes the beam to follow a curved trajectory (Vivo-Vilches, 2018). The ion beam is introduced to the gas ionization chamber (GIC) detector, where the ion beam is ionized. The ionization causes releases of electrons which are driven to the anode by the electric field, causing signals of the measured ions (Vivo-Vilches, 2018).

2.4.2 Inductively Coupled Plasma Mass Spectrometry

Inductively coupled plasma mass spectrometry (ICP-MS) is a mass spectrometric technique utilized to measure the abundance and elemental composition of environmental- and biological samples. ICP-MS is a multielement determination technique and can be used to measure several isotopes simultaneously at trace levels. The elements are separated and measured based on their mass-to-charge ratio (m/z). This allows for beneficial measurements and separation of isotopes of the same element. The major components of the ICP-MS are illustrated in *Figure 5*.

The samples are introduced to the spray chamber, through a nebulizer, by a peristaltic pump. The nebulizer serves the purpose of converting the samples to fine aerosol particles, and selectively filter out larger particles (Wilschefski & Baxter, 2019). The samples will then be transported into a plasma torch, ionizing the sample to a high-energy ion beam due to the high temperature of the argon gas present in the torch. The ICP-MS instrument consists of ion lenses that focus and guide the ion beam into the quadrupole mass analyzer (Wilschefski & Baxter, 2019). The different isotopes in the ion beam are filtered based on the mass-to-charge ratio (m/z) by the quadrupole mass analyzer. The separated ion signals strike the electron multiplier (EM) detector, which cumulates signal pulses and detects them as ion counts per second (CPS) (Mazarakioti et al., 2022).

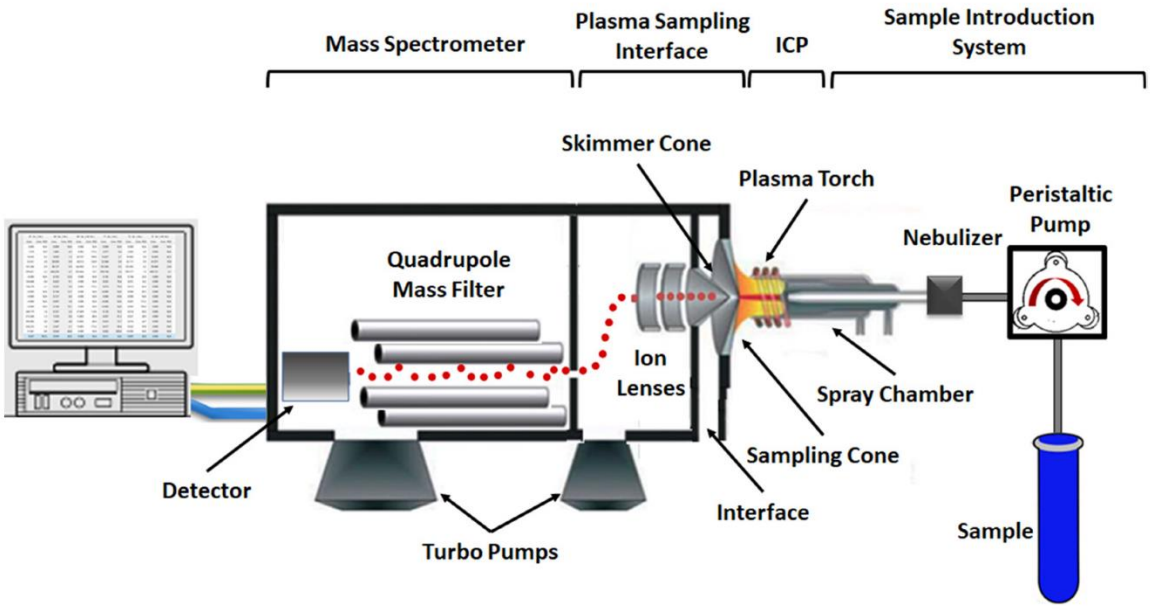

Figure 5: Schematic illustration of an inductively coupled plasma mass spectrometer system and major components. Figure derived from Mazarakioti, E. C., Zotos, A., Thomatou, A.-A., Kontogeorgos, A., Patakas, A., & Ladavos, A. (2022). Inductively Coupled Plasma-Mass Spectrometry (ICP-MS), a Useful Tool in Authenticity of Agricultural Products' and Foods' Origin.

2.5 Modeling of Radionuclide Transport in the Marine Environment

Hydrodynamic ocean models can simulate oceanic processes such as ocean currents, tidal waters and sedimentation. Ocean transport models can in combination with hydrodynamic ocean models be able to predict behavior and changes in the continuous ocean state. Transport models use flow fields from the hydrodynamic ocean model to predict the transport of trajectories. The three main types of radionuclide transport models are box-models, Eulerian models and Lagrangian models (Periáñez et al., 2019). Box models divide the marine area into interconnected boxes, and assume uniform and instantaneous mixing of radionuclides within each box (Periáñez et al., 2019). Eulerian models utilize differential equations to give temporal and spatial evolution of the radionuclides in different states (Periáñez et al., 2019). While the Lagrangian model utilizes several trajectories representing an equivalent number of radionuclides (Periáñez et al., 2019).

Ocean transport models of radionuclides can be valuable in supporting decision-making risk following nuclear accidents. Transport models are especially useful in the emergency phase after a nuclear accident in a coastal facility (Periáñez & Cortés, 2023). The models could contribute to protecting both man- and ecosystems from ionizing radiation following a nuclear accident. Therefore, the development of adequately accurate transport models is necessary to fast-respond to emergency situations, and to reduce the potential harmful effects following ionization (Duffa et al., 2016). The purpose and motivation for using ocean models with radionuclide discharges as model input lies in the need for more accurate, high-resolution oceanographic transport models. Ocean models are valuable

tools during nuclear emergencies and as a part of nuclear preparedness, and in conjunction with releases of toxic pollutants or discharges of radionuclides. Ocean models could also provide valuable information when predicting the state of ocean currents, and to see potential changes in the ocean current patterns. Changing ocean currents is a climate change indicator (EPA, 2023), and by validating accurate and efficient ocean models, better understanding and predictions about the continuously changing climate can be achieved.

2.5.1 Lagrangian Approach

In this study, the ocean transport model in the project is based on a Lagrangian approach. This approach implements large sets of virtual particles integrated within a model area over a selected time period (Sebille et al., 2018). The virtual particles for this research represent the radionuclides ^{236}U and ^{129}I discharged from Sellafield and La Hague. However, a Lagrangian particle does not directly correspond to a physical radionuclide particle. Every single Lagrangian particle can have unique properties and be regarded as a possible pathway of a water mass initiated at a specific position and time. Since every trajectory has unique properties and acts independently of the other trajectories, the model will not calculate the exact concentrations of the radionuclides. Instead, concentrations can be derived from this density of trajectories within a volume during a selected time period, and can be presented as time series or a map of the changing model concentrations over time.

To validate the Lagrangian model, documented discharge data of radionuclides are necessary to compare the model simulations to actual dispersion scenarios. During model simulations of this research, relatively well-documented- and estimated discharges of ^{129}I and ^{236}U have been identified at Sellafield and La Hague nuclear reprocessing plants. These discharges were primarily annual estimations from a reconstructed input function (Christl et al., 2015b). However, the annual estimated discharges were converted to monthly discharges to get sufficient temporal variability in the ocean model.

2.5.2 OpenDrift

OpenDrift is an open-source Python-based framework utilized for Lagrangian particle modeling developed by the Norwegian Meteorological Institute (MET) (Dagestad et al., 2018). OpenDrift is generic and considered a “framework” rather than an actual trajectory model (Dagestad & Hope, 2020). The generic approach of OpenDrift makes it useful in modeling various kinds of drifting ocean particles, offering great flexibility and multipurpose.

Modules within the OpenDrift framework correspond to traditional trajectory models, and modules for oil drift, search-and-rescue, a basic module for atmospheric drift and a high-resolution aluminum transport model (Simonsen et al., 2023) have already been developed (Dagestad et al., 2018). OpenDrift is designed with focus on performance, and even simulations of millions of trajectories could run and perform on a standard laptop (Dagestad et al., 2018). The OpenDrift design is rather

generic and performance-focused, but also robust and in daily operational use for emergency preparedness at the Norwegian Meteorological Institute (Dagestad et al., 2018).

2.5.3 Applications of Ocean Modeling

Environmental monitoring and measurements are valuable tools for risk assessments and understanding the behavior of contaminants in the environment. However, the combination of observational data and transport models is complementary regarding risk assessment and the fate of radionuclides in the environment. The use of transport models provides additional beneficial properties, including the provision of estimates for locations and times in which observational data are unavailable, predicting future transport and process investigation (Simonsen, 2019).

3 Materials and Methods

3.1 Sampling Location Area

The Norwegian Sea is considered a part of the North Atlantic Ocean, and covers an area of approximately 250,000 km^2 (Henriksen et al., 2005) and reaches depths of 3,970 m (Britannica, 2024). Literature research for ^{129}I and ^{236}U observations within the model area revealed scarce sampling points in the Norwegian Sea.

A total of 20 seawater samples, 10 x 5 L samples and 10 x 1 L samples, were collected by The Institute of Marine Research (IMR) between April and May 2023. The samples were collected from six different sampling stations in the Norwegian Sea (*Figure 6*) as part of a G.O. Sars cruise. Samples from the stations were collected at surface level and depth, and additional sample details are presented in *Table 1*.

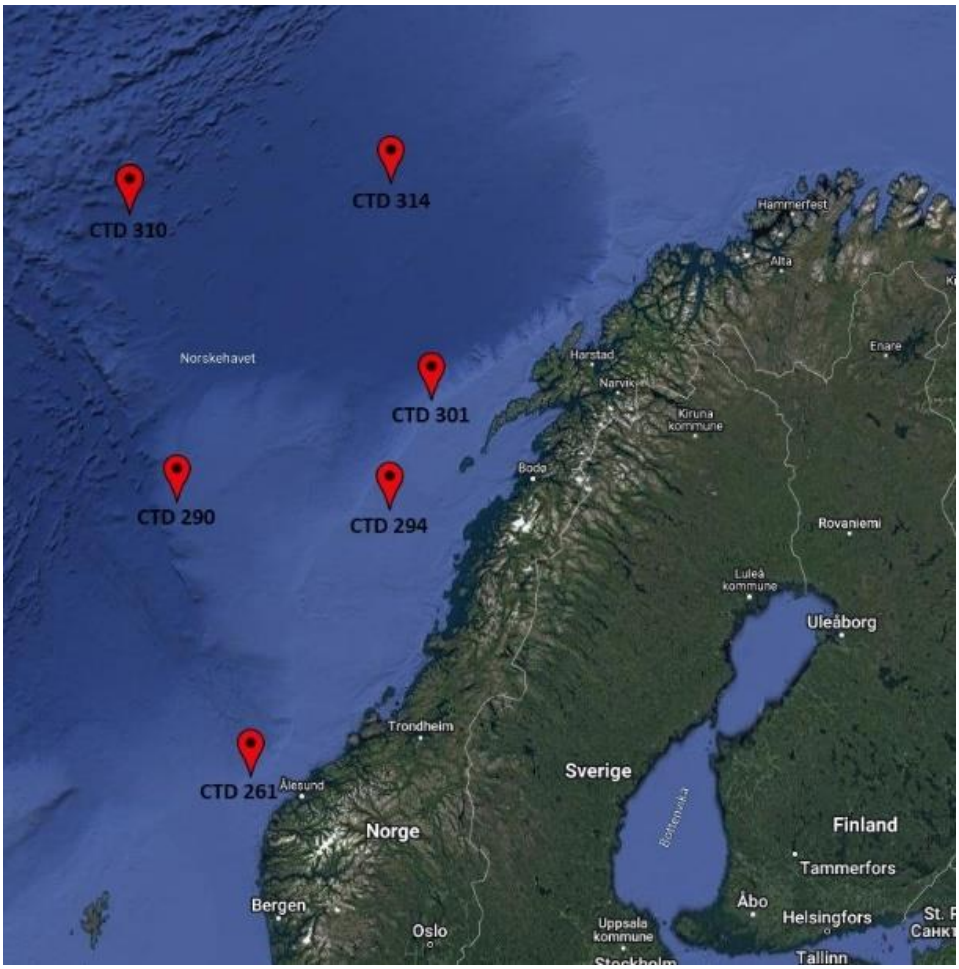

Figure 6: Map of the six sampling stations in the Norwegian Sea where samples for this research were collected. Each of the six stations (CTD261, CTD290, CTD294, CTD301, CTD310 and CTD314) is marked as a red pin. The Institute of Marine Research collected twenty seawater samples from these stations.

Table 1: Number of samples collected, coordinates and depth levels (m) for each sampling station.

Station	Number of Samples	Latitude (N)	Longitude (E)	Sampling Depth (m)
CTD 261	2	62.7718	4.3663	5
CTD 261	2	62.7718	4.3663	319
CTD 290	2	66.9385	1.7300	5
CTD 290	2	66.9385	1.7300	400
CTD 294	2	66.8345	9.3355	5
CTD 294	2	66.8345	9.3355	326
CTD 301	2	68.3150	10.7918	5
CTD 301	2	68.3150	10.7918	646
CTD 310	2	70.6392	0.0097	5
CTD 314	2	70.9970	9.3575	5

3.2 Radiochemical Separations of ^{129}I

The laboratory work conducted during this project included sample preparation of iodine from seawater samples. Radiochemical separation techniques utilized during sample preparation included filtrations, centrifugations and liquid extractions. The sample preparation of ^{129}I was performed at CTU, and the conducted procedure, developed by Hou (DTU) and Mindová (CTU), is found in *Appendix B* (Hou & Mindová, 2023). The resulting dry and homogenous sample powder was shipped to Centro Nacional de Aceleradores (CNA) in Seville for AMS measurements.

A total of 10 samples (1b-10b) and 1 blank were prepared. Each sample contained 1 L seawater, and an aliquot of 100 mL per sample was processed for measurements. The aliquot of 100 mL was poured into a weighed glass beaker, which was reweighed to obtain both volumetric and gravimetric measurements. To the beaker, 1 mL of stable I_2 carrier solution (Woodward iodine), with a known low amount $^{129}I/^{127}I$ of 2.0×10^{-14} (Niello Fernández et al., 2013) was added. The iodine carrier was added in a concentration of 2.0 mg stable iodine carrier per 100 mL sample to determine the chemical yield. The beaker was reweighed to acquire the added mass of the carrier, and then 1 mL of 0.5M $K_2S_2O_5$ and 2.5 mL of 3M HNO_3 were added and stirred in the beaker with a glass rod. The pH of the solution was measured to ensure a pH between 1-2, and pH values beyond this range were adjusted by additional 3M HNO_3. This solution was left for at least 5 min to convert the iodine (I_2) to iodide (I^-).

The solution was transferred to a 250 mL separation funnel, and 10 mL of $CHCl_3$ was added. The aqueous- and organic phases were mixed before 0.5 mL of 1M $NaNO_2$ was added to oxidize I^- to I_2. The I_2 was extracted into the organic phase and turned pink after mixing (*Figure 7*).

Figure 7: Extraction of I_2 to the organic phase in a separation funnel. The upper phase in the funnel is the aqueous phase and the organic phase is the bottom phase. The pink color in the organic phase indicates the presence of I_2 due to the phase extraction of I_2. Photo: J. Lauritsen.

The organic phase was separated and collected in a clean beaker. New portions of 10 mL $CHCl_3$ were added to repeat the extractions three times to ensure collection of the remaining I_2. Before the last extraction, 5 drops of 3M HNO_3 and 1 drop of 1M $NaNO_2$ were added to ensure an optimal surrounding environment of low pH and enough oxidizing agent in the solution. The organic phase lost the pink color, indicating complete extraction of I_2 (*Figure 8*).

Figure 8: Separation of the pink I_2 organic phase to the beaker. The remaining organic phase in the funnel (bottom) became transparent, indicating complete separation of I_2 to the beaker. Photo: J. Lauritsen.

The organic phase in the beaker was transferred to a new 100 mL separation funnel, together with 25 mL ultrapure water (18 MΩcm) and 1 drop of 0.5 M $K_2S_2O_5$, to back extract and reduce the iodine from I_2 to I^- in the aqueous phase. The phases were mixed and watched for at least 2 minutes, to ensure sufficient reducing agent ($K_2S_2O_5$) for the reaction. The reduction reactions were completed when both phases became colorless (*Figure 9*), and the organic phase was discarded into a waste beaker.

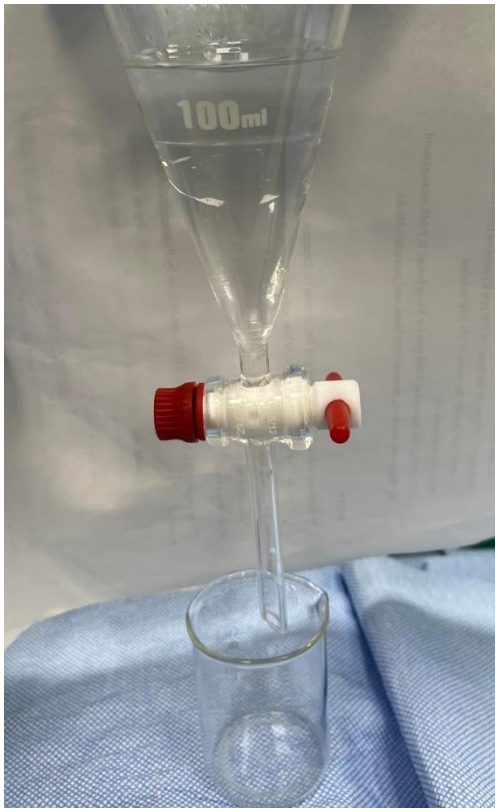

Figure 9: Back extraction of I_2 from the bottom organic phase to I^- in the upper aqueous phase. The colorless appearances indicate a complete reduction reaction of I_2 to I^-, which is transparent in the upper aqueous phase. Photo: J. Lauritsen.

After discarding the organic phase, a new portion of 10 mL $CHCl_3$, 5 drops of 3M HNO_3 and 1 drop of 1M $NaNO_2$ were added to the aqueous phase to re-extract the I^- to I_2 to the organic phase. The organic phase became pink due to I_2, and was collected in a beaker. The extractions were repeated until the pink color had completely disappeared, combining the organic phases from all extractions.

The combined organic phases were transferred to a new separation funnel, and 2.5mL of ultrapure water (18 MΩcm) and 1 drop of 0.5M $K_2S_2O_5$ were added to repeat the back extraction of I_2 to I^- into the aqueous phase. The organic phase was discarded into a waste beaker when both phases were colorless. The low-volume aqueous phase was transferred to a 15 mL centrifuge tube, and the separation funnel was cleaned with 2 x 3 mL ultrapure water added to the same centrifuge tube. To the centrifuge tube, 1 mL of 3M HNO_3 and 1 mL of 1M $AgNO_3$ were added. The reaction caused the formation of AgI precipitate, which was centrifuged at 3500 rpm for 3 min. The samples were washed several times, first with 1 mL 3M HNO_3, then 3 x 3 mL ultrapure water. The precipitate was agitated with a Pasteur pipette between each centrifugation and transferred into a weighed 1.5 mL Eppendorf tube following the final wash. The Eppendorf tube was centrifuged once with a smaller centrifuge at 4000 rpm for 3 minutes. The excess water was removed, and the precipitate was put in a drying cabinet. The dried and solid AgI (s) sample powder was shipped to CNA in Seville for the final part of

the preparation and AMS measurements. The solid sample powder was mixed with niobium (Nb) by Jose Maria López-Gutiérrez at CNA in Seville to obtain a fine homogeneous sample mix before being measured with the AMS.

The AMS measurements provided $^{129}I/^{127}I$ ratios in the samples which had to be converted to numbers of ^{129}I atoms, through ^{129}I concentrations (atoms/l), to be used as observations for the model validation. The ^{127}I concentrations (µg/l) of the samples were measured with three parallels for each sample by the ICP-MS for the conversions. Additional details regarding the conversion process and calculation can be found in *Section 4.2* and *Appendix E*.

3.3 Model Configuration

All model simulations and post processing in this project was conducted with an Asus VivoBook equipped with an Intel(R.) Core(TM.) i5-82658U CPU processor and Windows 11. The configuration of model parameters is crucial for achieving the desired outputs to test research questions and hypothesis. A big part of modeling is continuously changing and optimizing these parameters through trial and error, and several adjustments were made throughout this modeling project. This chapter describes how the OpenDrift model was set up and the most important parameters of both the run- and post-processing scripts are presented. The overall and generalized summary of the model setup is described in six major steps in *Figure 10* below.

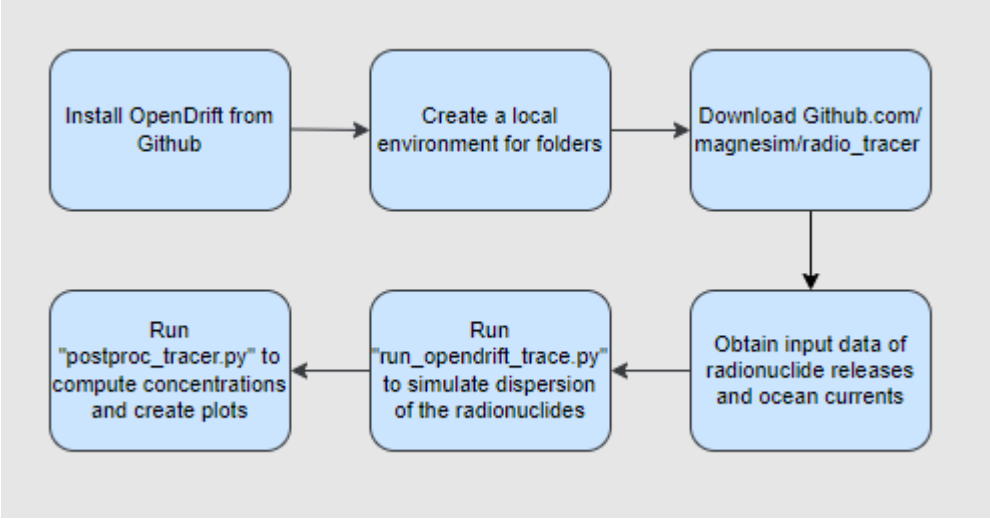

Figure 10: Flowchart illustrating the modeling setup process. From installation of the OpenDrift model to final runs of the post processing scripts. Follow the marked arrows between the boxes for the correct step order.

3.3.1 Model Simulation

The model simulation was set up for a period of 30 years, from 01.01.1993 to 01.10.2023. Due to the long simulation time, the total number of trajectories was set to 200,000. These model trajectories were split into two groups (one from Sellafield and one from La Hague) of 100,000, evenly distributed

throughout the model simulation. The number of trajectories is important to improve the predictability of ocean transport, and also make the model more susceptible to capture the natural variability in the ocean.

The model calculates a new position for each model particle for each time step. The time step for the model was set to four hours. The increments of the trajectories in the model are based on ocean current data retrieved from the Copernicus Marine Service database (Copernicus, 2023). This dataset has a spatial resolution of 0.083° x 0.083° and a daily/monthly temporal resolution (Copernicus, 2023). The spatial extent of the dataset covers the global ocean, with latitudes ranging from -80° to 90° and longitudes from -180° to 179.92° (Copernicus, 2023). This database contains important dynamic ocean variables like temperature, currents and salinity, which change over time. Therefore, it is important to continuously retrieve this information during the model simulation period, to accurately predict the transportation of trajectories. Printing every timestep and generating large volumes of data is not always necessary for post processing. The timestep output during this model simulation was set to 3600*240, indicating every 10^{th} day. This decision was based on the time period for the simulation and to reduce excessive storage consumption.

Another important decision was to determine the initial point release location of the trajectories in the model. The trajectories represented the discharges of ^{129}I and ^{236}U from Sellafield and La Hague, so the chosen locations were close to the shore by the two nuclear reprocessing plants (*Figure 11*). The trajectories were deployed at a random depth between 0-10 m and in a radius of 1000 m of the chosen location.

Figure 11: Map of Sellafield location (north orange marker) and La Hague location (south orange marker), as well as the corresponding release point of model trajectories from the two discharge sources during the model simulation (black markers). Sellafield release point was set at 54.357N -3.9232E and La Hauge release point was set at 49.744N and -2.05.

Trajectories transported outside the northern area limits at 80.1N and eastern area limits at 26.0E during the model simulation were deactivated. The deactivation was conducted to maintain focus on the specific area of interest and to reduce computational resources. The model simulation operated for about 200 hours, while gradually increasing the size of the generated file to a final 28.4 GB ready for post processing. The GitHub-link to the model simulation script is located in *Appendix C*.

3.3.2 Post Processing

Following the model simulation, the generated data was subjected to post processing to analyze the model output. The post processing produced several plots and time series of concentrations, isotope ratios and model age trajectories.

The main principle of a Lagrangian approach is to convert trajectories to concentrations. The model area was divided into grids with pixel sizes of 40 km x 40 km. The pixel size needs to be refined since too large grids can dampen variations while too small grids can cause much noise. The concentrations were calculated by the number of trajectories within each grid and time step, and divided by volume. In addition, each trajectory was assigned a weighting factor depending on the time of the model release compared to the documented discharge used as model input. Trajectories released at a time of

high discharge from the source were assigned a higher weighting factor compared to trajectories released during lower discharges.

The model filtered out trajectories below 20 m, indicating that the model concentrations are based on the trajectories present at [0-20m] depth interval. This interval was determined by viewing the vertical distributions of trajectories at various locations, and the trajectories were primarily found at these depth levels. In addition to depth filtration, latitude and longitude limitations were set to analyze specific areas of interest within the model area.

The model concentrations were compared to several observations of ^{129}I and ^{236}U concentrations from the literature as well as measurements of this study, aiming to validate the model. The observations were included in the figures of time series from the model, making it easy to compare them to model concentrations at specific positions.

To see differences in model concentrations, $^{129}I/^{236}U$ ratios, source contribution and model particle age, model data was extracted from nine locations. An important aspect when determining the box locations was the inclusion of at least one comparative observation data point for model validation. The boxes should have various distances from the sources and be a certain size to obtain homogenous water masses within one box. The chosen boxes analyzed during this research were the English Channel, the Irish Sea, the North Sea (South, East and North), the Norwegian Sea, the Barents Sea, Fram Strait and Komsomolets (*Figure 12*).

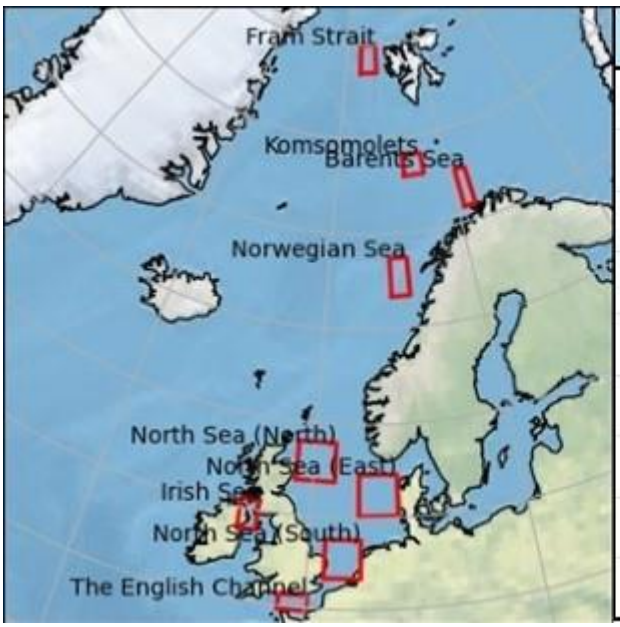

Location	Lon 1	Lon 2	Lat 1	Lat 2
The English Channel	-2.20	0.18	49.83	50.66
The Irish Sea	-6.50	-4.80	53.90	55.53
North Sea (South)	1.50	4.60	51.70	53.80
North Sea (East)	4.40	8.10	55.10	57.30
North Sea (North)	-1.70	2.10	56.90	59.00
Norwegian Sea	8.55	11.00	66.71	68.69
Barents Sea	21.10	22.90	70.80	72.80
Fram Strait	3.80	8.00	78.50	80.00
Komsomolets	12.07	15.50	72.96	74.04

Figure 12: Map of the analyzed model locations. The nine locations are marked as red boxes, and the corresponding coordinates for each box are presented next to the map.

The post processing could be utilized and optimized based on what model outputs were beneficial in the context of this research. The start- and end date within the model simulation time could be adjusted during post processing, aiming to look at model concentrations and ages within a specific timeframe. Another possibility during post-processing was to close in on one or more specific boxes for further analysis and insight into the obtained model data. The GitHub-link to the post processing script is presented in *Appendix C*.

4 Results and Discussion

4.1 Literature Data for Model Validation

Model validations are important to ensure model reliability in estimating real-world processes and strengthen the confidence of decision-making. During this project, an extensive literature review was initiated to provide observational data needed for the marine transport model validation. In recent years, ^{129}I and ^{236}U have proven very useful as radionuclide tracers of ocean transport (Christl et al., 2015a; Daraoui et al., 2016; Wefing et al., 2021). The literature research provided useful observations mainly in the North Atlantic Ocean, Barents Sea and Fram Strait. Most common were observations of ^{129}I, but samples measured for ^{129}I and ^{236}U simultaneously were found at some locations in the North and Barents Seas. However, additional samples were needed to compare and validate the ocean transport model for areas between the Irish Sea and the Barents Sea. Further literature data from (Christl et al., 2015a), (Daraoui et al., 2016) and (Wefing et al., 2021) provided additional observations in the North Sea and Fram Strait. In addition, seawater samples collected from the vicinity of the sunken nuclear submarine, Komsomolets (K278), as part of still unpublished research by the Institute of Marine Research (IMR), the Norwegian Radiation and Nuclear Safety Authority (DSA) and the Norwegian University of Life Sciences (NMBU) were used as additional observations for model validation (Heldal et al., 2024). Information regarding Komsomolets and the specific sampling location is found in *Appendix D*. The summary of observations used for validating the model is presented in *Table 2*, sorted by model location, year of sampling and reference to the literature where the observations were acquired.

Table 2: Literature observations used for model validation. The number of observations, years of sampling, measured radionuclide(s) and the literature reference for all locations are highlighted. The observations in the Norwegian Sea were measured as a part of this project.

Location	Number of Observations	Year	Radionuclide(s)	References
The Irish Sea	3	2012	^{129}I	(Vivo-Vilches et al., 2018)
The English Channel	11	2009	$^{129}I + ^{236}U$	(Christl et al., 2015a; Daraoui et al., 2016)
North Sea (South)	18	2009	$^{129}I + ^{236}U$	(Christl et al., 2015a; Daraoui et al., 2016)
North Sea (East)	17	2009	$^{129}I + ^{236}U$	(Christl et al., 2015a; Daraoui et al., 2016)
North Sea (North)	11	2009	$^{129}I + ^{236}U$	(Christl et al., 2015a; Daraoui et al., 2016)
Norwegian Sea	2	2023	^{129}I	This study (2024)
Barents Sea	8	2015	$^{129}I + ^{236}U$	(Castrillejo et al., 2018)
Fram Strait	1	2021	^{236}U	(Wefing et al., 2021)

Komsomolets	3	2019 + 2023	$^{129}I + ^{236}U$	(Heldal et al., 2024)

The literature review revealed a lack of ^{129}I and ^{236}U observations in the Norwegian Sea, and to obtain comparable observation data for the transport model, additional sampling points were needed. Through collaboration with IMR, twenty additional samples from various locations in the Norwegian Sea were collected and made available for the present project (*Figure 6*). The samples were subjected to radiochemical separations and mass spectrometric analyses to fill some of the data gaps.

4.2 Results from Mass Spectrometric Methods

Results from the ICP-MS and AMS measurements, including standard deviations (1σ) and relative standard deviations (%), from the Norwegian Sea samples are presented in *Table 3*. The ^{127}I concentrations (µg/l) of the samples were measured with the ICP-MS technique, as well as three blank parallels which showed no background signals. The ten samples were measured with three parallels, and the average ^{127}I concentrations (µg/l) for samples 1-10 varied between 47.4 to 55.1 µg/l and are presented in *Table 3*. The SD (1σ) range for each sample was between 0.06 and 0.43, and the relative standard deviations between the three parallels for every sample were less than 1%. All measurements of ^{127}I were above the limit of detection (LOD) of 0.16 and the limit of quantification (LOQ) of 0.52. The $^{129}I/^{127}I$ ratios for the ten samples were measured with the AMS technique, along with one blank sample measured to 9.0 (± 2.7) x 10^{-14}. Sample 3 was measured with two parallels yielding similar $^{129}I/^{127}I$ ratios of 2.8 (± 0.31) x 10^{-11} and 2.9 (± 0.30) x 10^{-11}. The average concentration of sample 3 is presented in *Table 3*, together with the measured $^{129}I/^{127}I$ ratios for the remaining samples.

The ^{129}I concentrations (atoms/l) obtained based on a combination of AMS ($^{129}I/^{127}I$) and ICP-MS (^{127}I) measurements are also presented in *Table 3*, and a detailed table with raw data for all sample masses and measurements used for the conversion is found in *Appendix E*.

Table 3: Results based on ICP-MS and AMS analyses. The average measured concentration of ^{127}I (µg/l) from three parallels by the ICP-MS and the measured $^{129}I/^{127}I$ ratio from the AMS for the 10 samples are presented together with standard deviations (SD) and relative standard deviation (RSD). The resulting concentrations of ^{129}I (atoms/l) from the conversion of the ICP-MS and AMS results are also presented.

	ICP-MS			AMS			Conversion to ^{129}I		
Sample	**^{127}I (µg/l)**	**SD (1σ)**	**RSD (%)**	**$^{129}I/^{127}I$**	**SD (1σ)**	**RSD (%)**	**^{129}I (atoms/l)**	**SD (1σ)**	**RSD (%)**
1	50.4	0.27	0.53%	3.9×10^{-10}	0.11×10^{-10}	2.8%	3.5×10^{10}	0.11×10^{10}	3.1%
2	52.9	0.38	0.71%	7.5×10^{-12}	0.082×10^{-12}	1.1%	7.7×10^{8}	0.13×10^{8}	1.7%
3	53.5	0.32	0.60%	2.8×10^{-11}	0.30×10^{-11}	11.0%	2.6×10^{9}	0.29×10^{9}	11.0%
4	55.1	0.43	0.77%	8.8×10^{-12}	0.14×10^{-12}	1.6%	8.4×10^{8}	0.17×10^{8}	2.0%
5	47.4	0.06	0.12%	6.5×10^{-11}	0.18×10^{-11}	2.8%	6.2×10^{9}	0.18×10^{9}	2.9%
6	52.4	0.18	0.34%	1.0×10^{-11}	0.013×10^{-11}	1.3%	9.8×10^{8}	0.16×10^{8}	1.6%
7	51.3	0.25	0.49%	7.6×10^{-11}	0.38×10^{-11}	5.0%	7.2×10^{9}	0.37×10^{9}	5.1%
8	53.4	0.11	0.21%	6.4×10^{-12}	0.17×10^{-12}	2.7%	6.3×10^{8}	0.18×10^{8}	2.9%
9	53.6	0.08	0.15%	1.3×10^{-11}	0.030×10^{-11}	2.3%	1.3×10^{9}	0.032×10^{9}	2.5%
10	54.4	0.27	0.49%	1.5×10^{-11}	0.023×10^{-11}	1.5%	1.4×10^{9}	0.027×10^{9}	1.9%

The concentrations of ^{129}I in seawater samples at all sampling stations in the Norwegian Sea varied between 0.63 x 10^9 and 35.0 x 10^9 atoms/l. These concentrations are higher than the one previously measured ^{129}I concentration (0.13 x 10^9 atoms/l) reported in the Norwegian Sea at surface level in 2012 (Vivo-Vilches et al., 2018). However, previous measurements sampled in 2015 in the southwestern part of the Barents Sea ranged between 5.1 to 17.1 x 10^9 (Casacuberta et al., 2018), overlapping with the measurements of this project.

The measured ^{129}I concentrations in the surface waters (1.3 to 35.0 x 10^9 atoms/l) were higher than the measured ^{129}I concentrations at depth (0.63 to 0.98 x10^9 atoms/l) for all sampling stations. The highest ^{129}I concentration of 35.0 x 10^9 atoms/l was seen at the sampling station furthest south in the Norwegian Sea at surface level (5m), while the sample collected at the deepest depth (646m) exhibited the lowest measured ^{129}I concentration of 0.63 x 10^9 atoms/l. The sampling stations in *Figure 13* are arranged from left to right according to distance to the Norwegian Coast, meaning station CTD 261 was closest to the coast and station CTD 310 was furthest from the coast. The ^{129}I concentrations in the surface waters (blue bars) decreased with increasing distance to the shore, as illustrated in *Figure 13* below.

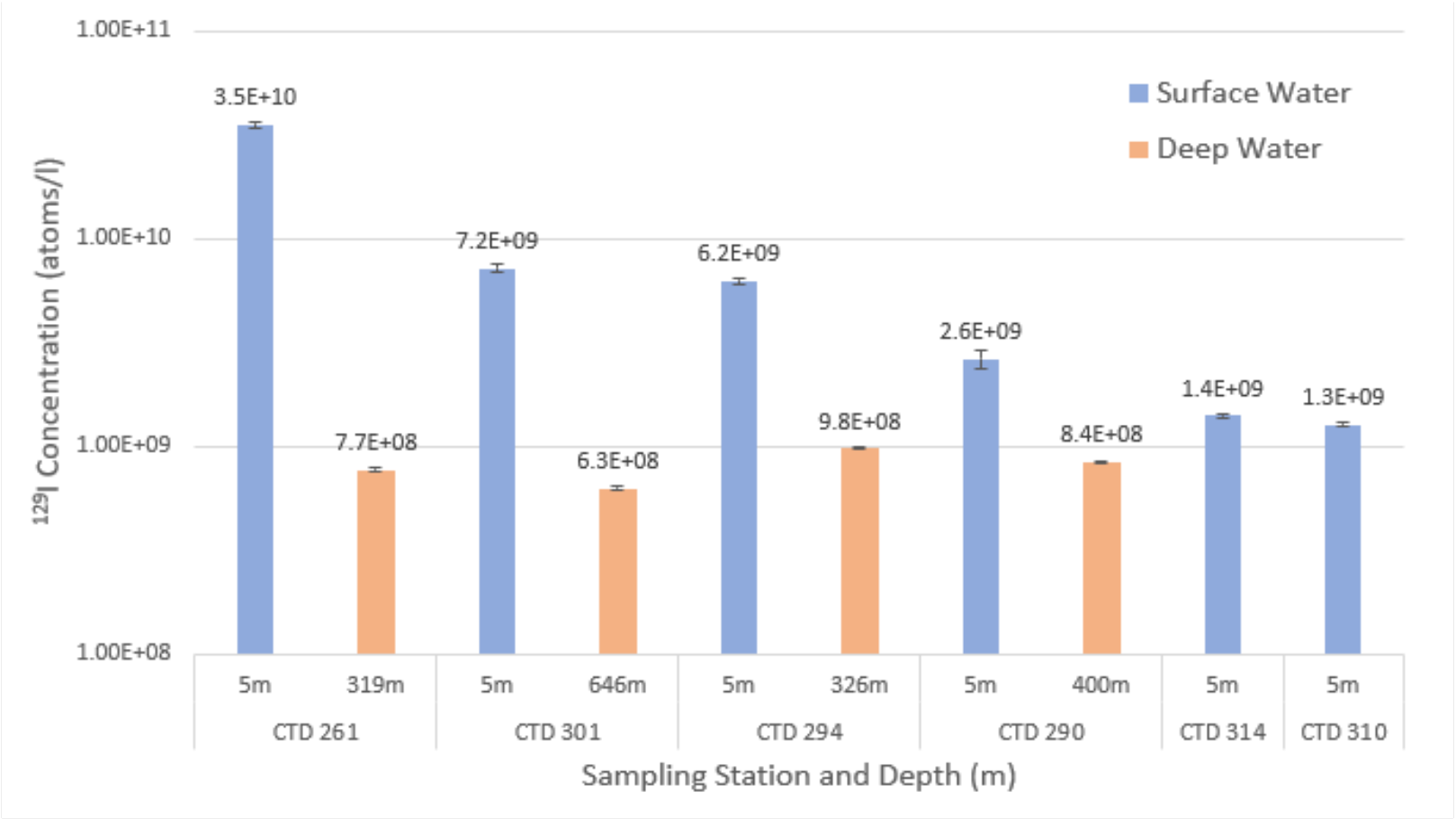

Figure 13: Measured ^{129}I concentrations (atoms/l) of samples collected from the six different sampling stations in the Norwegian Sea , including uncertainty bars (1σ). The sampling stations are arranged from left to right in order of increasing distance from the Norwegian coast. Station CTD 261, 290, 294, and 301 had samples collected at surface level at 5m (blue) and at depth (orange), while CTD 310 and 314 only had samples collected at surface level (5m

4.3 Documented Discharge Data as Model Input

OpenDrift utilized relatively well-documented discharge data as model input. Discharge data of ^{129}I and ^{236}U from Sellafield and La Hauge was gathered through published estimated data (Christl et al., 2015a; J.Gwynn, personal communication, January 9, 2024) and annual reports from Sellafield LTD (Sellafield, 2022) and Orano Group (Orano, 2022). Discharge data from several sources was gathered, but even after extensive research, the data remained incomplete. This caused the need to extrapolate the missing data of ^{129}I and ^{236}U from both Sellafield and La Hague.

Particularly, the discharge data of ^{236}U was quite difficult to gather. Information on historical ^{236}U discharges is sparse and not well-published, although the total annual uranium (kg) is more accessible (Christl et al., 2015b). The Sellafield discharge data are heavily based on estimations derived from a publication where modeling was utilized to reconstruct the discharge data of ^{236}U from Sellafield and La Hague (Christl et al., 2015b). The estimations provided annual concentrations of ^{236}U from Sellafield from 1952 until 2013 and La Hague from 1966 to 2012. Annual ^{129}I concentrations were provided for 1966 to 2012 from Sellafield and 1966 to 2013 from La Hague. Since monthly discharge data was available for some parts of the simulated model period, all of the discharge data was entered into the model as monthly discharge. Periods with only annual discharges were converted to identical monthly discharges, seen in *Figure 15* from 1952-2006 by the flat lines, while the highly variable lines from 2007 onwards highlight discharge data with monthly variations.

Additional monthly discharge data provided by J.Gwynn (personal communication, January 9, 2024), was utilized from 2007 through 2019. Discharge data of uranium from Sellafield was provided as total uranium (kg), not ^{236}U concentrations. To convert the total uranium (kg) to ^{236}U atoms, an assumption that the total uranium (kg) consisted of only ^{238}U was made. The ^{238}U is the major radionuclide, but there is also ^{235}U abundant, especially in enriched uranium fuel utilized in nuclear reactors.

The reconstructed annual discharge of ^{236}U (kg) from the published study (Christl et al., 2015b) were divided by the annual total uranium (kg) provided by J.Gwynn (personal communication, January 9, 2024) for the years of 2007 to 2012. This resulted in $^{236}U/^{238}U$ ratios for each year, plotted in a diagram (*Figure 14*), revealing relatively similar $^{236}U/^{238}U$ ratios between 2007 and 2012. The average ratio was 3.52×10^{-3}, and this ratio was utilized to convert the total uranium (assumed to consist of only ^{238}U) to ^{236}U.

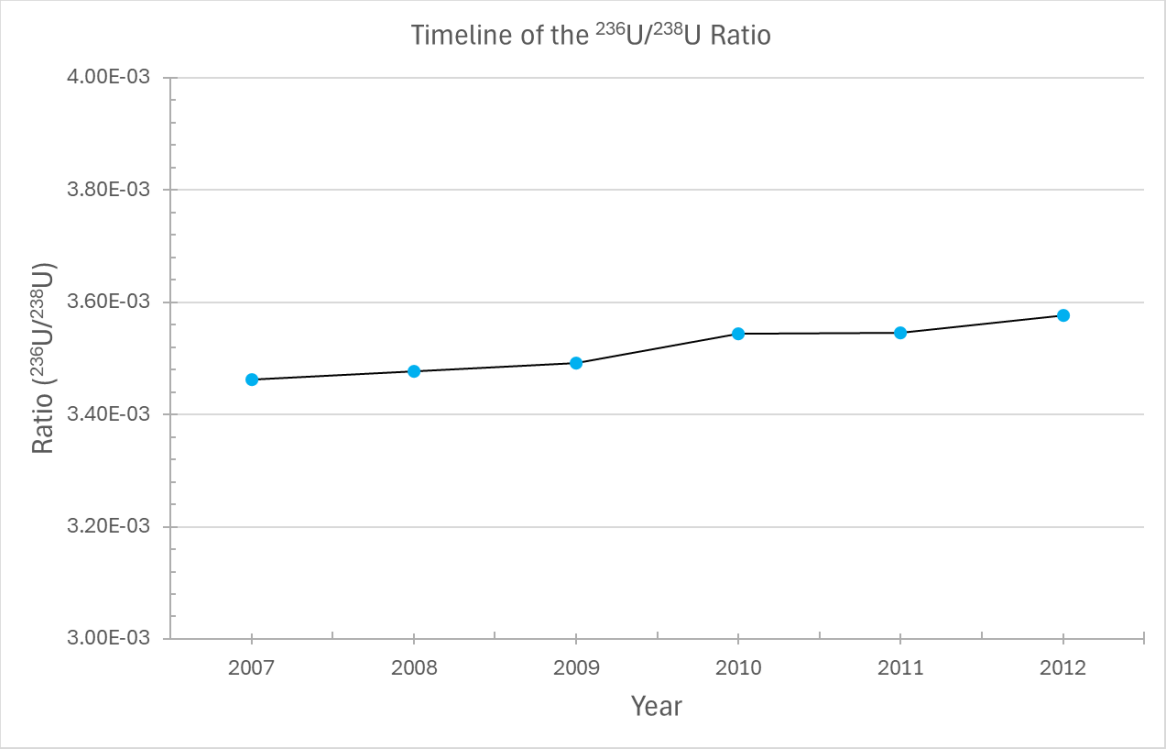

Figure 14: The average $^{236}U/^{238}U$ of the discharge data between 2007-2012. The ratio was derived from reconstructed estimates of ^{236}U (Christl et al., 2015b) and provided total uranium (assumed to consist of only ^{238}U) from J.Gwynn (personal communication, January 9, 2024). This ratio was utilized to convert total uranium to ^{236}U.

Extrapolations to fill the gaps of missing discharge data were conducted by observing general release trends in the published data to try and get as close to the actual discharges as possible. Especially discharge data from 2023 was not yet available through annual reports at the time of this project. The model utilized monthly discharge data as input, and in cases where only annual estimated discharges were provided, a conversion to monthly estimates was conducted. The resulting discharge data from documented discharges and extrapolations were visualized in diagrams. Diagrams of ^{236}U (*Figure 15*), ^{129}I (*Figure 16*) and the $^{129}I/^{236}U$ ratio (*Figure 17*) for Sellafield, La Hague and total were constructed to visualize how the monthly discharge varied over time. The diagrams display how ^{236}U discharged from Sellafield dominated after 1990, while ^{129}I discharges were dominated by La Hague. Only discharge data between 1993 and 2023 was used as input data for the model simulations.

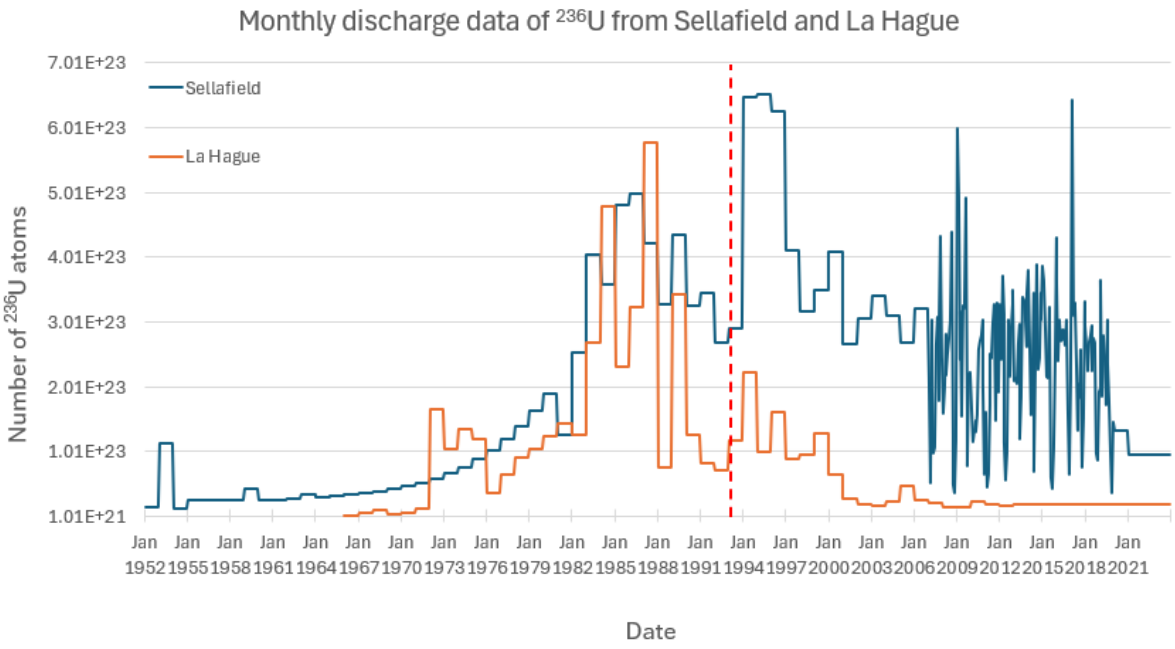

Figure 15: Monthly discharged ^{236}U atoms from Sellafield and La Hague from 1952-2023. The estimated ^{236}U discharges were provided from 1952 and onwards for Sellafield, and from 1966 and onwards for La Hague. The red dashed line marks the simulation starting period (January 1993), which was the discharge data used as model input.

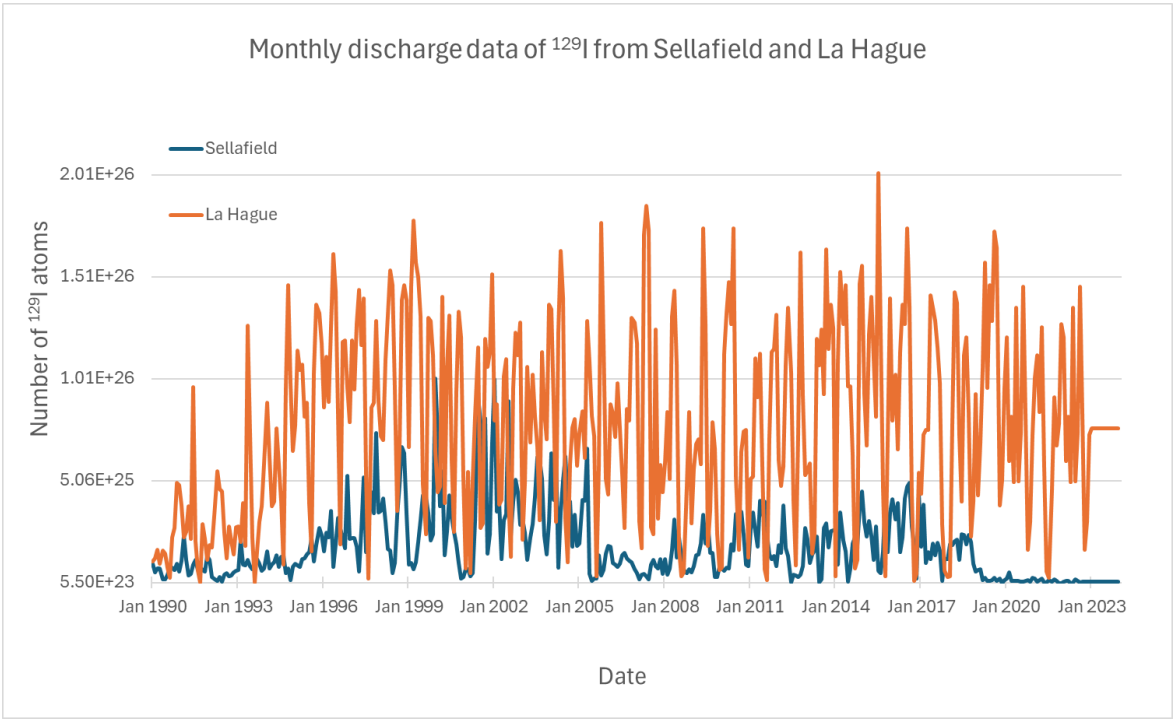

Figure 16: Monthly discharged ^{129}I atoms from Sellafield and La Hague from 1990-2023. Discharge data from 1993 to 2023 were used as model input during simulations.

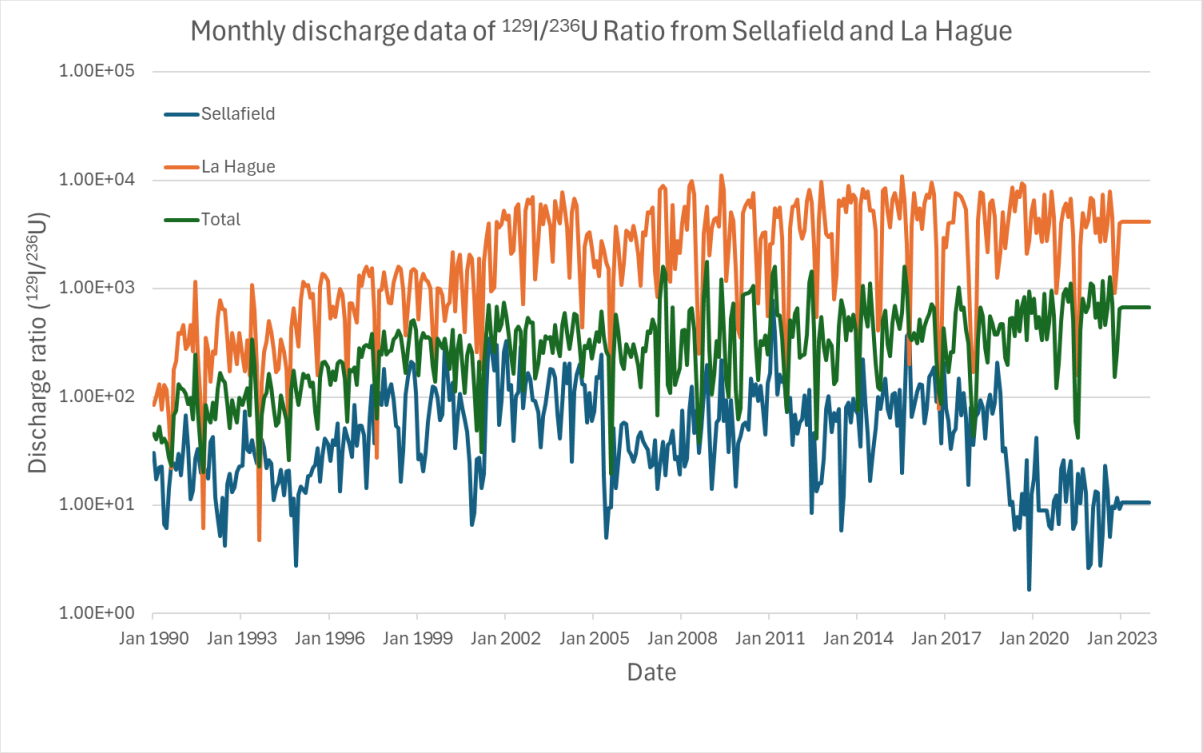

Figure 17: Monthly discharged $^{129}I/^{236}U$ ratio from Sellafield, La Hague and total. The total $^{129}I/^{236}U$ ratio is derived from ^{129}I from SF + LH divided by ^{236}U from SF + LH. Note the logarithmic y-axis.

4.4 Model Uncertainties and Limitations

Modeling is a method of calculating numbers that can be visualized and presented in a more comprehensive way than just raw numbers. Modeling is a great method of estimating and predicting the ocean transport of particles, but also has its limitations. Ocean transport models are generally simplifications of the actual real ocean processes, as the ocean is way more complex than described in the actual model. Even though the OpenDrift model used for this research is a simplification, the model complexity fits the purpose of this thesis.

The major model uncertainties of this project are related to the model input data. The input data of this model is mainly the hydrodynamic model and the documented discharge data from Sellafield and La Hague. Uncertainties are also related to flow fields which predict the processes through numerical calculations. These uncertainties arise from simplifications of complex processes, discretization in time and space and initial fields and boundary conditions. When utilizing radionuclide tracers from documented discharge data there will be uncertainties related to the source term. Inaccurate discharge estimations and parameterizations of unavailable data could lead to further uncertainties of the source terms. The uncertainties need to be reduced to improve the accuracy of the ocean transport estimates further. Validated transport models and continuous development of ocean transport models are essential for future modeling.

Limitations regarding source terms, radionuclide properties and oceanic parameters were decided for this project. The reasons for these limitations were to reduce the scope and run model simulations that aligned with the objectives and purpose of this thesis.

The utilized source term of this project was limited to the ^{129}I and ^{236}U discharges from the nuclear reprocessing plants, Sellafield and La Hague between 01.01.1993 and 01.10.2023. Therefore, discharges from Sellafield and La Hague before 1993 and other nuclear installations such as the Springfields nuclear fuel production facility, were neglected during model simulation. In addition, other major radionuclide sources like global fallout and discharge resulting from nuclear accidents were also disregarded.

The released trajectories of ^{129}I and ^{236}U from the nuclear reprocessing plants were assumed to have identical properties and behavior. In reality, the chemistries of iodine and uranium are different, and in research conducted by (Simonsen, 2019) the speciation of the radionuclides can greatly affect the model estimations. The trajectories of ^{236}U and ^{129}I were also assumed to be of completely conservative behavior, meaning the radionuclides will not be retained in the sediments or bind to other particles in the marine environment.

Tidal advection was also disregarded, resulting in estimation inaccuracies of the transport pathway of the model trajectories. By neglecting tidal advection, an increased number of trajectories were transported southwards of Sellafield and into the English Channel, while in reality more trajectories were transported northwards (Simonsen et al., 2017). The inclusion of tidal advection has been highlighted in the research of Simonsen (Simonsen et al., 2017), which concludes that the outflow from the Irish Sea and downstream activity concentration levels in remote areas are affected by the inclusion of tidal waters in the model (Simonsen et al., 2017).

4.5 Source Contribution of ^{129}I and ^{236}U from Sellafield and La Hague

A method of improving the source term of nuclear reprocessing discharge to the marine environment is to separate the radionuclide discharges from Sellafield and La Hague. Instead of assuming the radionuclide concentration as originating from one mixed source, the discharge could be separated between each source. The OpenDrift model which was utilized during this project was able to estimate the contribution from each of the two sources of ^{129}I and ^{236}U discharge in any part of the model domain.

The contributions of ^{129}I discharges from Sellafield (SF) and La Hague (LH) discharges can be seen from a [^{129}I] SF/ [^{129}I] LH ratio map (*Figure 18*). Based on this map, the contribution from LH discharges dominates most of the model domain, whereas the SF-derived ^{129}I dominates the Irish and Celtic Seas as well as the western parts of the North Seas. These contributions from SF and LH align with the known ocean circulation patterns and the northward transportation pathway from Sellafield as

seen in *Section 2.2*. A darker shade of red implies a higher ^{129}I discharge contribution from La Hague in contrast to ^{129}I from Sellafield. Even if the map (*Figure 18*) is mostly red, some lighter shades of blue can be observed around the UK. In these specific locations, the contribution of ^{129}I discharge is higher from Sellafield rather than La Hague. In between the red- and blue areas there is a layer of white, indicating a ratio of 1 (10^0) where the ^{129}I contribution to total concentration averaged over the simulation period is equal between Sellafield and La Hague.

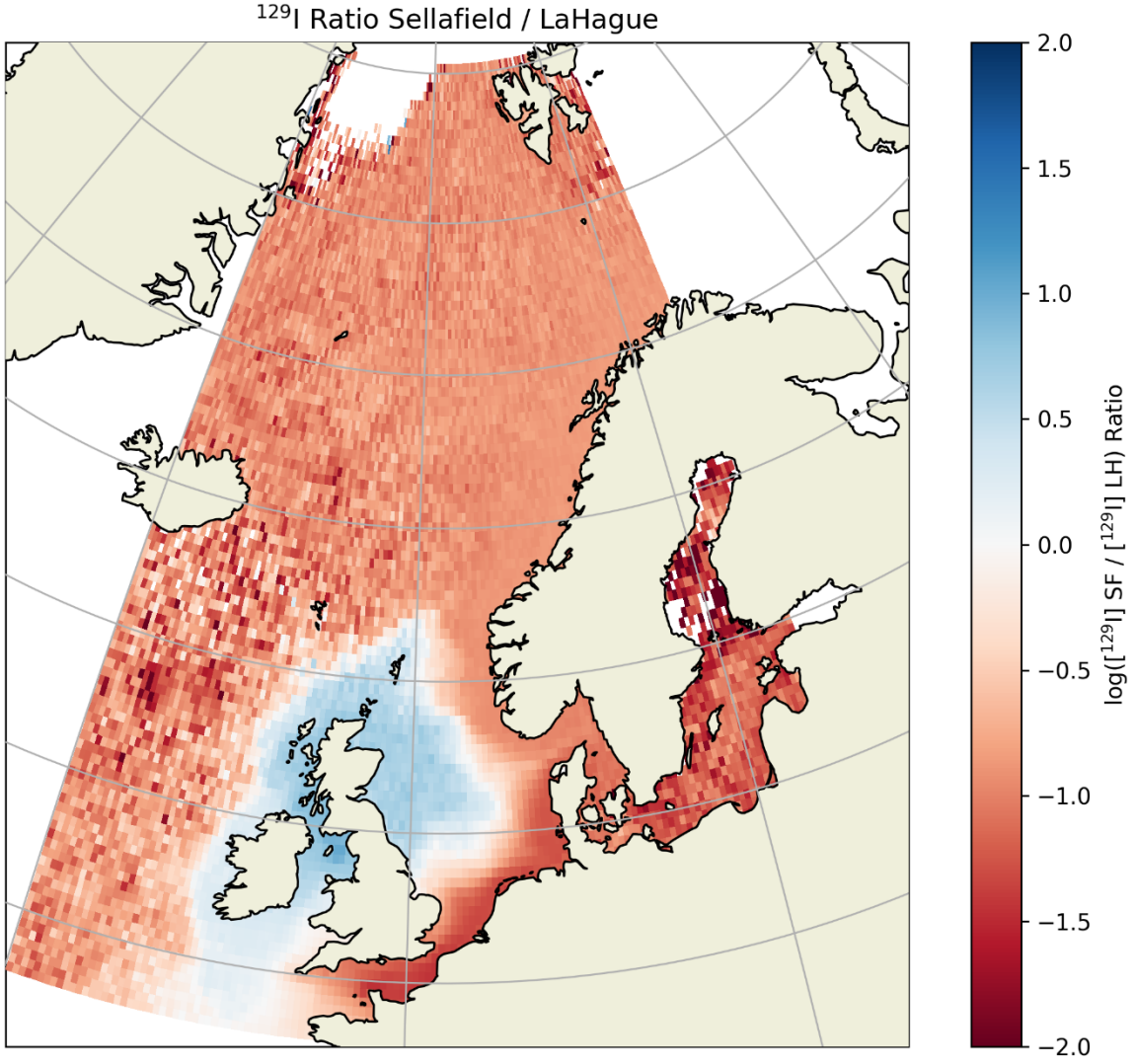

Figure 18: Map illustrating the estimated ^{129}I SF/ ^{129}I LH ratio. Red indicates a higher contribution from La Hague and blue indicates a higher contribution from Sellafield. The color scale represents the log[^{129}I] SF/[^{129}I] LH ratio from -2 to 2.

In contrast to the ^{129}I ratio between Sellafield and La Hague, the ^{236}U ratio is primarily blue, with an especially dark blue shade around the UK (*Figure 19*). This indicates that the modeled contribution of ^{236}U is generally higher for Sellafield compared to La Hague. In the English Channel right outside of La Hague, where you would expect higher ^{236}U contributions from La Hague there is a white area, indicating an even source contribution.

The model concentrations of ^{236}U in the Baltic Sea show minor red spots, implying that Sellafield is the major source contributor. However, this result is likely due to generally lower estimated model concentrations in this area, resulting in increased variability. The high variability in low-concentrated areas reduces the precision and reliability of the prediction, making it difficult to draw certain conclusions.

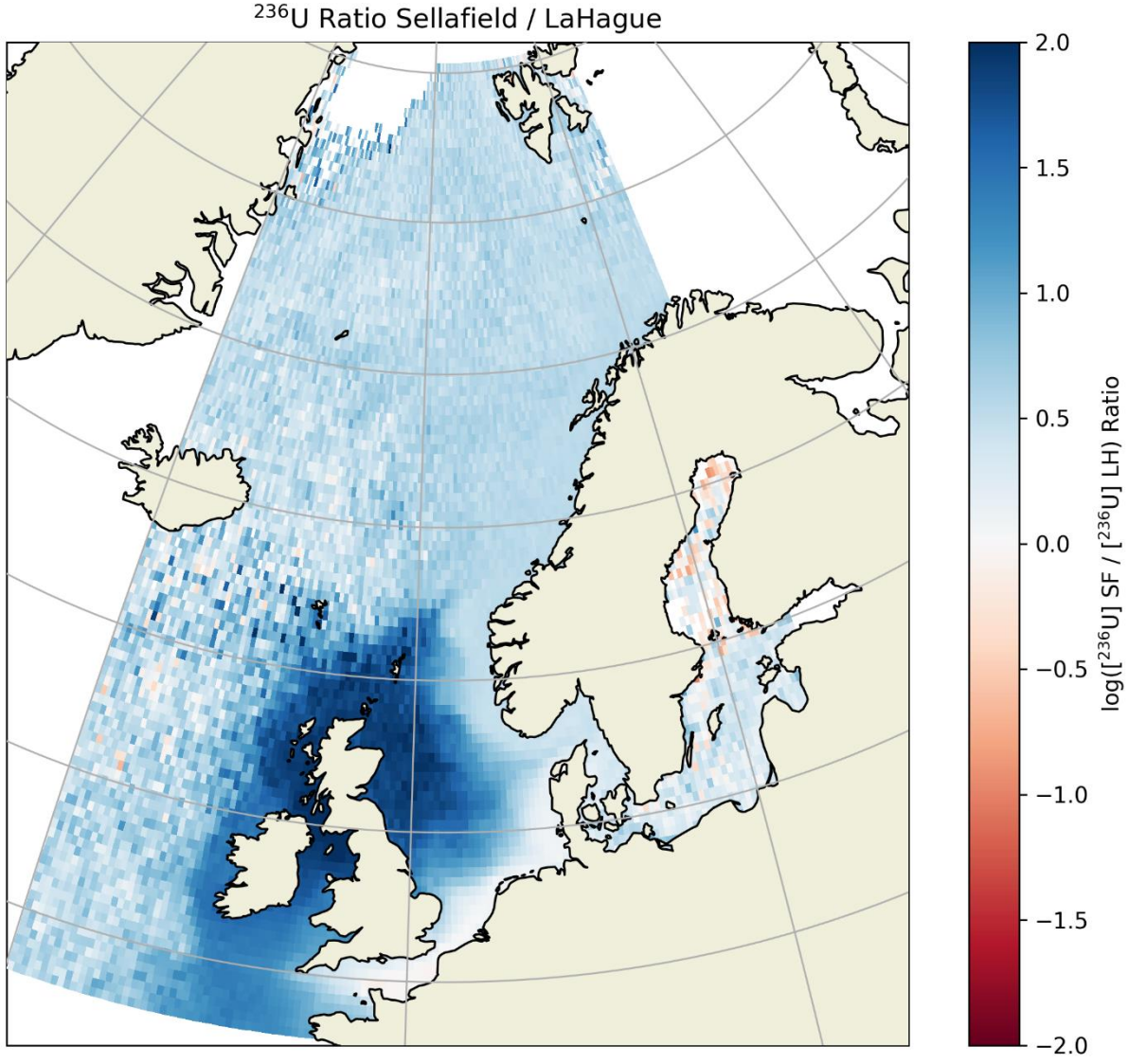

Figure 19: Map illustrating the ^{236}U SF/ ^{236}U LH ratio. Red areas indicate a higher ^{236}U contribution from La Hague and blue areas indicate a higher ^{236}U contribution from Sellafield. The color scale represents the log[^{236}U] SF/ [^{236}U] LH ratio from -2 to 2.

Both maps (*Figures 18 & 19*) show clear patterns in the isotope ratios of ^{236}U and ^{129}I between Sellafield and La Hague. The observation that the ratio of ^{129}I is generally higher from La Hague, while the ^{236}U is higher from Sellafield is expected and in line with the documented discharge data

utilized as model input. From these ratio maps, an increased understanding of transportation pathways from each source can be made.

4.6 Validation of the Marine Transport Model

The use of ocean transport models has become an important part of predicting how contaminants are transported through the marine environment. However, ocean transport models need to be validated, and non-validated models have increased uncertainties which limits their usefulness. Thus, an important part of ocean transport modeling is to validate the model through comparison with observations. The OpenDrift model simulation of this project utilized documented discharge data of ^{129}I and ^{236}U from Sellafield and La Hague (*Section 4.3*) as model input. The model simulation produced both concentration- and $^{129}I/^{236}U$ isotope ratio outputs, which in combination with observations at various locations could be applied to validate OpenDrift.

4.6.1 Validation from ^{129}I and ^{236}U Concentrations

Observations of ^{129}I and ^{236}U in the box locations were included as circles in the time series plots of the model concentration. In the time series plot of modeled radionuclide concentrations, we have divided the sum of both sources (total concentration, green line) into Sellafield contribution (blue line) and La Hague contribution (orange line).

As we can observe from the time series plot of ^{129}I from The English Channel (*Figure 20*), the main source contributor was La Hague. Model estimations from La Hague varied between 10^{10} and 10^{11} atoms/l, while estimations from Sellafield mostly varied between 10^{9} to 10^{10} atoms/l. The La Hague estimations align fairly well with the total ^{129}I concentration throughout the model period. The ^{236}U concentration time series of the English Channel shows a similar trend of higher La Hague contribution from 1993 to 2001, while from 2001 to 2023 the ^{236}U contribution is higher from Sellafield. The model concentrations in the time series are in line with what could be expected from the documented discharge data of both Sellafield and La Hague, which were utilized as model input.

The documented discharges of ^{129}I from Sellafield and La Hague presented in *Figures 15 &* 16, showed that the La Hague discharges were the major ^{129}I contributors. The differences between ^{129}I discharges from Sellafield and La Hague from 1995 to 2023 were substantial, with discharges from La Hague being about one order of magnitude higher, reaching 10^{26} ^{129}I atoms per month, while discharges from Sellafield reached 10^{25} ^{129}I atoms per month. The documented discharges from 1990 to 2023 suggest Sellafield as the major source contributor of ^{236}U. The peak discharge of ^{236}U from Sellafield was estimated in 1995, with a discharge of approximately 6.50 x 10^{23} atoms, while La Hague discharged about 2.2 x 10^{23} atoms in the same period. The differences in discharged ^{129}I and ^{236}U data could be seen in the time series plot of model concentrations (*Figures 20 & 21*), where the source contribution differences for ^{236}U are less prominent than for ^{129}I. This is indicated by the order

of magnitude of the ^{129}I and ^{236}U concentrations (atoms/l) on the y-axes, as well as the closer and more alternating Sellafield and La Hague contribution in the ^{236}U time series.

In the English Channel time series (*Figure 20*), seven ^{129}I and four ^{236}U observations are plotted against the model concentrations. There are some differences between ^{129}I observations and the corresponding model estimations, where the observations are generally higher. For the ^{236}U observations, the concentration of the model is more comparable, although one of the observations is somewhat higher. Based on these concentration time series from the English Channel, the model performs relatively well even if it slightly underestimates.

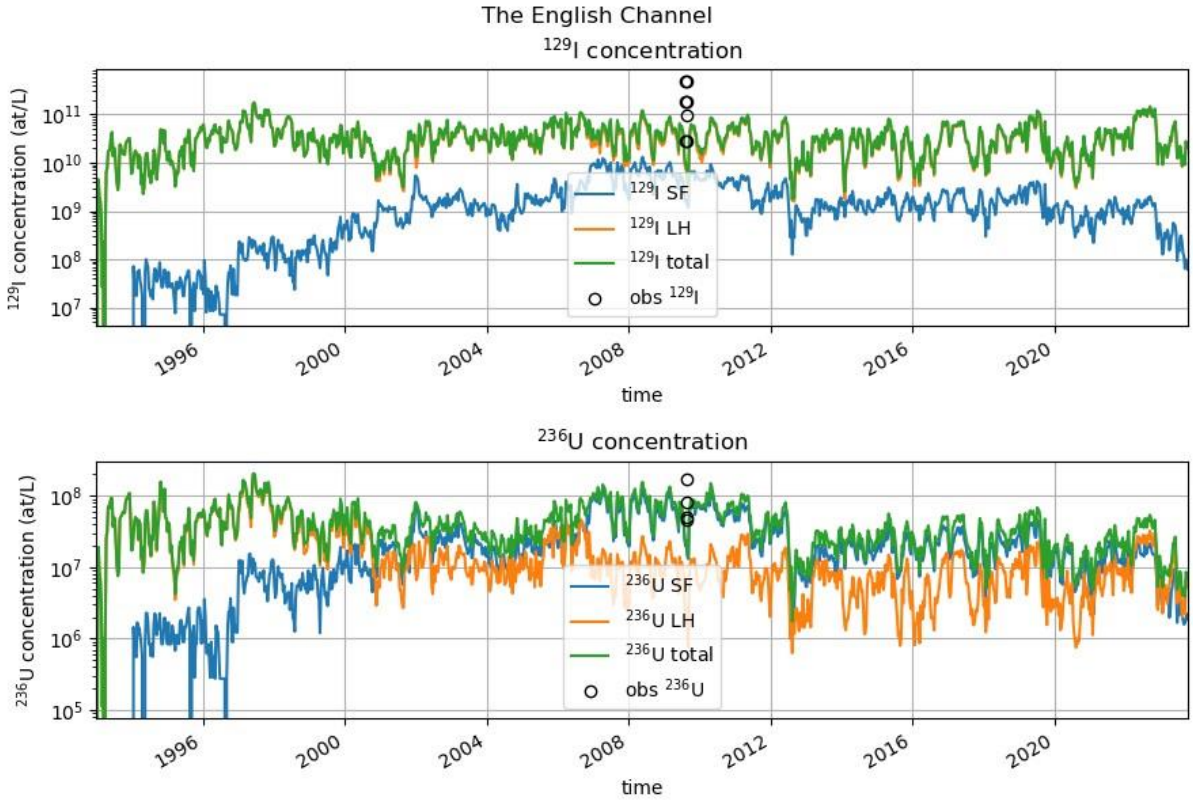

Figure 20: Model concentration time series for ^{129}I (upper) and ^{236}U (lower) in the English Channel. The concentrations (atoms/l) are divided by source origins: Sellafield, La Hague and total (SF + LH). The plotted circles represent literature data observations (Christl et al., 2015a).

To compare the model skill in a location further away from the source, a time series in the Barents Sea was produced (*Figure 21*). The source contribution of both ^{129}I and ^{236}U discharges from Sellafield and La Hague appears more similar compared to what was observed for the English Channel between 1996 and 2023. The total model concentrations (green line) of ^{129}I are reduced by one order of magnitude, from 10^{10} to 10^{11} atoms/l in the English Channel (*Figure 20*) to 10^{9} to 10^{10} atoms/l in the Barents Sea (*Figure 21*). The total model concentrations of ^{236}U are also reduced by one order of

magnitude, from 10^7 to 10^8 in the English Channel (*Figure 20*) to 10^6 to 10^7 atoms/l in the Barents Sea (*Figure 21*). However, most of ^{129}I still originate from La Hague and ^{236}U mainly from Sellafield for both locations, in line with the discharge data and the source contribution discussed in *Section 4.5*.

Substantial differences between observations and the model concentrations for the English Channel (*Figure 20*) and the Barents Sea (*Figure 21*) are noticed in the time series. The model estimations are relatively close to the observations in the English Channel, while the model estimations for the Barents Sea underestimate concentrations compared to observations by one order of magnitude for both ^{129}I and ^{236}U.

Another interesting observation is the concentration variations of the observations within one location. In the English Channel, there is a larger variability between the measured observations, while in the Barents Sea, the observations are more similar. One plausible reason for this observation is that the water masses transported into the Barents Sea are getting progressively more diluted and homogeneous (Christl et al., 2015a), while in the English Channel, the local variations are bigger due to the continuous discharge. The water masses in the English Channel are more heterogeneous, and time and space will affect the measured concentrations to a greater extent.

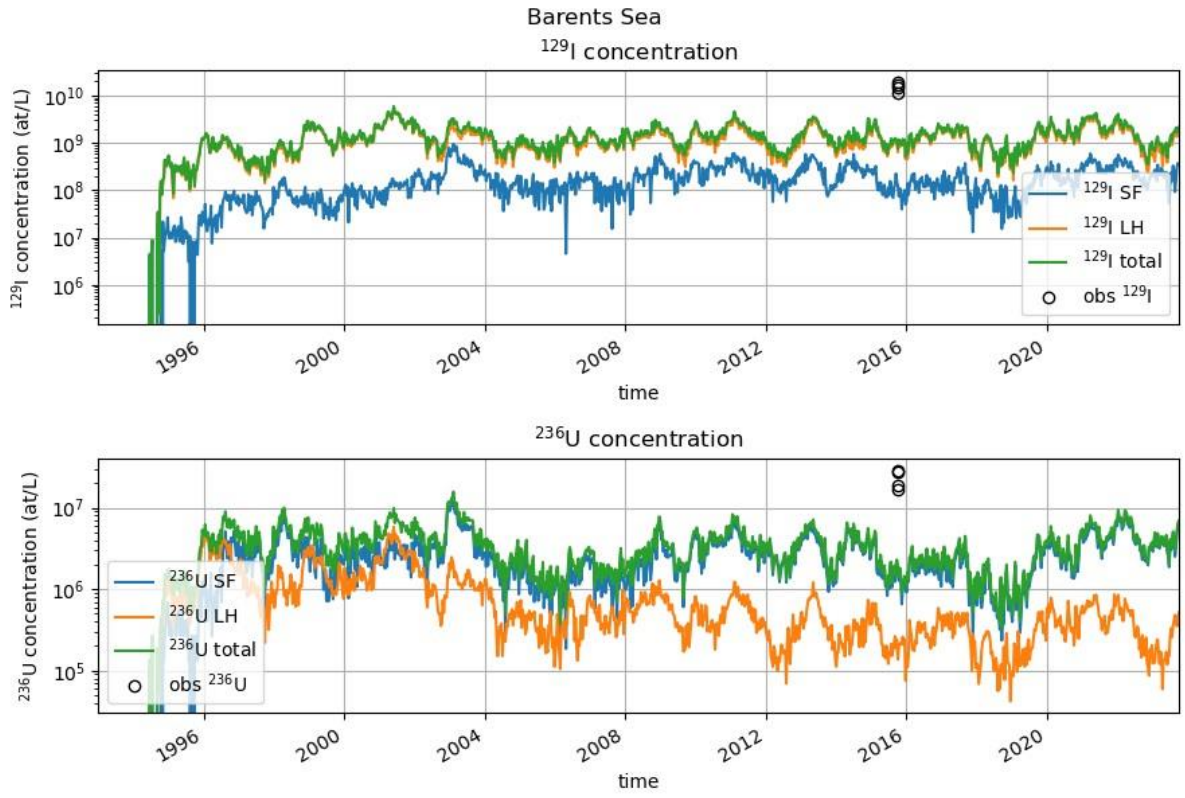

Figure 21: Model concentration time series for ^{129}I (upper) and ^{236}U (lower) in the Barents Sea. The concentrations (atoms/l) are divided by source origins: Sellafield, La Hauge and total (SF+LH). The plotted circles represent literature data observations (Casacuberta et al., 2018).

Two of the prepared and measured ^{129}I samples (samples 5 &7) from the Norwegian Sea were used as observations for model validation, resulting in the time series presented in *Figure 22*. The two samples are overlapping due to similar concentrations (7.18 x 10^9 atoms/l and 6.24 x 10^9 atoms/l). The time series of the Norwegian Sea shows that the model underestimates the concentrations of ^{129}I compared to the observations. In the Norwegian Sea, the model underestimates less than in the Barents Sea (*Figure 21*), but more than in the English Channel (*Figure 20*). This aligns with the distance of the location to the nuclear reprocessing sources, where the English Channel is closest and the Barents Sea is the furthest away, while the Norwegian Sea is in-between.

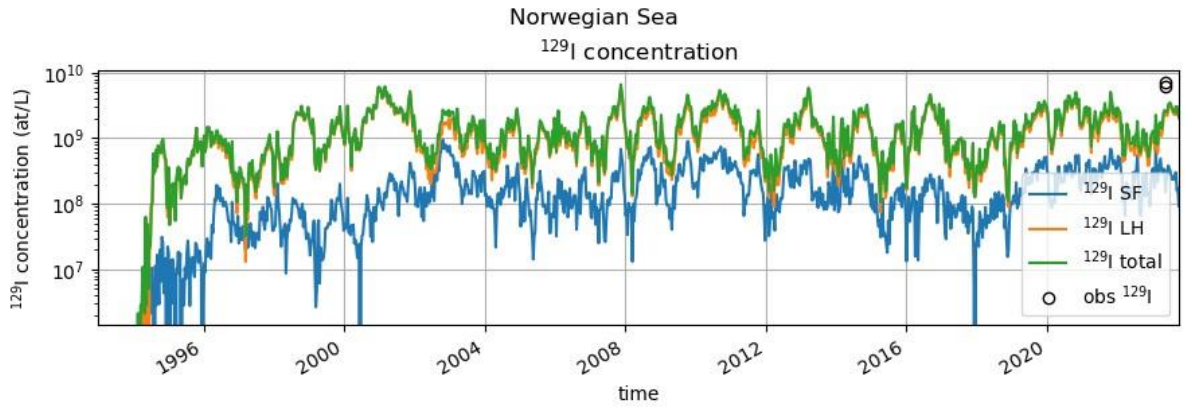

Figure 22: Model concentration time series for ^{129}I in the Norwegian Sea. The concentrations (atoms/l) are divided by source origins: Sellafield, La Hague and total (SF+LH). The plotted circles represent observations obtained in the present work.

Time series plots of ^{129}I and ^{236}U concentrations were produced for all nine locations, and in *Figures 23 & 24,* summaries of the average estimated concentrations compared to the corresponding average observations of ^{129}I and ^{236}U for the different locations are presented. The model underestimates the ^{129}I concentrations more than the ^{236}U concentrations in locations closer to the discharge sources in the English Channel and the North Sea (East and South). For the Komsomolets location, there are larger discrepancies in ^{236}U model estimations and observations. The ^{129}I concentrations are underestimated within the range of 2.5 to 23.0 (*Figure 23)* and ^{236}U concentrations are underestimated within the range of 2.1 to 58.0 (*Figure 24*) for all locations.

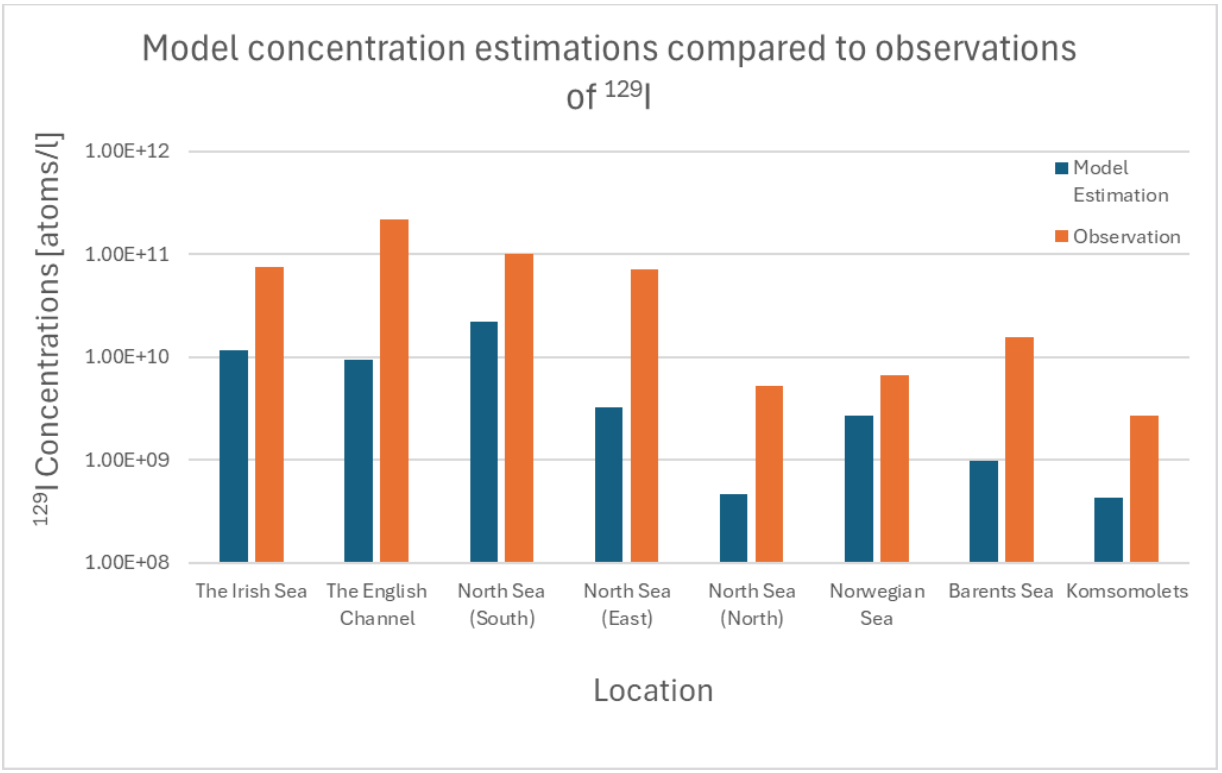

Figure 23: Model concentration estimations compared to observations of ^{129}I (atoms/l) within various model locations. Note that the average ^{129}I observation for each location is used.

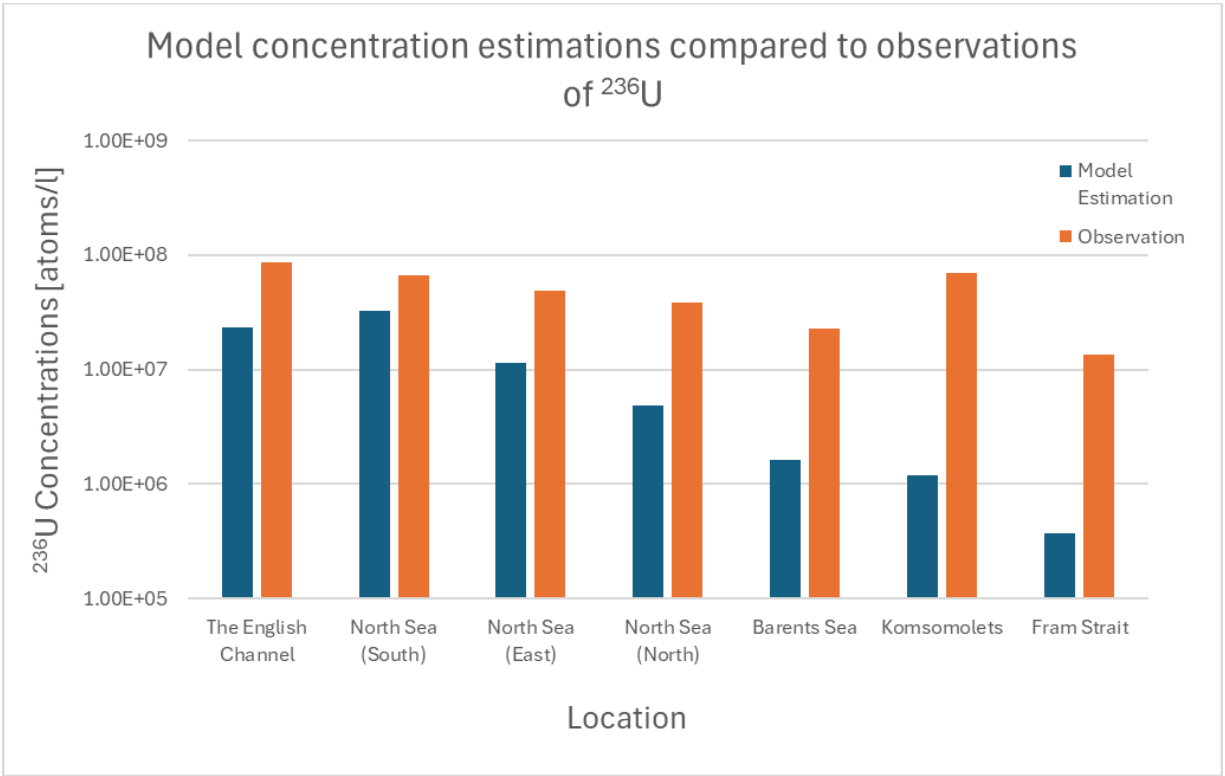

Figure 24: Model concentration estimations compared to observations of ^{236}U (atoms/l) within various model locations. Note that the average ^{236}U observation for each location is used.

The plotted observations in the time series for the English Channel, the Barents Sea and the Norwegian Sea indicate that the model generally underestimates the concentrations of actual observations, which is also illustrated in *Figures 23 & 24*. The underestimation increases with increased distance from Sellafield and La Hague. This underestimation of the actual observations is generally expected due to model uncertainties and the neglect of source terms like releases before 1990, global fallout and the Springfield facility, which is a major source contributor of ^{236}U in the Northeast Atlantic Ocean (Christl et al., 2015b). The releases before 1990 would contribute to the overall model concentrations, even if these releases were significantly lower. The estimated model concentrations of ^{236}U would increase if global fallout was considered, as a large amount of ^{236}U was released during the atomic weapon testing (Shao et al., 2019). The neglect of other sources than the nuclear reprocessing plants might greatly affect locations further away, as the importance of other sources increases. Whereas the locations closer to the source are more impacted by the local discharges from Sellafield and La Hague, and the model estimates the concentrations of ^{129}I and ^{236}U more accurately.

4.6.2 Validation from $^{129}I/^{236}U$ ratios

Another approach to validate the ocean transport model is to utilize $^{129}I/^{236}U$ isotope ratios. These isotope ratio observations were gathered from locations where ^{129}I and ^{236}U concentrations were measured simultaneously and plotted against the estimated model ratios at various locations (*Figure 25*).

The scatter plot shows the observed $^{129}I/^{236}U$ ratios compared to the model ratio. The dashed line in the middle represents where the points would be if the model perfectly correlated to the observations. The filled circles represent each observation from the various locations, while the open circles represent the average ratios of each location. By utilizing the isotope ratios, the locations further away from the sources compare better than the locations closer to the sources. The observed Barents Sea ratios (purple) align well with the model, on both sides of the dashed line. The English Channel has larger variations, and the average observed ratio is much higher than the model ratio from the same location. At two out of three locations in the North Sea (South and East), large variations can be seen for each location. The isotope ratios vary much less for the ocean model than the observations since the model calculates equations that can reduce fluctuations and smooth out the signal. In addition, the model estimates an average $^{129}I/^{236}U$ ratio for a larger area, while the observations are measured at one specific point within the larger area.

The estimated isotope ratios are identical and can be seen as a straight horizontal line in *Figure 25* for all locations except the Barents Sea. This is because the model includes a corresponding estimated ratio for every observed isotope ratio, and most observed ratios were measured from samples collected

on the same date. The model estimated one general ratio for the specific locations and time, and for the Barents Sea (purple) the model estimated two different isotope ratios because observed ratios from two different dates were available for this location.

The isotope ratio observations further away from the source fit the estimated isotope ratios of the model to a larger extent. A reason for this could be that the water masses are mixed better to a homogenous mix, and the exact sampling location might not affect the measured ratios too much. In the English Channel, a more heterogeneous water mass can be found, and the observed ratios can vary to a greater extent within the same box location. The additional large variation in the North Sea also strengthens the indication that locations closer to the source have larger variations.

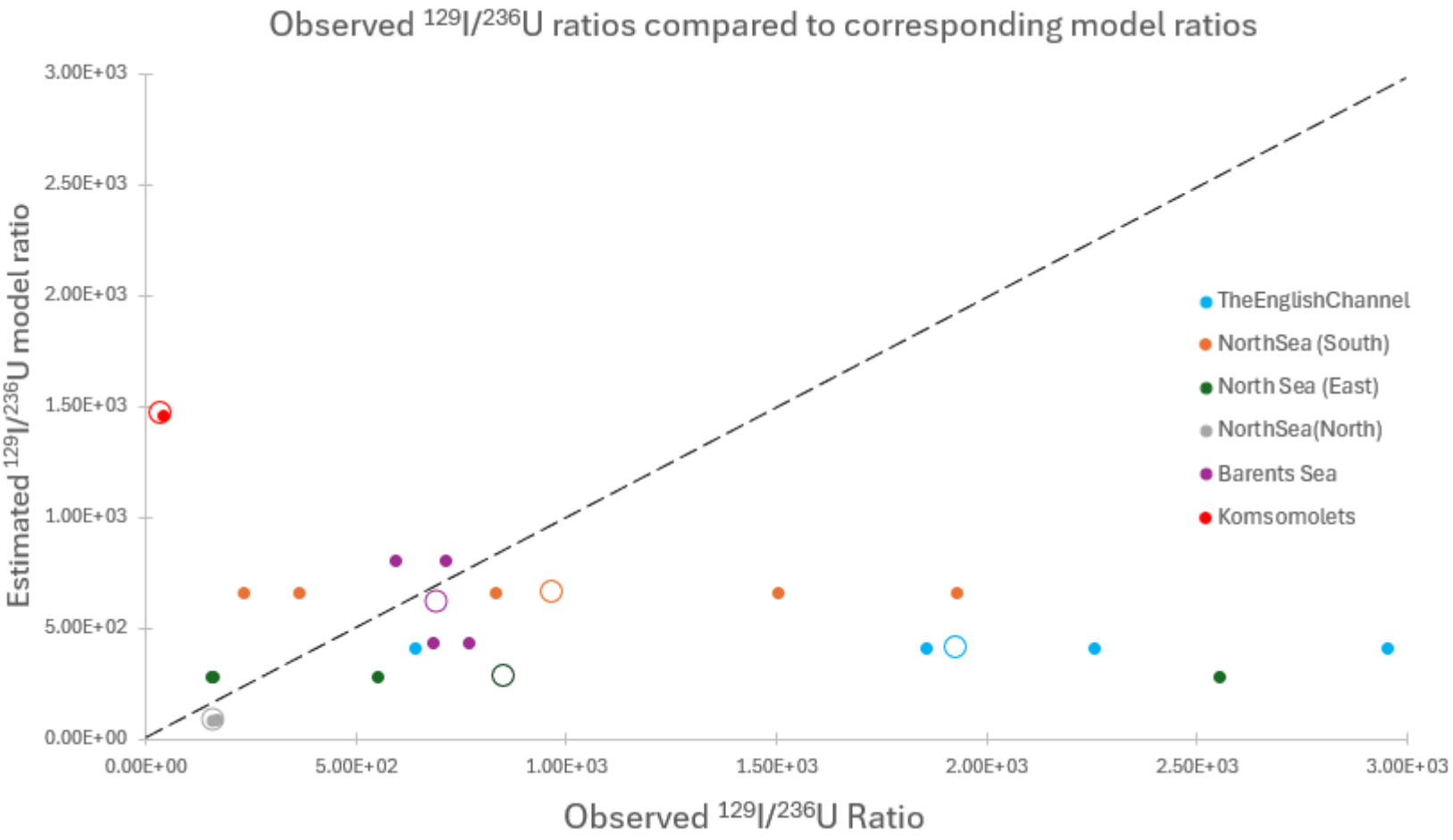

Figure 25: Observed $^{129}I/^{236}U$ ratios compared to estimated $^{129}I/^{236}U$ model ratios for various model locations. The open circles represent the average observations within each model location, and the dashed line marks the positions where observed ratios equal model ratios.

Estimated $^{129}I/^{236}U$ model ratios were also compared to the $^{129}I/^{236}U$ ratios from the discharge data from Sellafield and La Hague. The annual minimum- and maximum isotope ratios of the discharge from both reprocessing plants were implemented as dashed lines in the scatterplot (*Figure 26*). The observations plotted in the scatterplot were measured between 2009-2023. Due to the transport time, the oldest radionuclide concentrations in the Barents Sea from 2009 were assumed to result from discharges six to seven years prior. Therefore, the annual minimum- and maximum discharge ratios from Sellafield and La Hague between 2002-2023 were retrieved and marked as dashed lines in *Figure 26*. The min- and max ratio for Sellafield were 1.06×10^{1} and 1.44×10^{2}, while the min- and max ratio for La Hague were 1.80×10^{3} and 5.73×10^{3} for this period. In La Hauge, the discharged $^{129}I/^{236}U$ ratio remained high compared to the ratio at Sellafield between 1990 and 2023 (*Figure 17*). As previously seen, La Hague has the highest discharge of ^{129}I, while Sellafield has the highest ^{236}U discharge. The difference between ^{129}I and ^{236}U discharges is bigger for La Hague than Sellafield, resulting in the higher $^{129}I/^{236}U$ ratio for La Hague discharges.

In addition, the model simulations during this project only considered discharge data from Sellafield and La Hague as the source of contamination. Therefore, the global fallout (GF) was plotted to compare its $^{129}I/^{236}U$ ratio to the observation ratios. The values of the ratio of global fallout have previously been determined to be 0.5 in another study (Casacuberta et al., 2016), indicating a higher concentration of ^{236}U than ^{129}I. The observed $^{129}I/^{236}U$ ratios were all larger than 0.5 and fell to the right of the global fallout observation in *Figure 26*. The closest observed ratio to GF was the ratio of Komsomolets, which is the furthest location from the nuclear reprocessing (RP) sources. Indicating that GF discharge is more prominent further away from the nuclear reprocessing sources, affecting a larger part of the source contribution.

The observed isotope ratios for the English Channel (light blue points) were mostly in between the min- and max ratio discharge values from La Hague. This would be expected as the English Channel is located northwards of the La Hague reprocessing plant. The observations from the south of the North Sea (orange points) were also closer to the isotope ratio of La Hague, rather than Sellafield as this is also closer to this discharge source. The observed isotope ratios from the Barents Sea (purple points) are between the maximum ratio from Sellafield and the minimum ratio from La Hague. This could be a result of a mixed isotope ratio from both La Hague and Sellafield, as this is further away from both sources.

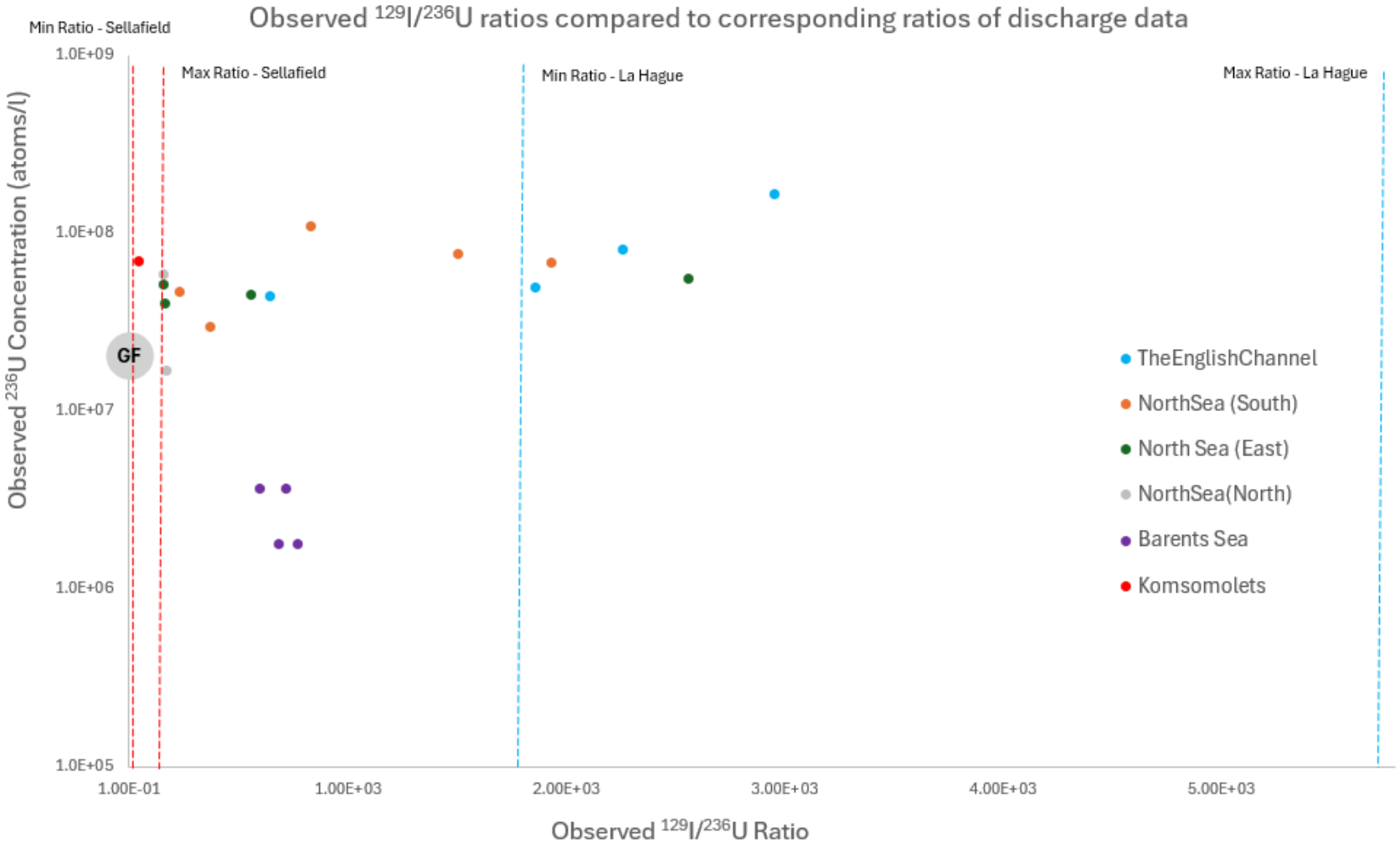

Figure 26: Observed $^{129}I/^{236}U$ ratios compared to $^{129}I/^{236}U$ ratios from the discharge data for various locations. The min- and max $^{129}I/^{236}U$ discharge ratios from Sellafield (red dashed lines) and La Hague (blue dashed lines) between 2002-2023 are marked in the scatterplot. The isotope ratio of global fallout (GF) is plotted as a large, gray mark. Note the logarithmic scale of observed ^{236}U concentrations on the y-axis, as well as the scale of the observed $^{129}I/^{236}U$ on the x-axis.

The estimated $^{129}I/^{236}U$ ratios were also compared directly to $^{129}I/^{236}U$ ratios from observations, by plotting observations in a time series of model estimations. The ratio time series was plotted to see differences between Sellafield and La Hague, and how the ratios developed over time. From the isotope ratio time series of the English Channel (*Figure 27*), three $^{129}I/^{236}U$ observations are seen close to the ratio estimation from La Hague (orange) and one $^{129}I/^{236}U$ observation is seen near the total (green). This supports the finding in the scatterplot (*Figure 26*), where the observed ratio from the English Channel was primarily between the min- and max ratio from the discharges of La Hague. This indicates that the isotope ratio seen in the English Channel is most probably affected by La Hague discharges.

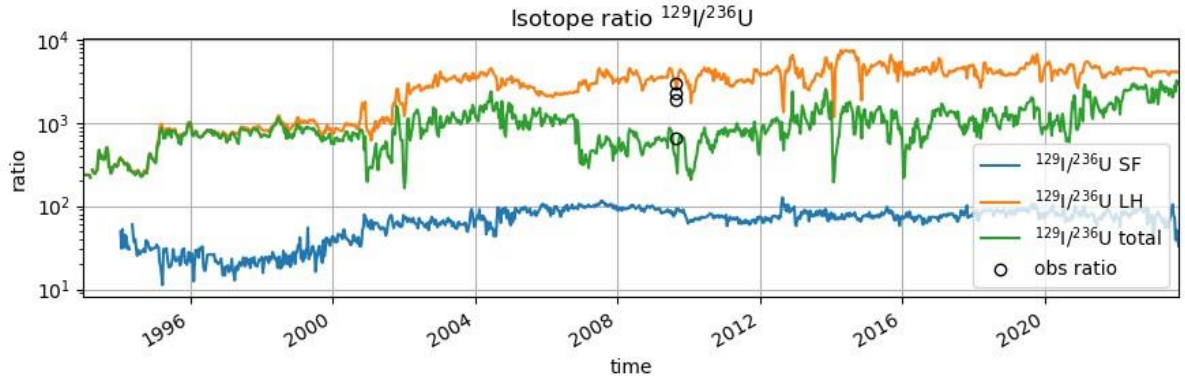

Figure 27: Time series of the estimated $^{129}I/^{236}U$ model ratio in the English Channel from 1993 to 2023. The isotope ratios ($^{129}I/^{236}U$) are divided by source origin: Sellafield, La Hague and total. Four observed $^{129}I/^{236}U$ ratios from 2009 are marked as circles.

From the scatterplot (*Figure 26*), the two observed $^{129}I/^{236}U$ ratios from north of the North Sea are plotted between the min- and max-discharge ratio from Sellafield. The model estimations were compared to two available observations of $^{129}I/^{236}U$, which were plotted in a time series (*Figure 28*). In the time series, these two observations are seen close to the Sellafield $^{129}I/^{236}U$ isotope ratio line (blue). Comparisons of the model estimations to the two observed $^{129}I/^{236}U$ ratios in the north of the North Sea indicate Sellafield as the main discharge source contributor, with some discharges from La Hague mixed in due to the slightly elevated observations above the Sellafield line (blue).

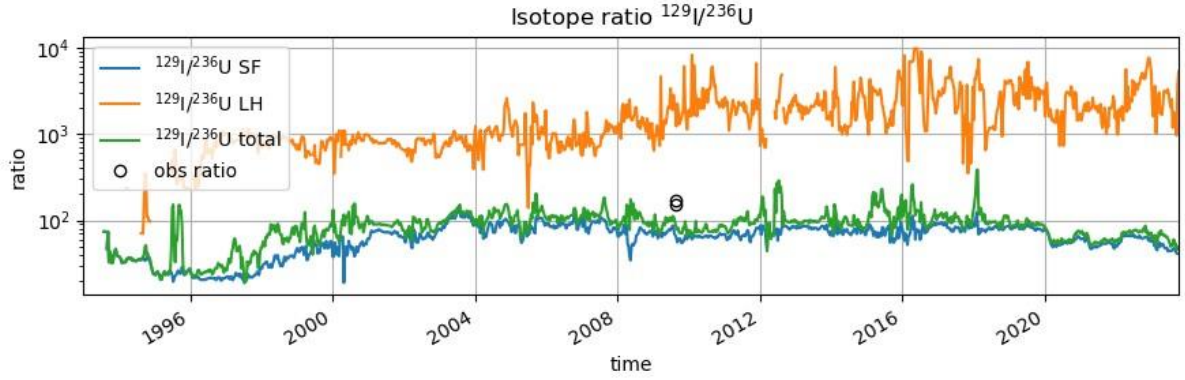

Figure 28: Time series of the estimated $^{129}I/^{236}U$ model ratio in the North Sea (north) from 1993 to 2023. The isotope ratios ($^{129}I/^{236}U$) are divided by source origin: Sellafield, La Hague and total. Two observed $^{129}I/^{236}U$ ratios from 2009 are marked as circles.

The four observed $^{129}I/^{236}U$ ratios in the Barents Sea were seen between the discharge ratio of Sellafield and La Hague (*Figure 26*), indicating a mixed ratio from both Sellafield and La Hague. The estimated model $^{129}I/^{236}U$ ratios were plotted as a time series, which implemented these ratio observations for comparison and validation of the model (*Figure 29*). The observations are seen on the $^{129}I/^{236}U$ estimated total (green), supporting the claim of a more mixed ratio origin from Sellafield and La Hague seen in the Barents Sea.

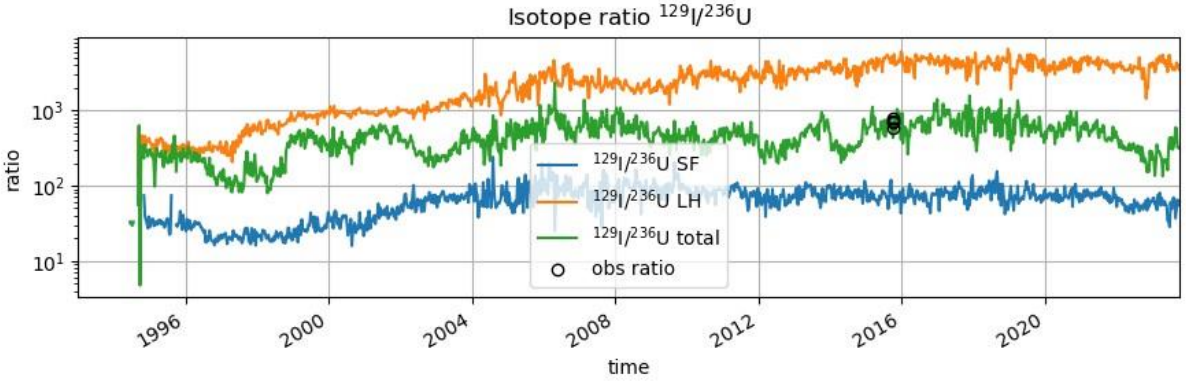

Figure 29: Time series of the estimated $^{129}I/^{236}U$ model ratios in the Barents Sea from 1993 to 2023. The isotope ratios ($^{129}I/^{236}U$) are divided by source origin: Sellafield, La Hague and total. Four observed $^{129}I/^{236}U$ ratios from 2009 are marked as circles.

The comparison of model ratio estimations in the English Channel, the north of the North Sea and the Barents Sea showed that the model makes better ratio estimations further away from the discharge sources. The locations closer to the source are more affected by the individual local discharges from La Hague (the English Channel) and Sellafield (the North Sea), while the model estimates a more mixed source contribution for the Barents Sea.

4.7 Model Age of Trajectories

The model simulation assumed the same behavior of ^{129}I and ^{236}U which resulted in identical transportation time and trajectory age in the model. To answer hypothesis H_1 regarding whether Lagrangian particles from Sellafield are older than the corresponding Lagrangian particles from La Hague, the model produced model age time series. The time series illustrate how the model particles ages from Sellafield (blue line) and La Hague (orange line) in the Barents Sea (*Figure 30*) and the Irish Sea (*Figure 31*) developed from 1993 to 2023. The thin lines represent the model trajectory age for every timestep (10^{th} day), while the thick lines represent a mean and smoothed trendline of running averages of the thirty nearest points. The green lines represent the total age from both Sellafield and La Hague, while the red dashed lines represent the smoothed trajectory ages of the Sellafield line (thick blue) minus the smoothed La Hague line (thick orange).

The thin lines show high variability in model particle age since these are values from every time step in the model. Increased heights of the thin lines can be seen over time, due to the increased number of model particles released from the discharge sources, resulting in more dispersion across the model area and higher variability. The thick trend lines are smoothed to see the development and trends of model particle ages over time, with reduced noise from the thin lines.

The trajectory age differences between locations from various distances to the discharge sources could be seen. The two age plots of the Irish Sea and the Barents Sea visualize clear age differences. The model ages of trajectories in the Barents Sea appeared in 1994 (*Figure 30*), implying that model particles observed in the Barents region have at least one year of transportation time. The particles from Sellafield in the Irish Sea began at 0 years in 1993 (*Figure 31*), indicating an immediate model trajectory concentration from Sellafield since 1993 is the first year of the model simulation. This occurs because the model particle release source of Sellafield was located in the Irish Sea.

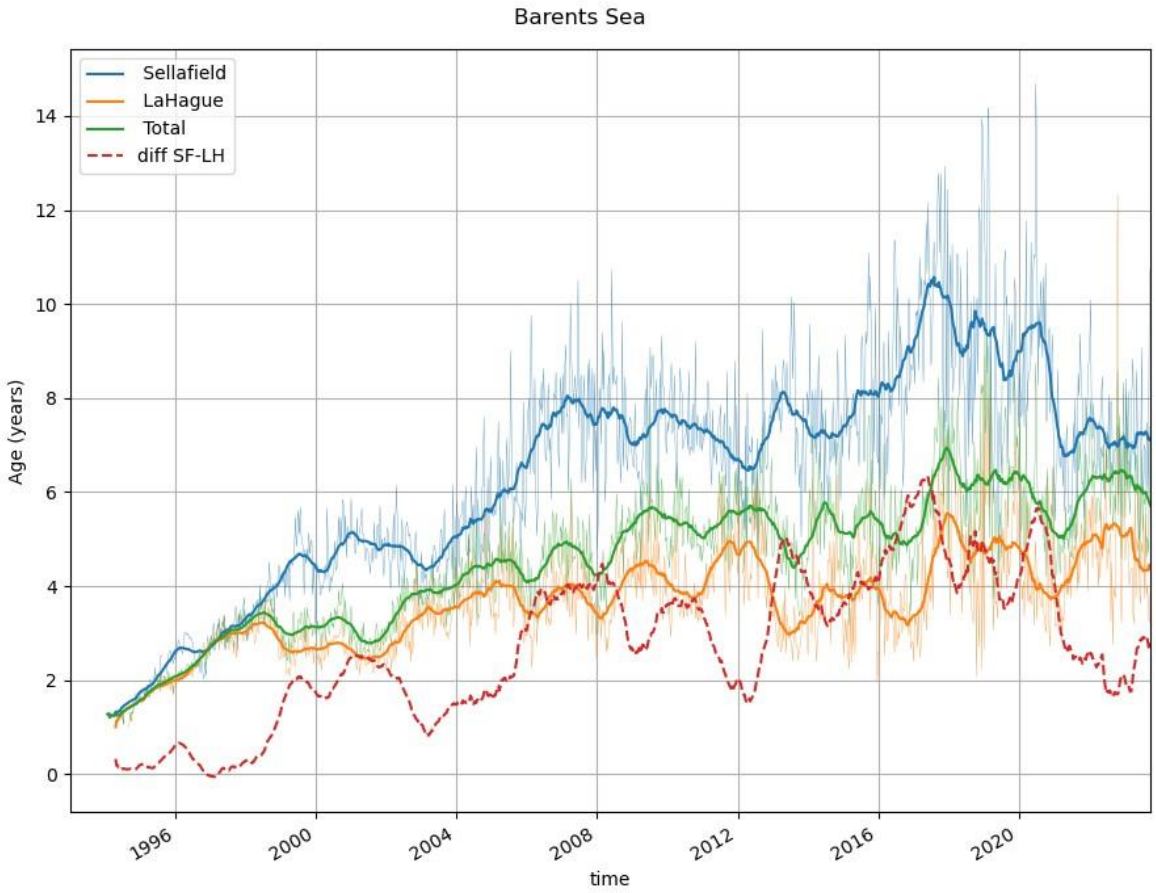

Figure 30: Time series of model particle age (years) from Sellafield, La Hague and total in the Barents Sea. The thin and colored lines represent the model particle age for every timestep (10th day) from the different source origins. The thick lines represent a mean trendline and smoothing of the thin lines. The red dashed line represents the age differences (SF-LH) between the smoothed Sellafield line (thick blue) and the smoothed La Hague line (thick orange).

The age of the model particles from Sellafield in the Irish Sea does not exceed 5 years, due to the assumed constant water mass transportation from the area. The trajectories from Sellafield are older than the trajectories from La Hague in the Barents Sea. This indicates that particles from Sellafield have a longer transportation time than particles from La Hague towards the Barents Sea. The opposite could be seen for the Irish Sea, however, where trajectories from La Hague are older due to longer transportation time. The red dashed line in the Irish Sea timeseries (*Figure 31*) show negative age values throughout the model period. Since this line is based on the differences between particle ages from Sellafield (SF) – La Hague (LH), the negative values indicate that model particles from La Hague are older than from Sellafield in the Irish Sea.

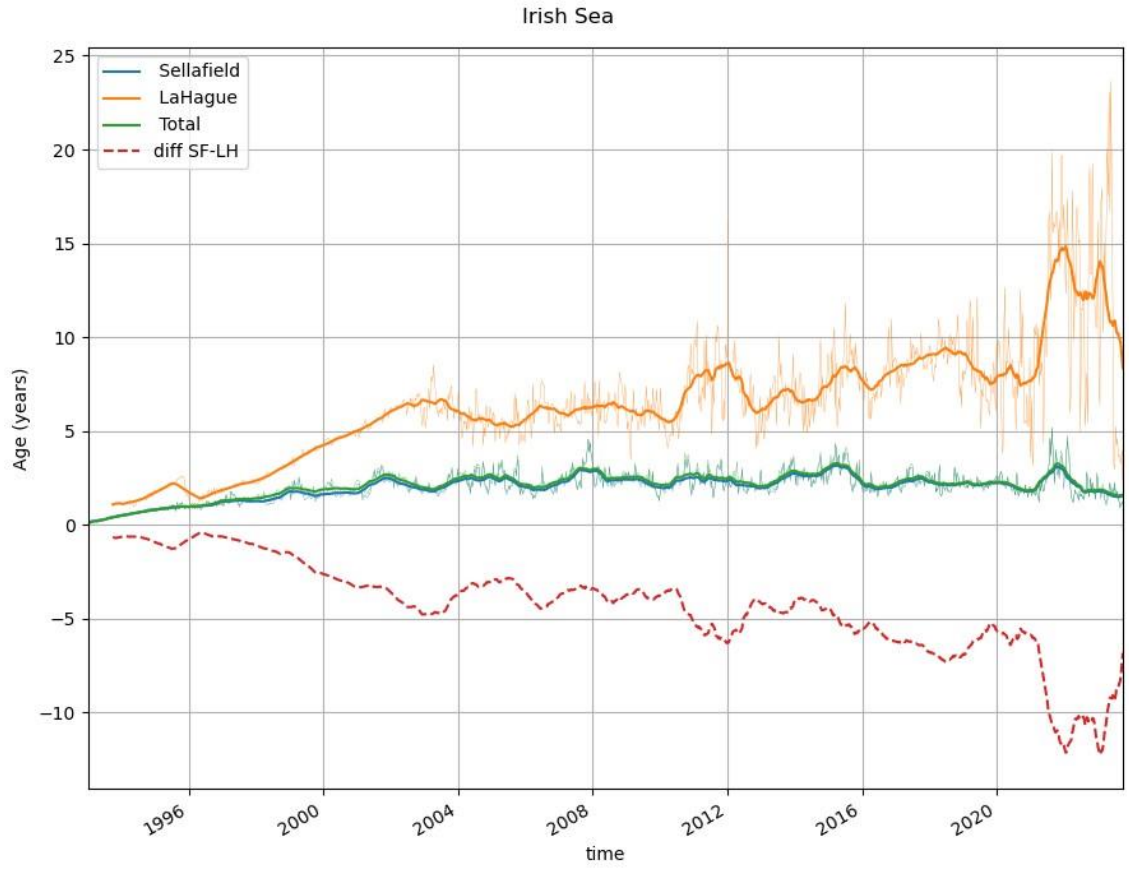

Figure 31: Time series of model particle age (years) from Sellafield, La Hague and total in the Irish Sea. The thin and colored lines represent the model particle age for every timestep (10th day) from the different source origins. The thick lines represent a mean trendline and smoothing of the thin lines. The red dashed line represents the age differences (SF-LH) between the smoothed Sellafield line (thick blue) and the smoothed La Hague line (thick orange).

The model produced a particle age time series for all nine locations. To answer H_1 and see if the model particle ages from Sellafield were older than for La Hague within the model area, the average age of Sellafield minus La Hague from all the nine separate locations is presented in *Figure 32*. The model estimated the model particle age from Sellafield and La Hague for the model timestep (every 10th day), and the average values for each location between 2003 and 2023 were used to compare model ages. Positive age values indicate older average particles from Sellafield (SF) and negative age values indicate older average particles from La Hague (LH). In the Irish and the northern North Seas, the average age difference from La Hague was 5.43 and 4.59 years, respectively. While for the remaining seven locations, the average Sellafield trajectories were older than the average La Hague trajectories with a range between 3.22 to 5.47 years.

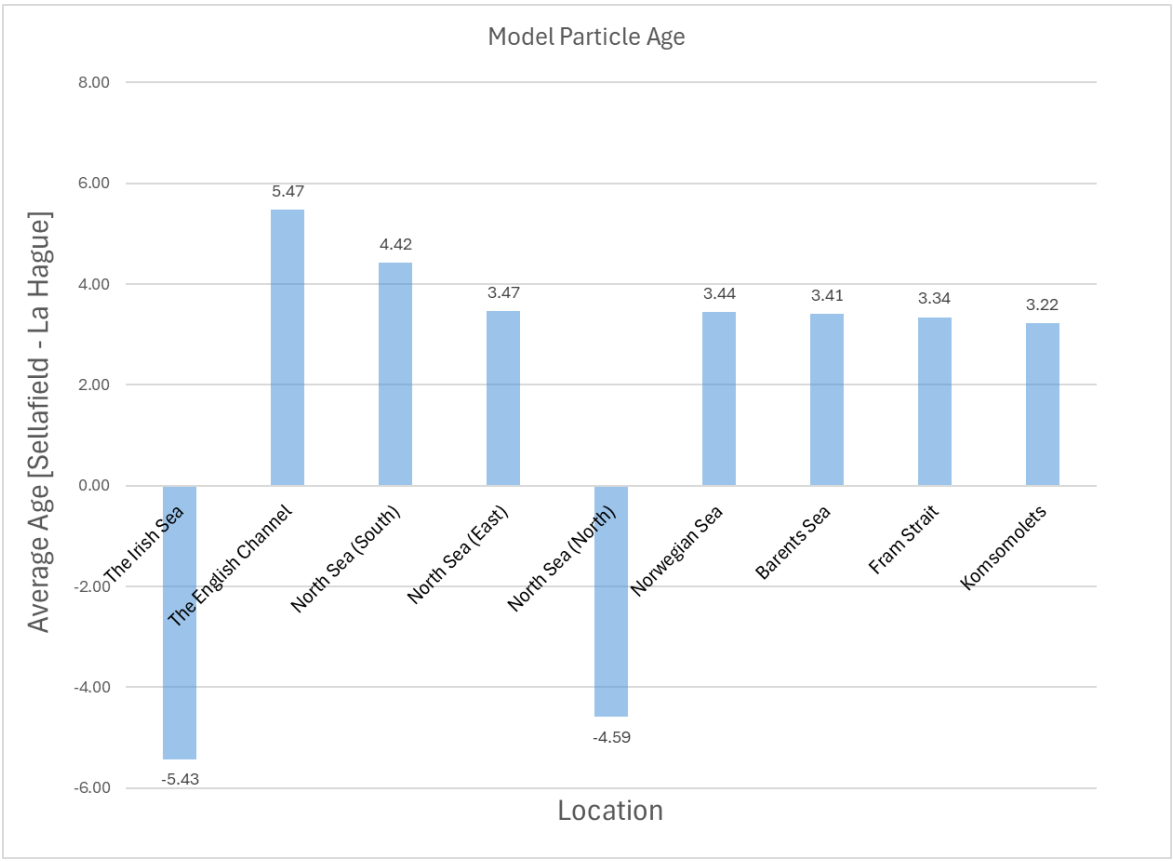

Figure 32: Average model particle age (years) differences between Sellafield and La Hague (SF – LH) for locations between 2003 and 2023. Positive values indicate older particles from Sellafield, and negative values indicate older particles from La Hague.

Based on *Figure 32,* the age of model particles is primarily higher for Sellafield compared to La Hague within the model area, except for the Irish Sea and the north of the North Sea, where older model particles from La Hague are seen. These findings correspond to the results in *Section 4.5*, which show a higher abundance of Sellafield trajectories at the locations that have a net negative age difference in *Figure 32*, indicating that the average La Hague trajectories in these Sellafield dominating locations are older. This suggests longer transportation time for model particles from Sellafield to the Norwegian Sea, the Barents Sea, Fram Strait and Komsomolets. A reason for the younger model particles from La Hague in most areas can be related to transportation with strong coastal currents, resulting in shorter transportation times, and thus younger trajectories.

4.8 Evaluation of ^{236}U Retention in the Irish Sea

Several studies regarding ocean transport modeling with radionuclide tracers have assumed that ^{236}U behaves conservatively in the marine environment (Casacuberta et al., 2018; Castrillejo et al., 2018; Christl et al., 2017). However, this assumption has recently been challenged in a Lagrangian ocean model study, which suggested that ^{236}U interactions with seabed sediments cannot be neglected, at

least in the shallow waters, if ^{236}U is used as an ocean tracer (Periáñez et al., 2023). In another previous study, it was suggested that only 52% of the discharged ^{236}U from nuclear reprocessing in the Irish Sea reaches the Arctic Ocean (Periáñez et al., 2018).

An interesting ocean process affecting the transportation of radionuclides from Sellafield is tidal advection. Research has proved that the estimated transport of ^{99}Tc out of the Irish Sea is affected by whether or not the ocean transport model includes tidal advection to the flow field (Simonsen et al., 2017). The inclusion of tidal drift in the model caused an increased northwards drift while neglecting the tidal drift tended to overestimate the southward transport into the Celtic Sea (Simonsen et al., 2017). The tidal drift inclusion was observed to affect the radionuclide concentration levels as far as the Barents Sea and the Arctic Ocean (Simonsen et al., 2017). The model simulations during this project, which neglected the tidal advection, likely overestimated the radionuclide transportation from Sellafield to the English Channel.

The model simulations during this project assume that the ^{129}I and ^{236}U behave conservatively in the marine environment, which translates to zero retention by binding reactions to other particles or the bottom sediments. If ^{236}U particles are significantly retained in the sediments of the Irish Sea, the model should overestimate the ^{236}U concentrations due to broadly assumed conservative behavior and transport. However, the marine environment is complex, and the transportation of ^{236}U is affected by various factors which makes model predictions more difficult.

To evaluate ^{236}U retention in the Irish Sea based on model simulations of this research, the model concentrations of ^{236}U and the $^{129}I/^{236}U$ ratio which have been used in combination with observations to validate the transport model in *Section 4.6* can be analyzed. The model concentrations of ^{236}U in the English Channel (*Figure 20*) and the Barents Sea (*Figure 21*) are underestimated compared to observations. The underestimation also increase further away from the source like in the Barents Sea compared to observations closer to the source, such as the North Sea (south). Since the model assumes conservative behavior of ^{236}U, the model would more likely overestimate the concentration of ^{236}U from Sellafield due to more binding reactions in the Irish Sea if there was substantial ^{236}U retention. The estimated model ratios of $^{129}I/^{236}U$ could also contribute to evaluating ^{236}U retention in the Irish Sea. In *Section 4.6.2* the estimated model ratios were compared to observed ratios throughout the model area. This comparison revealed more accurate model estimations further away from the nuclear reprocessing sources in the Barents Sea, north of the North Sea and Komsomolets, compared to the English Channel and south of the North Sea. The conservative assumption of ^{236}U in the transport model would likely result in a lower $^{129}I/^{236}U$ ratio due to increased ^{236}U concentrations. While potential retention would decrease the ^{236}U concentrations, causing a higher $^{129}I/^{236}U$ ratio. For this reason, the transport model would likely underestimate the $^{129}I/^{236}U$ ratio from Sellafield compared to observations if there was substantial ^{236}U retention in the Irish Sea. The estimated $^{129}I/^{236}U$ ratios were

relatively comparable, even if ^{236}U was assumed to be completely conservative. These comparable results indicate that the transportation of ^{236}U from Sellafield is less affected by retention in the Irish Sea.

Another approach to evaluate the retention of ^{236}U in the Irish Sea is to estimate the model age of particles released from Sellafield as seen in *Section 4.7*. A high ^{236}U retention in the sediment would result in a higher particle age of ^{236}U than ^{129}I in the Irish Sea. This model simulated 200,000 trajectories with unique properties, including specific age and source of origin. By combining the source of origin and the age of the trajectories, the suggestion that ^{236}U is retained in the shallow Irish Sea could be evaluated. The assumed conservative behavior of ^{236}U in this project naturally resulted in zero retention in the Irish Sea as seen in *Figure 31*. Therefore, the model particle ages from Sellafield were less than three years throughout the model simulation period due to continuous transportation. To utilize the trajectory age of particles from modeling to evaluate ^{236}U retention in marine particles or sediments in the future, several simulations including and excluding speciation and tidal advection should be conducted. During this pilot project, the behavior of ^{236}U and ^{129}I are identical and conservative, resulting in the same trajectory age. This makes it difficult to conclude ^{236}U retention based on model particle age analysis.

The model estimates of ^{236}U concentrations and $^{129}I/^{236}U$ ratios from Sellafield and La Hague revealed indications of no significant ^{236}U retention in the Irish Sea, when compared to observations. Sellafield was the highest source contributor to ^{236}U discharges, and the model estimations of ^{236}U concentrations from Sellafield were generally underestimated compared to corresponding observations. The underestimations indicate a higher degree of ^{236}U transportation in the real world compared to the estimated transportation in the ocean model which assumed completely conservative behavior of ^{236}U, as well as neglecting source contribution from global fallout. The same signals regarding no significant ^{236}U could be found in the analysis of the estimated $^{129}I/^{236}U$ ratios. The model estimates compared well to the observations, while still assuming conservative behavior of ^{236}U. Any retention of ^{236}U in the Irish Sea should decrease the ^{236}U concentrations within the areas downstream, and since the model assumes conservative behavior of ^{236}U, it would cause the model to underestimate the $^{129}I/^{236}U$ ratios.

Analysis of model particle age could also be a viable method of testing ^{236}U retention in the Irish Sea, but since the modeling conducted during this project excluded speciation it would be difficult to verify any possible retention. The ^{236}U concentrations and $^{129}I/^{236}U$ ratio simulations have revealed signals of no significant ^{236}U retention, but further work is needed to reach a firm conclusion.

4.9 Future Research

The research conducted during this project was mainly a pilot study to achieve a future, overarching goal of testing ^{236}U retention. This study focused on validating the OpenDrift ocean transport model by comparing estimated model concentrations of ^{129}I and ^{236}U and isotope ratios to observations. The modeling part conducted during this research was a simplified ocean transport model, which considered ^{129}I and ^{236}U to be completely conservative.

The real world is more complex, and future work should consider the speciation of radionuclides as part of the modeling. By analyzing differences in model concentration estimates including speciation to model estimates excluding speciation, a conclusion regarding ^{236}U retention could be made. In addition, tidal advection has been proven to affect the transportation pathways (Simonsen et al., 2017), and future research would gain from including tides in the ocean transport simulation.

All this considered, the simplified OpenDrift estimations during this pilot study still provided relatively comparable results to the observations. This study has shown the potential of the ocean transport model, OpenDrift, and by further increasing detail levels in future research, more accurate estimations can be made.

5 Conclusions

The initial literature research for ^{129}I and ^{236}U observations for model validation in the North Atlantic- and Arctic Ocean uncovered existing data gaps in the Norwegian Sea. As a result, samples from six different sampling stations in the Norwegian Sea were collected by The Institute of Marine Research (IMR). These samples were brought to laboratories at NMBU and CTU for radiochemical separations and measured at the accelerator mass spectrometer at CNA in Seville. These measurements provided a ^{129}I concentration range between 0.63 to 35.3 x 10^9 atoms/l in the Norwegian Sea, and these data were subsequently used for model validation.

The source terms of ^{129}I and ^{236}U from Sellafield and La Hague have been improved by source contribution separation of the two nuclear reprocessing plants. The source separation revealed distinct estimated age differences of model particles discharged from Sellafield and La Hague in the North Atlantic- and Arctic Ocean. Sellafield trajectories were generally older within the modeling area, except for locations in the Irish Sea and north of the North Sea. Thus, H_1 is strengthened since Sellafield particles are generally older than La Hague particles within most model locations.

The OpenDrift ocean transport model was validated by comparing model estimations of ^{129}I- and ^{236}U concentrations and $^{129}I/^{236}U$ ratios to corresponding observations. These model estimations were based on relatively well-documented discharges from Sellafield and La Hague, and the observations were gathered from various previous studies and measurements of this study. The validation showed that the model underestimated both the ^{129}I and ^{236}U concentrations compared to the corresponding observations at the same time and location, even if both radionuclides were assumed to behave completely conservative.

The model underestimates the concentrations, especially the ^{236}U concentrations, more at locations further away from the nuclear reprocessing sources like in the Barents Sea compared to locations closer to the sources like in the English Channel. This aligns with expectations that seawater farther from the nuclear reprocessing plants is more influenced by other discharge sources, such as global fallout and accumulated discharges from nuclear installations. In contrast, water masses closer to the nuclear reprocessing sources are more affected by local discharges.

The $^{129}I/^{236}U$ model estimations were most comparable to observations in locations further away from the nuclear reprocessing sources. The model estimated these ratios well, even if some important real-world dynamics and discharge sources were neglected. The reason for better model ratio estimations further away from the sources might be related to more mixed and homogenous water masses in these areas, while a more heterogeneous mix is present in the locations closer to the sources. The existence of heterogeneous masses is supported by the large variations in the observation measurements. Since the estimated $^{129}I/^{236}U$ isotope ratio is more comparable further away from the discharge sources, hypothesis H_2 could not be refuted.

The ^{236}U ocean tracer has been suggested not to be as conservative in the ocean as previously assumed due to substantial retention (Periáñez et al., 2023). The ocean transport model in this study underestimated the ^{236}U concentrations from Sellafield, which indicated greater transport of ^{236}U from Sellafield to the North Atlantic Ocean in field observations compared to the model. Since the model assumed a completely conservative behavior of ^{236}U, signs of significant ^{236}U retention in the Irish Sea would more likely cause the model to overestimate the ^{236}U concentration within the model area. The estimated $^{129}I/^{236}U$ isotope ratios compared well to corresponding observations. Signs of ^{236}U retention in the Irish Sea would decrease the ^{236}U concentrations in the real world, and the conservative assumptions of ^{236}U in the model would more likely cause an underestimation of the $^{129}I/^{236}U$ ratio.

The modeling conducted during this research excluded speciation and assumed conservative behavior of ^{236}U causing any substantial ^{236}U retention difficult to verify. Hypothesis H_3 could not be fully tested in this research, even if the compared ^{236}U concentrations and $^{129}I/^{236}U$ ratios in this study revealed signals of no substantial ^{236}U retention. However, this research has laid the groundwork for the further exploration of ^{236}U retention. To obtain more conclusive results on this topic, additional model simulations with and without speciation codes should be conducted.

References

Albretsen, J. (2019, 12.04.2021). *Ocean models*. Institute of Marine Research (IMR). Retrieved 12.04.2024 from https://www.hi.no/en/hi/forskning/research-data-1/models/ocean-models.

Be, M. M., Chiste, V., Dulieu, C., Browne, E., Chechev, V., Kuzmenko, N., Helmer, R., Nichols, A., Schonfeld, E., & Dersch, R. (2004). *Table of Radionuclides* (Vol. 1). Bureau International des Poids et Mesures. http://www.bipm.org/utils/common/pdf/monographieRI/Monographie_BIPM-5_Tables_Vol1.pdf.

Be, M. M., Chiste, V., Dulieu, C., Browne, E., Chechev, V., Kuzmenko, N., Kondev, F., Luca, A., Galan, M., Pearce, A., & Huang, X. (2008). *Table of Radionuclides* (Vol. 4). Bureau International des Poids et Mesures. http://www.bipm.org/utils/common/pdf/monographieRI/Monographie_BIPM-5_Tables_Vol4.pdf.

Britannica. (2024). Norwegian Sea. In A. Tikkanen (Ed.), *Britannica*.

Casacuberta, N., Christl, M., Vockenhuber, C., Wefing, A.-M., Wacker, L., Masqué, P., Synal, H.-A., & Rutgers van der Loeff, M. (2018). Tracing the Three Atlantic Branches Entering the Arctic Ocean With 129I and 236U. *Journal of Geophysical Research: Oceans*, *123*(9), 6909-6921. https://doi.org/10.1029/2018JC014168.

Casacuberta, N., Masqué, P., Henderson, G., van-der-Loeff, M. R., Bauch, D., Vockenhuber, C., Daraoui, A., Walther, C., Synal, H.-A., & Christl, M. (2016). First 236U data from the Arctic Ocean and use of 236U/238U and 129I/236U as a new dual tracer. *Earth and Planetary Science Letters*, *440*, 127-134. https://doi.org/10.1016/j.epsl.2016.02.020.

Castrillejo, M., Casacuberta, N., Christl, M., Vockenhuber, C., Synal, H. A., García-Ibáñez, M. I., Lherminier, P., Sarthou, G., Garcia-Orellana, J., & Masqué, P. (2018). Tracing water masses with 129I and 236U in the subpolar North Atlantic along the GEOTRACES GA01 section. *Biogeosciences*, *15*(18), 5545-5564. https://doi.org/10.5194/bg-15-5545-2018.

Christl, M., Casacuberta, N., Lachner, J., Herrmann, J., & Synal, H.-A. (2017). Anthropogenic 236U in the North Sea – A Closer Look into a Source Region. *Environmental Science & Technology*, *51*(21), 12146-12153. https://doi.org/10.1021/acs.est.7b03168.

Christl, M., Casacuberta, N., Lachner, J., Maxeiner, S., Vockenhuber, C., Synal, H.-A., Goroncy, I., Herrmann, J., Daraoui, A., Walther, C., & Michel, R. (2015a). Status of 236U analyses at ETH Zurich and the distribution of 236U and 129I in the North Sea in 2009. *Nuclear Instruments and Methods in Physics Research SEction B: BEam Interactions with Materials and Atoms*, *361*, 510-516. https://doi.org/10.1016/j.nimb.2015.01.005.

Christl, M., Casacuberta, N., Vockenhuber, C., Elsässer, C., Bailly du Bois, P., Herrmann, J., & Synal, H.-A. (2015b). Reconstruction of the 236U input function for the Northeast Atlantic Ocean: Implications for 129I/236U and 236U/238U-based tracer ages. *Journal of Geophysical Research: Oceans*, *120*(11), 7282-7299. https://doi.org/10.1002/2015JC011116.

Christl, M., Gautschi, P., Maxeiner, S., Müller, A. M., Vockenhuber, C., & Synal, H.-A. (2023). 236U analyses with the ETH Zurich MILEA prototype system. *Nuclear Instruments and Methods in Physics Research Section B: Beam Interactions with Materials and Atoms*, *534*, 61-71. https://doi.org/10.1016/j.nimb.2022.11.009.

Copernicus. (2023). *Global Ocean Physics Reanalysis* https://doi.org/10.48670/moi-00021.

Costa Peluzo, B. M. T., & Kraka, E. (2022). Uranium: The Nuclear Fuel Cycle and Beyond. *Int J Mol Sci*, *23*(9). https://doi.org/10.3390/ijms23094655.

Dagestad, K. F., Röhrs, J., Breivik, Ø., & Ådlandsvik, B. (2018). OpenDrift v1.0: a generic framework for trajectory modelling. *Geosci. Model Dev.*, *11*(4), 1405-1420. https://doi.org/10.5194/gmd-11-1405-2018.

Dagestad, K.-F., & Hope, G. (2020). *OpenDrift*. In https://opendrift.github.io/index.html.

Daraoui, A., Tosch, L., Gorny, M., Michel, R., Goroncy, I., Herrmann, J., Nies, H., Synal, H.-A., Alfimov, V., & Walther, C. (2016). Iodine-129, Iodine-127 and Cesium-137 in seawater from the North Sea and the Baltic Sea. *Journal of Environmental Radioactivity*, *162-163*, 289-299. https://doi.org/10.1016/j.jenvrad.2016.06.006.

Duffa, C., Bois, P. B. d., Caillaud, M., Charmasson, S., Couvez, C., Didier, D., Dumas, F., Fievet, B., Morillon, M., Renaud, P., & Thébault, H. (2016). Development of emergency response tools for accidental radiological contamination of French coastal areas. *Journal of Environmental Radioactivity*, *151*, 487-494. https://doi.org/10.1016/j.jenvrad.2015.04.019.

EPA. (2023). *Climate Change Indicators: Oceans*. Retrieved 10.04.2024 from https://www.epa.gov/climate-indicators/oceans.

Forwood, M. (2008). *The Legacy of Reprocessing in the United Kingdom*. https://fissilematerials.org/library/rr05.pdf.

Froidevaux, P. (2023). *Chemical separation of U in water Ver. N° : 1*. Institut de Radiophysique (IRA), University of Lausanne.

Froidevaux, P. (2023). *Manufacture of AMS targets to be sent to the Ion Beam Physics Laboratory at ETH Zurich*. Institut de Radiophysique (IRA), University of Lausanne.

GOV.UK. (2022, 17.05.2022). *Operations to end at Sellafield's Magnox Reprocessing Plant*. https://www.gov.uk/government/news/operations-to-end-at-sellafields-magnox-reprocessing-plant.

Heldal, H. E., Gwynn, J., Teien, H.-C., Volynkin, A., Jensen, L. K., Scheibener, S., & Epifanov, A. (2019). *Investigation of the marine environment around the nuclear submarine "Komsomolets" 6.-10. July 2019 (No. 9-2019)* 1503-6294). https://www.hi.no/hi/publikasjoner/toktrapporter/2019/investigation-of-the-marine-environment-around-the-nuclear-submarine-komsomol-ets-6.-10.-july-2019-no.-9-2019.

Heldal, H. E., Teien, H.-C., Gwynn, J., Jerome, S. M., López-Gutiérrez, J. M., García-Tenorio, R., Tims, S., & Lind, O. C. (2024). *Komsomolets Report* [Unpublished manuscript].

Henriksen, S., Fichler, C., Grønlie, A., Henningsen, T., Laursen, I., Løseth, H., Ottesen, D., & Prince, I. (2005). The Norwegian Sea during the Cenozoic. In B. T. G. Wandås, J. P. Nystuen, E. Eide, & F. Gradstein (Eds.), *Norwegian Petroleum Society Special Publications* (Vol. 12, pp. 111-133). Elsevier. https://doi.org/10.1016/S0928-8937(05)80046-3.

Hou, X., & Mindová, M. (2023). *Iodine separation procedure from seawater for ^{129}I AMS measurement*. Technical University of Denmark.

IAEA. (2005). *Status and Trends in Spent Fuel Reprocessing*. INTERNATIONAL ATOMIC ENERGY AGENCY. https://www.iaea.org/publications/7107/status-and-trends-in-spent-fuel-reprocessing.

IAEA. (2012). *Worldwide Marine Radioactivity Studies (WOMARS): Radionuclide Levels in Oceans and Seas*. INTERNATIONAL ATOMIC ENERGY AGENCY. https://www.iaea.org/publications/7003/worldwide-marine-radioactivity-studies-womars-radionuclide-levels-in-oceans-and-seas.

Lehto, J., & Hou, X. (2010). *Chemistry and Analysis of Radionuclides*. WILEY.

Mazarakioti, E. C., Zotos, A., Thomatou, A.-A., Kontogeorgos, A., Patakas, A., & Ladavos, A. (2022). Inductively Coupled Plasma-Mass Spectrometry (ICP-MS), a Useful Tool in Authenticity of Agricultural Products' and Foods' Origin. *Foods*, *11*(22), 3705. https://doi.org/10.3390/foods11223705.

Niello Fernández, J., Negri, A., Wallner, A., Arazi, A., Fifield, L. K., & Tims, S. (2013). *Determination of total I and 129I concentrations in freshwater of Argentina* EPJ Web of Conferences, https://doi.org/10.1051/epjconf/20136303007.

Orano, G. (2022). *Rapport annuel de surveillance de l'environnement Orano la Hague*. https://www.orano.group/en/group/reference-publications.

Orre, S., Gao, Y., Drange, H., & Nilsen, J. E. Ø. (2007). A reassessment of the dispersion properties of 99Tc in the North Sea and the Norwegian Sea. *Journal of Marine Systems*, *68*(1-2), 24-38. https://doi.org/10.1016/j.jmarsys.2006.10.009.

Orre, S., Smith, J. N., Alfimov, V., & Bentsen, M. (2010). Simulating transport of 129I and idealized tracers in the northern North Atlantic Ocean. *Environmental Fluid Mechanics*, *10*(1), 213-233. https://doi.org/10.1007/s10652-009-9138-3.

Periáñez, R., Abascal-Ruíz, U., López-Gutiérrez, J. M., & Villa-Alfageme, M. (2023). Sediments as sinks and sources of marine radionuclides: Implications for their use as ocean tracers. *Marine Pollution Bulletin*, *194*. https://doi.org/10.1016/j.marpolbul.2023.115316.

Periáñez, R., Bezhenar, R., Brovchenko, I., Duffa, C., Iosjpe, M., Jung, K. T., Kim, K. O., Kobayashi, T., Liptak, L., Little, A., Maderich, V., McGinnity, P., Min, B. I., Nies, H., Osvath, I., Suh, K. S., & With, G. d. (2019). Marine radionuclide transport modelling: Recent developments, problems and challenges. *Environmental Modelling & Software*, *122*(104523). https://doi.org/10.1016/j.envsoft.2019.104523.

Periáñez, R., & Cortés, C. (2023). A Numerical Model to Simulate the Transport of Radionuclides in the Western Mediterranean after a Nuclear Accident. *Journal of Marine Science and Engineering*, *11*(1), 169. https://doi.org/10.3390/jmse11010169.

Periáñez, R., Suh, K.-S., Min, B.-I., & Villa-Alfageme, M. (2018). The behaviour of ^{236}U in the North Atlantic Ocean assessed from numerical modelling: A new evaluation of the input function into the Arctic. *Science of The Total Environment*, *626*, 255-263. https://doi.org/10.1016/j.scitotenv.2018.01.058.

Raisbeck, G. M., & Yiou, F. (1999). ^{129}I in the oceans: origins and applications. *Science of The Total Environment*, *237-238*, 31-41. https://doi.org/10.1016/S0048-9697(99)00122-9.

Salbu, B. (2009). Fractionation of radionuclide species in the environment. *Journal of Environmental Radioactivity*, *100*(4), 283-289. https://doi.org/10.1016/j.jenvrad.2008.12.013.

Schneider, M., & Marignac, Y. (2008). *Spent Nuclear Fuel Reprocessing in France*. https://fissilematerials.org/publications/2008/05/spent_nuclear_fuel_reprocessin.html.

Sebille, E. v., Griffies, S. M., Abernathey, R., Adams, T. P., Berloff, P., Biastoch, A., Blanke, B., Chassignet, E. P., Cheng, Y., Cotter, C. J., Deleersnijder, E., Döös, K., Drake, H. F., Drijfhout, S., Gary, S. F., Heemink, A. W., Kjellsson, J., Koszalka, I. M., Lange, M., . . . Zika, J. D. (2018). Lagrangian ocean analysis: Fundamentals and practices. *Ocean Modelling*, *121*, 49-75. https://doi.org/10.1016/j.ocemod.2017.11.008.

Sellafield, L. (2022). *Discharges and Environmental Monitoring Annual Report 2021*. https://www.gov.uk/government/publications/discharges-and-environmental-monitoring-annual-report-2021/discharges-and-environmental-monitoring-annual-report-2021.

Shao, Y., Yang, G., Xu, D., Yamada, M., Tazoe, H., Luo, M., Cheng, H., Yang, K., & Ma, L. (2019). First report on global fallout 236U and uranium atom ratios in soils from Hunan Province, China. *Journal of Environmental Radioactivity*, *197*, 1-8. https://doi.org/10.1016/j.jenvrad.2018.11.009.

Simonsen, M. (2019). *Marine transport modeling of radionuclides using a dynamic speciation approach* Norwegian University of Life Sciences (NMBU)]. https://www.researchgate.net/publication/335834712_Marine_transport_modeling_of_radionuclides_using_a_dynamic_speciation_approach.

Simonsen, M., Albretsen, J., Saetra, Ø., Asplin, L., Lind, O. C., & Teien, H.-C. (2023). High resolution modeling of aluminium transport in a fjord estuary with focus on mean circulation and irregular flow events. *Science of The Total Environment*, *867*(161399). https://doi.org/10.1016/j.scitotenv.2023.161399.

Simonsen, M., Saetra, Ø., Isachsen, P. E., Lind, O. C., Skjerdal, H. K., Salbu, B., Heldal, H. E., & Gwynn, J. P. (2017). The impact of tidal and mesoscale eddy advection on the long term dispersion of 99Tc from Sellafield. *Journal of Environmental Radioactivity*, *177*, 100-112. https://doi.org/10.1016/j.jenvrad.2017.06.002.

Simonsen, M., Teien, H.-C., Lind, O. C., Saetra, Ø., Albretsen, J., & Salbu, B. (2019). Modeling key processes affecting Al speciation and transport in estuaries. *Science of The Total Environment*, *687*, 1147-1163. https://doi.org/10.1016/j.scitotenv.2019.05.318.

Snyder, G., Aldahan, A., & Possnert, G. (2010). Global distribution and long-term fate of anthropogenic 129I in marine and surface water reservoirs. *Geochemistry, Geophysics, Geosystems*, *11*(4). https://doi.org/10.1029/2009GC002910.

Steier, P., Bichler, M., Fifield, L. K., Golser, R., Kutschera, W., Priller, A., Quinto, F., Richter, S., Srncik, M., Terrasi, P., Wacker, L., Wallner, A., Wallner, G., Wilcken, K. M., & Wild, E. M. (2008). Natural and anthropogenic 236U in environmental samples. *Nuclear Instruments and Methods in Physics Research Section B: Beam Interactions with Materials and Atoms*, *266*(10), 2246-2250. https://doi.org/10.1016/j.nimb.2008.03.002.

Thompson, C., Leavy, I., & Baum, S. (2023). *Sample Preparation Method for Low-Level Total 129I Measurements by ICP-MS*. https://www.pnnl.gov/publications/sample-preparation-method-low-level-total-129i-measurements-icp-ms.

Trautmann, N., Happel, S., & Roesch, F. (2022). 7 Radiochemical separations. In R. Frank (Ed.), *Volume 2 Modern Applications* (Vol. 2, pp. 225-286). De Gruyter. https://doi.org/10.1515/9783110742701-007.

U.S.NRC. (2020). *Natural Background Sources*. Retrieved 12.04.2024 from https://www.nrc.gov/about-nrc/radiation/around-us/sources/nat-bg-sources.html.

Vivo-Vilches, C. (2018). *41Ca measurement with Low Energy Accelerator Mass Spectrometry (LEAMS) at the Centro Nacional de Aceleradores* Centro Nacional de Aceleradores]. https://www.researchgate.net/publication/363271228_41Ca_measurement_with_Low_Energy_Accelerator_Mass_Spectrometry_LEAMS_at_the_Centro_Nacional_de_Aceleradores.

Vivo-Vilches, C., López-Gutiérrez, J. M., Periáñez, R., Marcinko, C., Moigne, F. L., McGinnity, P., Peruchena, J. I., & Villa-Alfageme, M. (2018). Recent evolution of 129I levels in the Nordic Seas and the North Atlantic Ocean. *Science of The Total Environment*, *621*, 376-386. https://doi.org/10.1016/j.scitotenv.2017.11.268.

Wang, Y., Hou, X., Zhang, W., Zhang, L., & Fan, Y. (2021). Determination of ultra-low 236U in environment samples using ICP-MS/MS measurement and chemical separation. *Talanta*, *224*, Article 121882. https://doi.org/10.1016/j.talanta.2020.121882.

Wefing, A. M., Casacuberta, N., Christl, M., Gruber, N., & Smith, J. N. (2021). Circulation timescales of Atlantic Water in the Arctic Ocean determined from anthropogenic radionuclides. *Ocean Sci.*, *17*(1), 111-129. https://doi.org/10.5194/os-17-111-2021.

Wilschefski, S. C., & Baxter, M. R. (2019). Inductively Coupled Plasma Mass Spectrometry: Introduction to Analytical Aspects. *Clin Biochem Rev*, *40*(3), 115-133. https://www.researchgate.net/publication/335921363_Inductively_Coupled_Plasma_Mass_Spectrometry_Introduction_to_Analytical_Aspects.

WNA. (2020). *Processing of Used Nuclear Fuel*. Retrieved 12.04 from https://world-nuclear.org/information-library/nuclear-fuel-cycle/fuel-recycling/processing-of-used-nuclear-fuel.aspx.

Appendix

Appendix A – Uranium Separation Procedure

Chemical separation of U in water (Froidevaux, 2023a):

1. Weigh accurately a certain volume of water not exceeding 5 litre and acidify with HNO_3 65% (2ml/l). Filter if necessary.

2. Add the ^{232}U tracer (purified from ^{228}Th if necessary). Shake with a magnetic stirrer.

3. Add 50 mg Fe^{3+} per litre of water (240 mg $FeCl_3 \cdot 6H_2O$).

4. Carefully add NH_4OH 30% until the iron hydroxide precipitate appears.

5. Test the pH with pH paper, and adjust the pH to 8 by adding acid or alkali

6. Put on a watch glass and heat to about 70°C for ½ hour. Remove the stirrer and allow to settle.

7. Decant the supernatant and centrifuge (3000 rpm for 20 min) into Teflon flasks or plastic test tubes

8. Decant the supernatant and dissolve the precipitate in about 20-30 ml of 8M HNO_3. Dissolution may be assisted by the addition of a drop of 30% H_2O_2.

9. Condition one Eichrom U/TEVA cartridge with 10 ml of 8M HNO_3.

10. Pass the solution from point 8 through the column. Wash the beaker with 2x3 ml of 8M HNO_3 which is passed through the cartridge.

11. Wash the cartridge with 20 ml of 8M HNO_3

12. Wash the cartridge with 15 ml of 6M HCl

13. Elute U of the cartridge with 20 ml of 0.01 M HCl

14. Dry evaporate the U fraction on a hot plate. The sample is ready for plating onto a steel disc.

AMS – Target Fabrication of Uranium (Preparation of sample powder) (Froidevaux, 2023b):

1. After radiochemical separation, evaporate the eluate containing U, Pu or Am+Cm from the columns to dryness in the acid fume hood.

2. Resuspend the residue in 10 mL of 0.1 M HCl in a small beaker (20/50 mL). It is advisable to immerse the beaker containing the HCl in the ultrasonic bath for several seconds to ensure that the residue is well dispersed in the solution.

3. Add 1 mL of the Fe^{3+} 2 mg.mL-1 solution

4. Add a small magnetic stirrer to the beaker. Heat it slightly on the hot plate to 50°C and stir gently at 150 rpm. Allow the solution to warm up and equilibrate for about 10 minutes.

5. Add concentrated ammonia drop by drop until the pH of the solution is >7. This usually only requires a few drops and is visually evident when the solution changes color slightly to orange. Then allow the solution to equilibrate for 10 minutes.

6. Remove the magnetic stirrer and wash it in the beaker using a deionized water nozzle.

7. Transfer the solution to a yellow-lidded centrifuge tube, washing the beaker with deionized water and adding the washings to the tube.

8. Centrifuge the beakers at 3000 rpm for 10 min.

9. Discard the supernatant, resuspend the precipitate in deionized water and shake the closed beaker vigorously to disperse the precipitate into solution. This step is essential to ensure that any remaining ammonia is washed away before heating to high temperature. Centrifuge a second time.

10. Discard the supernatant. Prepare a fine plastic pipette.

11. Place the required quantity of small quartz crucibles in the brass sample wheel. Numbers are marked in the wheel, but these will fade after several uses. It is therefore advisable to leave spaces in some places between the samples, so that they can be identified after heating to high temperature.

12. Transfer the sample precipitate to its designated quartz crucible using the thin plastic pipette. The addition of a very small amount of deionized water to the precipitate will facilitate this operation. If the crucible is full and there is still precipitate to be added, proceed to step 13 and return to step 12 as many times as necessary to completely transfer the precipitate to its designated quartz crucible.

13. Without adding the lids to the quartz crucibles, place the sample wheel in the desiccator at 80°C. Leave until the water has evaporated from the crucibles and only the precipitate powder remains in the crucibles.

14. With the lids added to the quartz crucibles, bake the samples at 650°C for at least 4 hours.

Appendix B – Iodine Separation Procedure

Iodine Separation Procedure from Seawater for ^{129}I AMS Measurement (Hou & Mindová, 2023):

1. Water samples are filtered through 0.45 μm filter within 2 days after sampling. In case of transportation or storage, samples can be pretreated by adding of 12.6 g Na_2SO_3 per 1 dm^3.

2. Take the 100 cm^3 of borehole water to a beaker, weigh the mass of the water.

3. Add 2.0 mg of stable iodine carrier** (Woodward iodine with the isotope ratio $^{129}I/^{127}I$ less than 2×10^{-14}) to the sample. To determine the chemical yield, 5 kBq of ^{125}I tracer with is added ($T_{1/2}$ = 59.388 d, E_γ = 35.5 keV, Y = 6.68%). Or ^{131}I can be used instead ($T_{1/2}$ = 8.0252 d, E_γ = 364.5 keV, Y = 81.5%). Then, add 1 cm^3 of 1 $mol \cdot dm^{-3}$ $NaHSO_3$*** solution to the sample solution, 0.5 cm^3 of concentrated HNO_3 (or 2 – 3 cm^3 of 3 $mol \cdot dm^{-3}$) to pH 1 – 2. Wait at least 5 minutes to convert iodine (I_2) to iodide (I^-).

4. Transfer the solution to a 250 cm^3 separation funnel. Add 10 – 15 cm^3 $CHCl_3$. Shake the phases. If a third phase is formed, it must be removed together with $CHCl_3$. Then, fresh 5 cm^3 of $CHCl_3$ is added to the aqueous phase. Then add dropwise 0.5 – 1 cm^3 of 1$mol \cdot dm^{-3}$ $NaNO_2$, until the pink color disappears. $NaNO_2$ oxidize I^- to I_2. Do extraction of I_2 to organic phase by shaking.

5. Separate the $CHCl_3$ phase (down) to the beaker. Add new portion of $CHCl_3$ to the separation funnel to extract the remained I_2. Combine organic phase. Repeat the extraction 2 – 3 times (or more) more, till the pink color disappears. During the very last extraction, add 5 drops of 3 $mol \cdot dm^{-3}$ HNO_3 and 1 drop of 1 $mol \cdot dm^{-3}$ $NaNO_2$****.

6. Transfer the organic phase to the washed and clean separation funnel (50 cm^3). Add 20 – 30 cm^3 of ultrapure water (18 MΩcm), then add 0.3 cm^3 of 0.05 $mol \cdot dm^{-3}$ $NaHSO_3$ to back extract iodine to the water phase by reducing I_2 to I^-. Wait ~2 minutes to see if the amount of reducing agent added is sufficient – both phases must be colorless. In case, that the water phase is yellow or organic phase is pink, it is necessary to add more $NaHSO_3$. Separate discard the organic phase to a waste bottle.

7. To the water phase in separation funnel, add 10 cm^3 $CHCl_3$, 5 drops of 3 $mol \cdot dm^{-3}$ HNO_3, and 0.1 cm^3 $NaNO_2$ (1 drop is enough) to oxidize I^- to I_2. Do extraction of I_2 to $CHCl_3$, separate the organic phase to the beaker. Add 10 cm^3 of fresh $CHCl_3$ to the separation funnel. Repeat the extraction, combine the organic phase. Repeat extraction if necessary.

8. Transfer the organic phase to a new separation funnel (the same one as in step 5 can be used). Add 3 cm^3 of ultrapure water (as less as possible), then 0.2 $cm^3$of 0.05 $mol \cdot dm^{-3}$ $NaHSO_3$ to back extract iodine to the water phase. Both phases must be colorless! Discard the organic phase to the waste bottle. If the solution becomes colored, add 1 drop of 1 $mol \cdot dm^{-3}$ $NaHSO_3$.

9. Transfer the water phase to a 10 mL centrifuge tube (max volume for sample should be ~ 7.5 mL). If there is free volume in the tube, fill this volume with water which was used for cleaning of the separation funnel. In case that the precipitation is doing later (or the solution is not yellow), after few hours or next day, add 1 drop of 1 $mol \cdot dm^{-3}$ $NaHSO_3$ into the sample in the tube.

10. For precipitation, to the water phase in the centrifuge tube, add 1 cm^3 of 3 $mol \cdot dm^{-3}$ HNO_3 and 1 cm^3 of 1 $mol \cdot dm^3$ $AgNO_3$. Mix it well (using Pasteur pipet) to let the AgI precipitate. Centrifuge at 2 300 rpm for 2 minutes.

11. Wash the precipitate with 0.5 – 1 cm^3 of 3 $mol \cdot dm^{-3}$ HNO_3, add water, mix it and centrifuge. Repeat the washing step with water only, 2 – 3 times. Then, transfer the precipitate with Pasteur pipet

into weighed 1.5 cm^3 centrifuge tube with the help of water. Remove excess water with the pipette. Centrifuge, and remove the water rest. Dry the precipitate in the centrifuge tube in an oven at 60 – 80 °C for not longer than 2 hours.

Procedure Blank Preparations:

12. Practically the same procedure is applied. Instead of seawater, ultrapure water is used. One blank sample should be sufficient. When a new sort of chemical is employed or samples are prepared in a different place, in this case, new blank samples must be prepared.

Pressing Target Material into Cathodes:

13. Target material preparation. Weight the mass of precipitate (the total mass minus the mass of the empty 1.5 cm^3 centrifuge tube). Grind the AgI precipitate to a fine powder using a glass or wood rod. Add niobium powder (325 mesh) to the centrifuge tube to achieve the mass ratio of 5:1 (Nb:AgI). Mix it well. Note all masses.

14. Put the Cu cathode into the press holder. Transfer the target material into the Cu cathode and press. Keep the prepared targets in a desiccator until AMS measurement. Normally, samples are stored in the dark using aluminum foil and without access to oxygen.

NOTES:

** Woodward iodine: 2.082 mg ^{127}I per g of the solution (in Denmark). It was the solution of I_2 in 0.5 $mol \cdot dm^{-3}$ NaOH + 0.05 $mol \cdot dm^{-3}$ K_2SO_3 as a reducing agent.

*** Instead of $NaHSO_3$, $KHSO_3$ can be used. $KHSO_3$ can be prepared as follows: 1 $mol \cdot dm^{-3}$ $K_2S_2O_5$ corresponds to 2 $mol \cdot dm^{-3}$ $KHSO_3$. A fresh solution of this compound must be prepared at least once a week.

**** Adding of $NaNO_2$, HNO_3, $NaHSO_3$/$KHSO_3$ can be done by Pasteur pipet. Only WW must be precise.

Appendix C – Model Scripts

Both the general run script and the final post processing scripts which were utilized can be found at the following GitHub:

- https://github.com/magnesim/radio_tracer

The more detailed and refined scripts utilized during this project can be made available upon request.

Appendix D – Sampling Komsomolets (K278)

Komsomolets was a Soviet nuclear submarine which sank on 7th April 1989. Komsomolets was powered by a single 190 MW OK-650b-3 pressurized water reactor and carried two nuclear torpedoes (Heldal et al., 2019). The total activity at the time of the sinking has been estimated to be 29 PBq with an additional 16 TBq of Pu-isotopes contained within the two torpedo warheads (Heldal et al., 2019). Due to the reactor and the torpedoes, the shipwreck has continuously released radionuclides to the surrounding marine environment. The submarine is resting in the Norwegian Sea, southwest of Bear Island (*Figure 33*), at a depth of 1673m (Heldal et al., 2019).

Figure 33: Sampling location of Komsomolets observations (73.81966379N, 13.27566556E).

The samples from the Komsomolets sampling location were provided by courtesy of the Institute of Marine Research (IMR), the Norwegian Radiation and Nuclear Safety Authority (DSA) and the Norwegian University of Life Sciences (NMBU), and measured by the National Accelerator Center (CNA) in 2019 and 2023. These samples were primarily collected to obtain comparable baseline data for future annual measurements. In this research, elevated background levels of radiation are expected in these samples, which hopefully can be observed when comparing observations to the model concentrations.

Appendix E – Raw Data and Conversion to ^{129}I (atoms/l) from Mass Spectrometric Measurements

Table 4: Raw data from ICP-MS and AMS measurements. Including masses of sample volume and iodine carrier (Woodward), uncertainties of measurements and blank corrections used for converting the $^{129}I/^{127}I$ ratio from the AMS and the ^{127}I (µg/L) from the ICP-MS to ^{129}I concentrations (atoms/l) for model validation.

Sample number	Latitude	Longitude	Date of sampling	Depth [m]	Mass [g]	ICP-MS ^{127}I [ug/L]	standard deviation 127I [ppb] (ICP-MS)	127I carrier spiked, WWI, mg	AMS $^{129}I/^{127}I$ [10^{-12}] raw data	AMS $^{129}I/^{127}I$ [10^{-12}] with corr.		129I/127I ratios correct for blank, [10-12]	^{129}I concentration in sample, Atom/L		$^{129}I/^{127}I$ atomic ratio in sample		
											err. (%)			Sigma	Value	Unc. %	Sigma
Sample 1	62.77	4.366	28.04.2023	5	104.1530	50.36	0.27	2.007	384.98	384.978	3.0	384.89	3.53E+10	1.13E+09	1.48E-07	3.17	4.69E-09
Sample 2	62.77	4.366	28.04.2023	319	89.4052	52.90	0.38	1.967	7.45	7.452	1.1	7.36	7.70E+08	1.27E+07	3.07E-09	1.49	4.57E-11
Sample 3	66.94	1.730	09.05.2023	5	100.0500	53.50	0.32	1.984	27.94	27.941	10.8	27.85	2.63E+09	2.85E+08	1.03E-08	10.84	1.12E-09
Sample 4	66.94	1.730	09.05.2023	400	101.0036	55.10	0.43	2.040	8.80	8.796	1.6	8.71	8.36E+08	1.73E+07	3.20E-09	1.92	6.15E-11
Sample 5	66.83	9.336	10.05.2023	5	99.8396	47.40	0.06	2.032	64.57	64.568	2.7	64.48	6.24E+09	1.81E+08	2.78E-08	2.90	8.05E-10
Sample 6	66.83	9.336	10.05.2023	326	99.8073	52.40	0.18	2.031	10.17	10.175	1.3	10.09	9.76E+08	1.64E+07	3.93E-09	1.65	6.47E-11
Sample 7	68.32	10.792	12.05.2023	5	102.6064	51.30	0.25	2.045	75.84	75.837	5.0	75.75	7.18E+09	3.65E+08	2.95E-08	5.07	1.49E-09
Sample 8	68.32	10.792	12.05.2023	647	97.8916	53.40	0.11	2.043	6.43	6.427	2.6	6.34	6.29E+08	1.77E+07	2.48E-09	2.81	6.99E-11
Sample 9	70.64	0.010	19.05.2023	5	100.4593	53.60	0.08	2.034	13.25	13.254	2.3	13.16	1.27E+09	3.17E+07	4.99E-09	2.49	1.24E-10
Sample 10	71.00	9.358	20.05.2023	5	103.1343	54.40	0.27	2.038	14.96	14.964	1.6	14.87	1.40E+09	2.68E+07	5.42E-09	1.85	1.00E-10

Norges miljø- og biovitenskapelige universitet
Noregs miljø- og biovitskapelege universitet
Norwegian University of Life Sciences

Postboks 5003
NO-1432 Ås
Norway